FACULDADE DE CIÊNCIAS E TECNOLOGIA
UNIVERSIDADE NOVA DE LISBOA

DEPARTAMENTO DE FÍSICA

The influence of geometric factors on the wall shear stress distribution in realistic human coronary arteries

Jorge André Piedade Pinhal dos Santos

Dissertação apresentada na Faculdade de Ciências e Tecnologia da Universidade Nova de Lisboa para a obtenção do grau de Mestre em Engenharia Biomédica.

A presente dissertação foi desenvolvida no Erasmus Medical Center em Roterdão, Holanda.

Orientadora:

Dr. Ir. Jolanda J. Wentzel

Lisboa
2009

Acknowledgments

In the first place I would like to thanks Dr. Ir. Jolanda Wentzel for her supportive supervision and for her patience for reading and correcting all the drafts I have written during this period.

My special thanks to Diana and Sandro, my cousins, and to “our Portuguese group” in Rotterdam, who helped and supported me during these six months abroad.

I would also like to thank all the researchers and colleagues in the Biomechanics Laboratory in the Erasmus MC, who welcomed me and treated me as one of them.

Thanks also to all of my friends, especially to Samuel, Eduardo, Daniel, Barros, Filipa, Sara, Osório and Hugo, without whom, the last five years wouldn’t have been so much fun and unforgettable.

To Inês, my special thanks for all the care and courage given. You are my ally.

Finally, my most special thanks to my brother Pedro, and my parents Luís and Carminda, who are always there for me and are the most important persons in my life.

Abstract

Background:

Atherosclerosis is the main cause of death in the Western society. It is a geometrically focal disease, affecting preferentially vessel areas of low wall shear stress (SS), which induces the expression of atherogenic genes. To predict wall SS several options are available. Among them Computational Fluid Dynamics (CFD) simulations on 3D reconstructed coronaries using Finite Element Modeling (FEM). However, to perform CFD a 3D representation is needed. To obtain a 3D representation of the coronary under study different methods can be applied.

Methods:

CFD calculations were performed using FEM on ten 3D reconstructed coronary arteries by the state-of-the-art ANGUS method (biplane angiography + Intravascular Ultrasound (IVUS)). The SS outcomes of the CFD calculations were compared with SS calculated by the Poiseuille equation, and with the SS outcomes of CFD simulations of the same 3D reconstructed arteries by QCA-3D (biplane angiography – no cross-sectional information) and Straight (IVUS images stacked on a straight centerline – no curvature information) methods.

Results:

The Poiseuille equation did not have any sensitivity in predicting any low SS (<0.5 Pa) per cross-section. However, the average correlation coefficient between the average SS per cross section from the Angus geometries and SS based on the Poiseuille equation was $r^2 = 0.65 \pm 0.09$. A strong correlation was obtained for the SS from the ANGUS and the Straight method, while only an average correlation was obtained between ANGUS and QCA-3D average SS. Bland-Altman analysis was performed to confirm the results agreement. The sensitivity and specificity of the QCA-3D and Straight method in predicting low and high SS was measured. Geometric factors, such as local curvature, area gradient and torsion were found to be related to the presence of SS peaks or to regions prone to plaque development. These geometric risk factors were utilized to give some guidelines on meshing optimization.

Conclusions:

The use of a simpler 3D reconstruction approach, such as the QCA-3D or the Straight method, in combination with the optimization of meshing based on the geometric features of the coronaries, has the potential to, in the future, bring CFD calculations of wall SS from bench to bedside.

Resumo

Introdução:

A aterosclerose é a principal causa de morte na sociedade ocidental. É uma doença geometricamente focal que afecta preferencialmente áreas da parede de vasos com baixa tensão de cisalhamento, induzindo a expressão de genes aterogénicos. Hoje em dia para prever a tensão de cisalhamento (SS) da parede arterial várias opções são viáveis. Entre elas, simulações de Dinâmica de Fluidos Computacional (CFD) em coronárias reconstruídas em 3D em conjugação com Modelação em Elementos Finitos (FEM). Assim sendo, para realizar cálculos CFD, a representação 3D das coronárias é necessária. Para obter estas representações 3D vários métodos podem ser usados.

Métodos:

Os cálculos CFD são realizados usando FEM em dez artérias coronárias reconstruídas em 3D pelo método padrão ANGUS (angiografia biplanar + Ultrassom Intravascular (IVUS)). Os valores de SS obtidos nos cálculos CFD são comparados com os valores de SS calculados pela equação de Poiseuille, e com o SS obtido pelos cálculos CFD para as mesmas artérias coronárias, mas reconstruídas em 3D pelo método QCA-3D (angiografia biplanar – sem informação sobre a forma de cada secção de corte) e pelo método Straight (imagens IVUS empilhadas ao longo de um eixo recto – sem informação da curvatura).

Resultados:

A equação de Poiseuille não tem sensibilidade para prever um valor de SS baixo (SS<0.5) em cada secção de corte. Contudo, o coeficiente de correlação média, entre o valor médio de SS em cada secção de corte por geometrias Angus e SS baseado na equação de Poiseuille são $r^2 = 0.65 \pm 0.09$. Uma forte correlação foi obtida a partir dos valores de SS obtido com ANGUS e o pelo método Straight, enquanto apenas foi obtida uma correlação média entre o SS médio por corte entre o método ANGUS e o método QCA-3D. Uma análise Bland-Altman foi realizada para confirmar a concordância dos resultados. A sensibilidade e a especificidade do método QCA-3D e do método Straight para prever baixos e altos valores de SS foram medidas. Factores geométricos, como a curvatura local, o gradiente em área e a torção foram relacionados com a presença de picos de SS ou com regiões propensas ao desenvolvimento de placas. Estes factores de risco geométricos foram usados para dar algumas orientações para optimização das malhas de elementos finitos.

Conclusões:

A utilização de reconstruções 3D mais simples, como o método QCA-3D ou o método Straight, em combinação com a optimização das malhas baseada nos parâmetros geométricos das artérias coronárias, tem potencial para, no futuro, trazerem os cálculos CFD do SS da parede arterial da teoria para a prática.

Abbreviations list

ANGUS – Angiography + Intravascular ultrasound

CAAS – Cardiovascular Angiography Analysis System

QCA-3D –Quantitative Coronary Analysis 3D

CFD – Computational Fluid Dynamics

De – Dean Number

eNOS – Endothelial nitric oxide synthase

ESS – Endothelial Shear Stress

FDA – Food and Drug Administration

FEM – Finite Element Method

IVUS – Intravascular ultrasound

LAD – Left anterior descending artery

LCA – Left coronary artery

LCX – Left circumflex artery

LDL – Low density lipoprotein

LMCA – Left main coronary artery

RCA – Right coronary artery

Re – Reynolds number

SS – Shear stress

VCAM-1 – Vascular cell adhesion molecule-1

Table of contents

List of figures

List of tables

Introduction

The research to this Master Dissertation in Biomedical Engineering was performed at the Biomechanics Laboratory of the Biomedical Engineering Department, which is part of the Thoraxcenter of the Erasmus Medical Center in Rotterdam, The Netherlands. The supervisor of this project and head of the Biomechanics Lab. is Dr. ir. Jolanda J. Wentzel. The Biomedical Engineering is a research group focused on the cardiovascular diseases, namely on its origin, diagnosis and treatment. The Biomedical Engineering is, then, divided in the Experimental Echocardiography group and the Biomechanics Lab. At the latest, researchers study the effects of the mechanical stresses on the development and progression of vascular disease, namely atherosclerosis. The research includes cell studies, animal experiments and patient studies. In order to study the relationship between biomechanical parameters and vascular disease is used the combination of imaging modalities and computer modeling, resulting in applications such as ANGUS.

Chapter 1. Background

1.1. Coronary Arteries

The coronary arteries are the vessels that supply blood rich in oxygen to the heart muscle. Only the main coronary arteries lie on the surface of the heart as the smaller arteries penetrate the surface into the cardiac muscle. The two main coronaries are the left coronary artery (LCA) and the right coronary artery (RCA), which derive directly from the aorta. The LCA then bifurcates into the left circumflex artery (LCX) and the left anterior descending artery (LAD) (see figure 1.1). The length of the LCA ranges from 1 to 25 mm, when it bifurcates into the LAD whose length varies from 10 to 13 cm and the LCX, which measures 6 to 8 cm in length. The RCA measures about 12 to 14 cm in length [1]. These vessels mean diameters and diameter ranges are presented below in the Table 1.1.

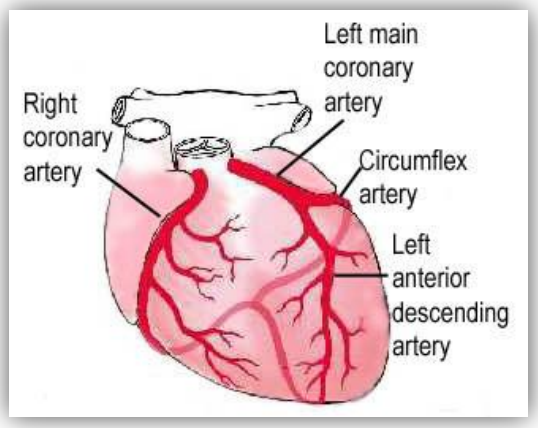

Figure 1.1 - Main coronary arteries (http://cognitorex.blogspot.com/2007/06/i-got-new-stent-today.html)

Coronary Artery	Mean Diameter (mm) ± SD	Range (mm)
LMCA	4.7 ± 1.0	3.6 – 7.2
Proximal LAD	3.9 ± 0.8	2.4 – 5.6
Distal LAD	1.7 ± 0.4	1.2 – 2.7
LCX	3.4 ± 0.8	1.5 – 5.2
Proximal RCA	3.6 ± 0.8	2.0 – 4.8
Distal RCA	2.7 ± 0.9	1.1 – 4.5

Table 1.1 - Mean diameters of the main coronaries according to Mosseri et al. [2]

The LCA supplies mainly the anterior and lateral portions of the left ventricle while the RCA supplies most of the right ventricle and the posterior part of the left ventricle in 80 to 90 percent of people [3].

The blood flow in coronary arteries is laminar, which means that it flows at a steady rate through the vessels, with each layer of blood remaining at the same distance from the wall. The central portion of the blood stays in the center of the vessel [3]. Since the flow in coronary arteries is laminar, the Reynolds number is also low. The non-dimensional Reynolds number is the measure of tendency for turbulence to occur and it is represented by the following equation:

$$\mathrm{Re} = \frac{\rho v d}{\eta} \quad (1)$$

In equation (1), v is the velocity of blood flow, d is diameter of the vessel, η is the viscosity and ρ is the density. The transition between laminar and turbulent flow

does not occur at a specific Reynolds number, even though, if the Reynolds number is below 2000 the fluid flow is laminar. Between 2000 and 4000 the flow is in transition between laminar and turbulent flow, and if the Reynolds number is over 4000 the flow is considered to be completely turbulent. The typical Reynolds number in coronary arteries is around 250[3].

1.2. Arterial Wall Anatomy

The arterial wall is composed of three layers (*tunicas*). As seen in figure 1.2, the innermost layer is called *tunica intima* and consists of a single layer of endothelial cells, connective tissue and some elastic fibers. The middle layer is called *tunica media* and it consists mainly of smooth muscle cells and elastic fibers. The outer layer is called *tunica adventitia* and is composed of collagen fibers as well as other elastic fibers. The *tunica adventitia* is the strongest of these three layers.

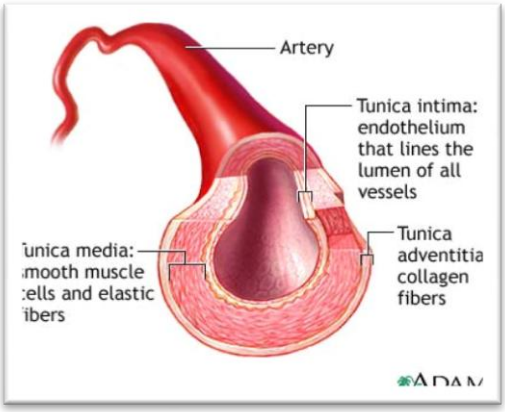

Figure 1.2 - Arterial wall layers (http://www.nlm.nih.gov/medlineplus/ency/imagepages/19194.htm)

Anatomically, the arterial walls are stronger than the venal walls, so they are less distensible [4]. Also, atherosclerotic arteries become hardened so they lose compliance.

1.3. Atherosclerosis

Atherosclerosis is the main cause of death in the developed world [5]. An atherosclerotic plaque is formed by deposits of lipids, macrophages, cellular debris, calcium, among other substances (see figure 1.3), in between the innermost layer (called intima) and the intermediate layer (called media) of the arterial wall. Atherosclerosis is generally associated with some risk factors, such as hypertension, smoking, hyperlipidemia, sedentary lifestyle, viral infection, diabetes mellitus, chronic infections and also with genetic predisposition [5].

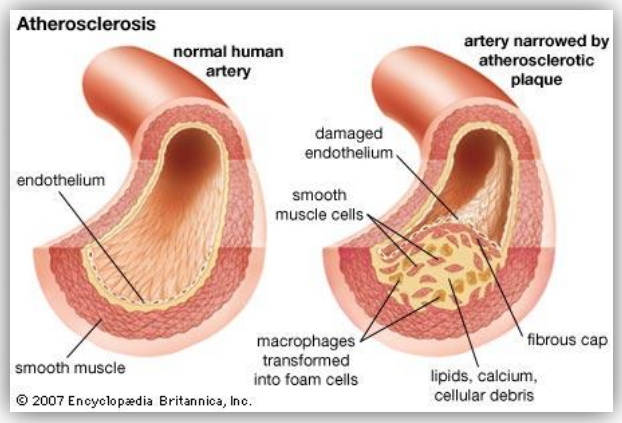

Figure 1.3 - Healthy human artery vs. artery narrowed by atherosclerotic plaque

The origin of an atherosclerotic plaque is due to the excessive accumulation of LDL (low-density lipoprotein, also known as bad cholesterol, and composed of lipids and a protein) particles in the arterial wall. Those LDL particles undergo some chemical alterations such as oxidation. The cells in the vessel interpret these modified LDLs as a danger sign, so the endothelial cells of the artery start to display adhesion molecules on their blood-facing surface. These adhesion molecules attract monocytes and T cells in the blood into the intima, where the monocytes mature into macrophages that will ingest the modified LDLs and produce inflammatory mediators. The macrophages become filled with fatty substances (they transform into foam cells) and along with the T cells they constitute the early form of a plaque. A fibrous cap is formed over the lipid core and smooth muscle cells migrate from the media to the top of the intima, multiply and produce a fibrous matrix that glues the cells together [6]. These plaques can grow into the artery lumen, restricting it, causing lumen narrowing, which can hamper the blood delivery to the tissues. Vessel stenosis can provoke, among others, angina pectoris. Plaques that are at high risk to rupture (called vulnerable plaques) are characterized by a certain composition: necrotic core, inflammatory cells infiltration (macrophage and T cells), large lipid pool and a thin fibrous cap. If a vulnerable plaque ruptures it can cause a thrombus or a clot. If a clot is big enough it can block a blood vessel causing a heart attack or a stroke, if it is a coronary or a brain artery respectively (figure 1.4).

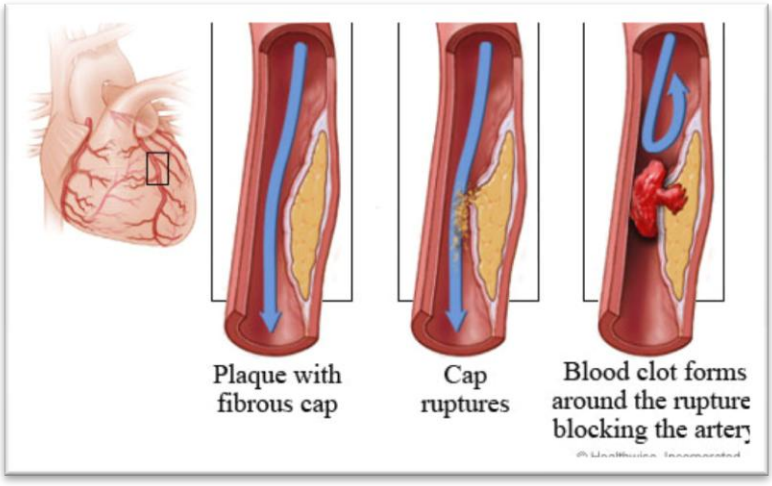

Figure 1.4 - Clot formation on a coronary artery (http://64.143.176.100/library/healthguide/en-us/support/topic.asp?hwid=zm2431)

1.4. The role of shear stress in Atherosclerosis

Forces are inflicted on vascular tissues in different directions. There are circumferential and radial forces (tensile or compressive), and there are tangential forces such as shear. The endothelial shear stress (ESS) is the tangential force derived by the friction of the flowing blood on the endothelial surface. It is the product of the shear rate (difference of velocity between two different layers divided by the distance between them, or dV/dr) at the wall and the blood viscosity (μ) [7].

$$\tau_s = \mu \frac{dV}{dr}$$

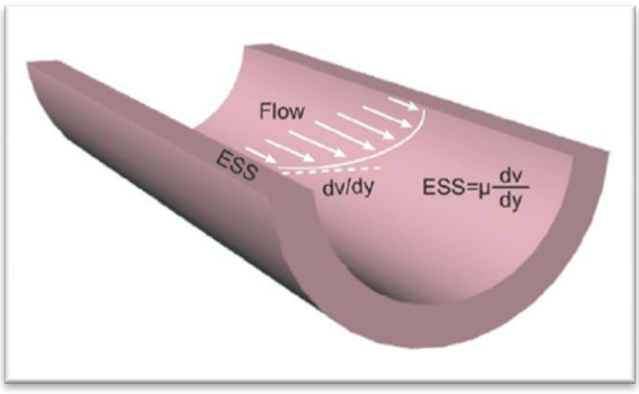

Figure 1.5 - Definition of endothelial shear stress [7]

Due to the pulsatile nature of the blood flow and the geometric configuration of the arteries, there are different patterns of endothelial shear stress. In the straight

parts of the arteries the shear stress varies from 1.5 to 7 Pa [7]. Though, in irregular regions, like outer walls of vessel bifurcations, the shear stress is usually low and oscillatory, with values ranging from <1 to 1.2 Pa.

The endothelial cells of the arteries respond to the different range of shear stress values in different ways. Even though the shear stress has magnitudes of only 5 Pa, the endothelial cells are specially equipped with a dedicated sensing mechanism, the mechanoreceptors, which are capable to detect those shear stress stimuli on the endothelial cells surface [8]. After detecting the shear stress stimulus, a complex pathway known as mechanotransduction is activated.

Different patterns of shear stress induce different phenotypes of the endothelial cells of the arteries. With physiological shear stress (>1.5 Pa), the endothelial cells will show an atheroprotective phenotype, although, if the shear stress is low and/or oscillatory (<0.4 Pa) the endothelial cells exhibit an atherogenic phenotype [5] (see figure 1.6). The low shear stress causes a change in the morphology of endothelial cells (which become less elongated and are not aligned with the direction of the blood flow); the atherogenic phenotype is mainly characterized by reduced production of eNOS (endothelial nitric oxide synthase, a vasodilator), reduced endothelial repair, increased amounts of reactive oxygen species, higher leukocyte adhesion (high expression of vascular cell adhesion molecule-1 also known as VCAM-1), higher permeability to lipoproteins and higher inflammation predisposition [9]. This atherogenic phenotype of the endothelial cells combined with the presence of the systemic risk factors will promote the atherosclerotic plaque formation at these sites.

Therefore, despite being associated with the risk factors mentioned above, the atherosclerosis is also a geometrically focal disease [5], which affects preferentially the areas where the shear stress caused by blood flow is low and oscillating, like the outer edges of artery bifurcations, inner curvatures and close to side branches. On the other hand, areas exposed to steady blood flow and higher shear stresses are normally disease free.

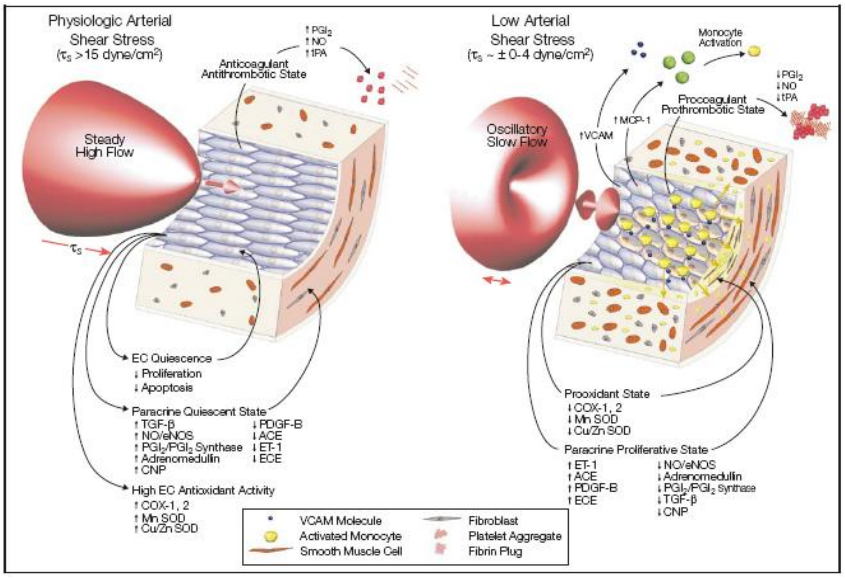

Figure 1.6 - Atheroprotective vs. atherogenic phenotype [5]

In addition to the role shear stress has in the atherosclerotic plaque formation, it is thought that it also plays an important role in the development of those plaques, into a quiescent or high-risk (vulnerable) atherosclerotic plaque [7, 10, 11].

As seen in figure 1.7 an eccentric vulnerable plaque can be divided in four regions: upstream and downstream, the midcap and the lateral shoulders. The upstream region of the plaque is submitted to high shear stress; meanwhile at the downstream regions the shear stress is low.

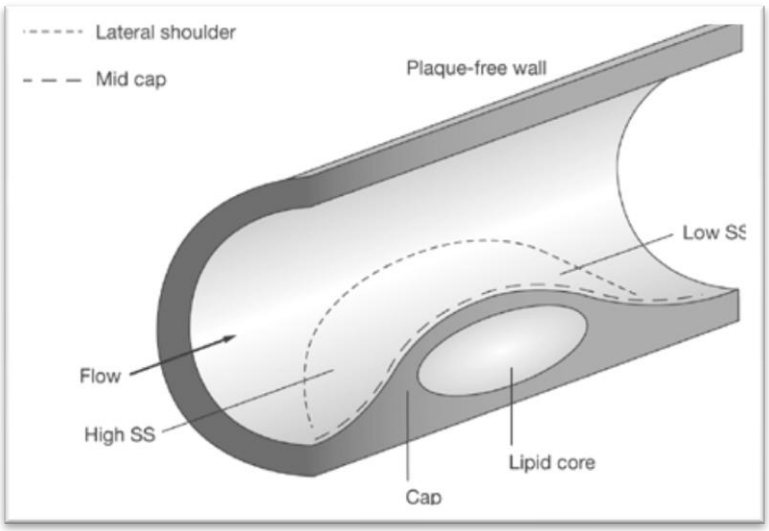

Figure 1.7 - Eccentric plaque regions [10]

When a plaque begins to grow, the lumen narrowing is prevented by outward vessel remodeling [10], in order to maintain normal values of shear stress. However, this vessel remodeling has some consequences. It can promote the plaque growth or even the plaque rupture. The plaque growth can occur in the downstream region of the plaque, due to low shear stress, which favors the atherosclerotic progression. The plaque fissuring occurs mainly at the upstream lateral plaque shoulders, and it is suggested that the high shear stress can be a reason for it, as it stimulates the endothelium to thin the fibrous cap [10]. Subsequently the tensile stress causes the plaque disruption at the lateral shoulders, because at those regions the fibrous cap is thinner and has, consequently, less resistance to tensile strength [12]. As the tensile stress is cyclic (due to oscillations in blood pressure), it can also lead to cap fatigue and rupture [12].

Thus it is important to continue studying new approaches on estimating wall shear stress in coronary arteries in order to predict atherosclerotic plaque development and progression.

1.5. Navier-Stokes equations – CFD and FEM

The Navier-Stokes equations are a set of differential equations that describe the motion of a viscous fluid. G.G. Stokes and C.L. Navier first derived them independently in the early 1800's. This set of equations consists of an equation for conservation of mass, conservation of momentum equations and a conservation of energy. Unlike algebraic equations, the Navier-Stokes's do not establish a relation among the variables of interest (like velocity or pressure). Instead, they establish relations among the rates of change of these variables [13, 14].

For an incompressible, Newtonian, temperature independent and uniform fluid, with a laminar flow, the continuity equation (a) and the Navier-Stokes equations (b), can be written as:

$$div \quad u = \frac{\partial u_1}{\partial x_1} + \frac{\partial u_2}{\partial x_2} + \frac{\partial u_3}{\partial x_3} = 0 \qquad \text{(a)}$$

$$\rho\left(\frac{\partial u}{\partial t}+(u.\nabla)u\right)-div\ \ \sigma=\rho f, \qquad \text{(b)}$$

In which $u=(u_1,u_2,u_3)^T$ stands for the velocity vector, ρ the density of the fluid, $f=(f_1,f_2,f_3)$ the body force per unit of mass, and σ the stress tensor. [15]

In theory, the Navier-Stokes equations, for a given flow problem can be solved analytically by using methods from calculus. Though, in practice, these equations are too difficult to solve analytically for real life geometries. So, nowadays, computers are used to solve approximations to the equations using techniques such as finite volume or finite element methods. This field of study is called Computational Fluid Dynamics (CFD).

In order to calculate SS through CFD, in any geometry, the 3D representation of that geometry in the computer software is needed.

The FEM is a general discretization tool for partial differential equations, alternative to the finite difference methods or finite volume methods. With FEM it is fairly easy to solve problems in complex geometries. On the other hand, the programming of FEM is more complicated than the previously mentioned methods.

In FEM, the region where the differential equation is defined Ω is subdivided into simple elements. In $\mathbb{R}$ the elements are intervals, in $\mathbb{R}^2$ are triangles or quadrilaterals and in $\mathbb{R}^3$ are usually tetrahedra or hexahedra. This subdivision of a region in elements, called mesh, is performed by a mesh generator. In each element are then chosen a number of nodal points [15] and the unknown function is approximated by a polynomial (it is common practice to restrict to lower degree polynomials – linear or quadratic).

1.6. Poiseuille flow model

As written above, the flow in the coronary arteries is considered to be laminar. So if we consider the blood as an incompressible fluid and the vessels as a stiff cylindrical tube with a constant diameter, the blood flow can be expressed by the Hagen-Poiseuille formula: $\Delta P=\frac{8\mu LQ}{\pi r^4}$. Where Δ P is the pressure drop between the ends of the cylinder, μ is the dynamic viscosity of the fluid, L is the length of the

tube, Q is the flow rate and r is the radius of the cylinder. According to Poiseuille's theory of flow the velocity has a parabolic profile, where the velocity is highest at the center of the tube and zero at the tube walls (figure 1.8).

The wall shear stress can be mathematically derived from the Hagen-Poiseuille equation: $\tau_s = \frac{4\mu Q}{\pi r^3}$

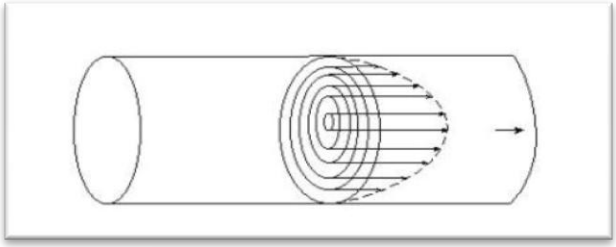

Figure 1.8 - Poiseuille flow (velocity) profile (adapted from http://www.columbia.edu/~kj3/Dslide4.jpg)

However, the flow in a realistic human coronary artery is not Poiseuille like. Depending on some geometric factors, the flow profile can exhibit different patterns. Figure 1.9 shows the different patterns of flow in a cylindrical tube. At location number 1 a Poiseuille (parabolic) flow is presented; number 2 corresponds to an asymmetric flow; number 3, which has a flattened profile, represents a turbulent flow (it can also represent a non-newtonian fluid velocity profile); and number 4 indicates a backflow or a retrograde flow.

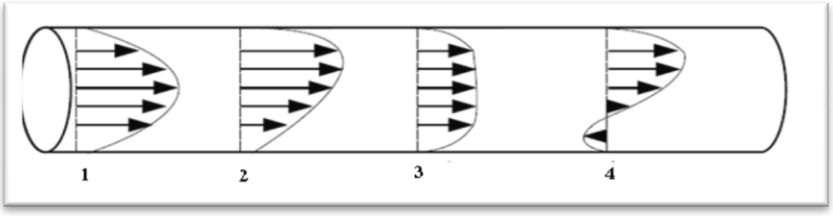

Figure 1.9 - Different flow profiles (adapted from Christian Poelma's Biological Fluid Mechanics lecture on Blood tissue interaction; the role of wall shear stress. Delft University of Technology)[16]

1.7. 3D Reconstruction Methods

The first step to perform CFD calculations on realistic human coronary arteries is to obtain the 3D geometry of those arteries. Therefore, 3D reconstruction methods are needed. The techniques used to obtain the geometries used in this study are described next in this section.

1.7.1. ANGUS

ANGUS is an application that allows the generation of 3D reconstructions of human coronary arteries in vivo, which involves the fusion of intravascular ultrasound (IVUS) and angiography. IVUS provides images with high spatial and temporal resolution. However, since it is a tomographic technique, it makes it difficult to confer a full 3D reconstruction of the vessel segment in investigation. Multiple IVUS images can be stacked up along a straight pullback centerline, which is a simple approach; however more realistic 3D reconstructions are needed. For that reason fusion of IVUS with biplane angiography was developed [17].

The ANGUS method uses a calibration cube to mathematically describe the 3D space. When a marker is imaged in this geometry, its 3D position can be determined. The IVUS images are acquired at the top of the R-wave of the ECG, to reduce the effect of the cardiac motion. Between each image, the IVUS catheter is pulled back 0.5mm. The X-ray biplane angiographic images are recorded; end-diastolic frames are selected, stored and used to define the centerline of the catheter, as such a 3D reconstruction of the catheter path can be obtained [17].

The lumen borders in the IVUS images are detected by a semi-automatic contour detection program. The contours are described with polar coordinates. By using the Fourier transform, a 2D Fourier description of the vessel segment is obtained.

Finally IVUS cross sections are distributed in equidistant intervals on the reconstructed centerline, with the imaging planes perpendicular to the reconstructed centerline and rotating it around the trajectory until it is in the right position [17].

In figure 1.10.A, is shown an example of two IVUS images of an RCA. In figure 1.10.B is shown an angiographic image of that same artery. Figure 1.10.C shows the 3D reconstruction of the artery shown in the previous two images.

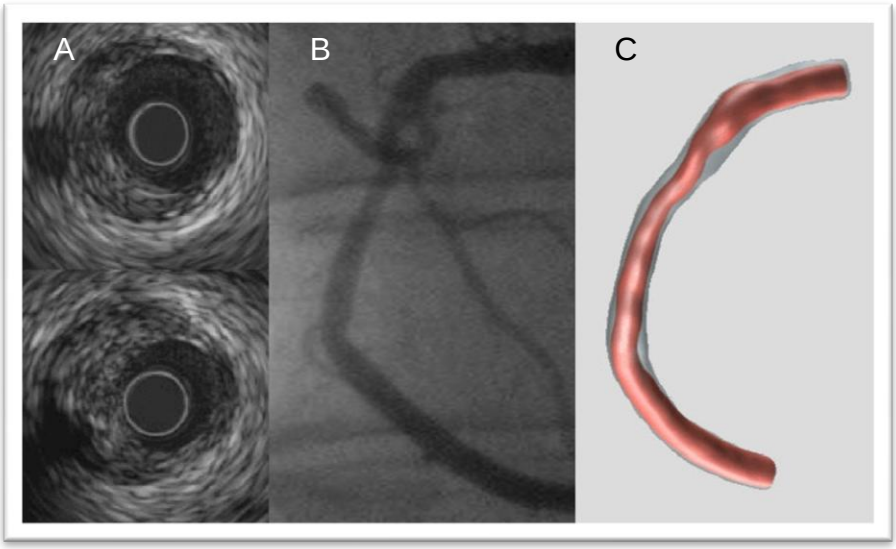

Figure 1.10 - A) IVUS images of a RCA; B) Angiographic image from the same artery; C) 3D reconstruction [18]

1.7.2. QCA-3D

The CAAS QCA-3D is a software package developed by Pie Medical Imaging BV, Maastricht, The Netherlands, approved by the FDA. The QCA-3D is a 3D reconstruction method of coronary arteries, included in the CAAS package, which uses biplane angiographic images and assumes elliptical shaped cross sections [19].

The X-ray biplane angiograms are first recorded, and a single biplane set of end-diastolic frames is selected. Then the QCA-3D automated contour detection finds the lumen borders at both projections. From the luminal borders a centerline was determined. The 3D reconstruction algorithm reconstructs the vessel lumen in 3D by assuming elliptical cross sectional shape, using the recording geometry of the X-ray images, the centerline and the lumen borders [19].

1.7.3. Straight

This 3D reconstruction method merely consists of stacking multiple IVUS images upon a straight centerline, therefore taking out the influence of the vessel curvature while preserving the cross-sectional information. This method was created and first used in this thesis; therefore, there is no literature background about it.

Chapter 2. Aim

The main aim of this project was to investigate the influence of the 3D geometry of realistic human coronary arteries on the wall shear stress distribution and to develop methods to estimate the shear stress based on flow and geometrical parameters.

Therefore, the task was to verify what the relationship is between the wall SS calculated by the finite element modeling using the gold standard ANGUS geometries (Fig. 2.1 A) with the wall SS calculated from other simplified geometries. Firstly the SS calculated from the ANGUS geometries as compared to SS calculated by the Poiseuille equation (Fig. 2.1 D). The influence of blood flow in this relationship was also tested.

Then, wall SS results from the ANGUS geometries were compared with the SS results from a geometry obtained by QCA-3D method and by the Straight method. The Straight method provides cross sectional information (from IVUS) but lacks the curvature information (Fig. 2.1 C). The QCA-3D technique provides curvature information (from the biplane angiography), but lacks in cross sectional information (Fig. 2.1 B).

Furthermore, geometrical parameters that are thought to influence the wall shear stress locally were examined, such as the vessel local curvature, the lumen area and the gradient in lumen area.

At the present time the goal is to calculate shear stress on-site at the catheterization laboratory, so, in order to make these calculations practical, the calculation time should be as low as possible. The use of a simpler 3D reconstruction method would have a positive impact in the pursuit of this goal. Also, the calculation time depends on the number of elements in the mesh. Consequently was given some insight on how to optimize the finite element meshing, making it finer or coarser, by predicting the geometrical locations where large shear stress and large gradient in shear stress are expected.

3D Reconstructions

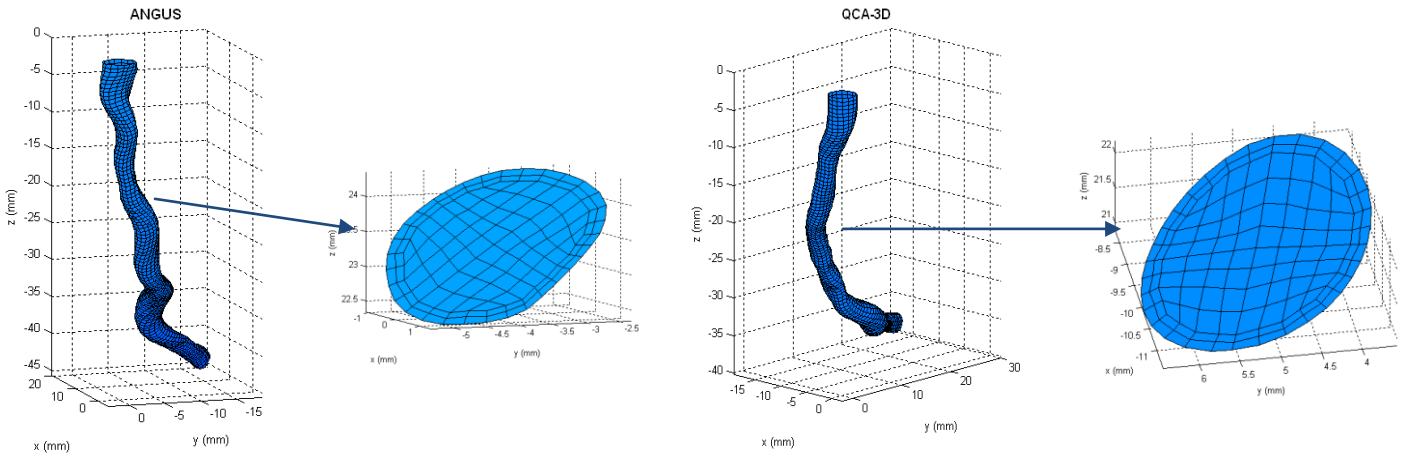

A **B**

ANGUS - IVUS + Angiography:

- Cross sectional information ✓
- Curvature information ✓

QCA-3D - Biplane Angiography:

- Cross sectional information ✘
- Curvature information ✓

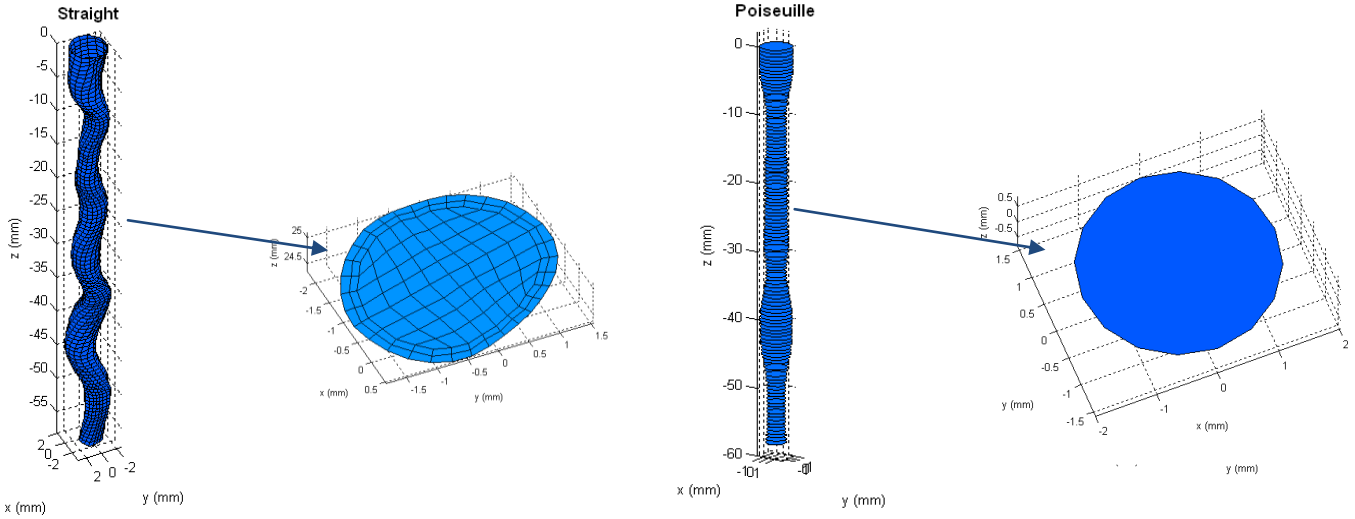

C **D**

Straight - IVUS:

- Cross sectional information ✓
- Curvature information ✘

Poiseuille - Cylindrical tube:

- Cross sectional information ✘
- Curvature information ✘

Figure 2.1 - ANGUS, QCA-3D, Straight and Poiseuille – 3D Reconstructions example and a corresponding cross-section from each method.

Chapter 3. Methods

Ten coronary arteries of ten different patients were analyzed. Three of those arteries were left circumflex arteries (LCX), two were left anterior descending arteries (LAD) and five of them were right coronary arteries (RCA).

The data for each artery was obtained by a 3D reconstruction technique, based on IVUS plus biplane angiography (ANGUS). This technique was described before in the Background chapter. Table 3.1 shows some geometrical information about the analyzed coronaries (such as the average lumen diameter, the range of diameters and the length of the segment) and some information about the blood flow (mean Reynolds number and the inlet flow rate).

Patient	Coronary Artery	Mean Reynolds Number	Inlet flow rate (ml/min)	Average lumen diameter (mm)	Range of diameter (mm)	Artery Length (mm)
p060028	LCX	269.8 ± 34.7	105.27	3.0 ± 0.4	2.5 - 3.7	68.8
p060065	RCA	172.7 ± 16.6	73.57	3.2 ± 0.3	2.5 - 3.8	79.6
p060125	RCA	200.6 ± 21.3	93.45	3.5 ± 0.4	2.8 - 4.3	66.7
p060204	LAD	350.1 ± 62.3	165.30	3.3 ± 0.6	2.5 - 4.6	59.8
p060233	LCX	332.9 ± 34.6	156.59	3.5 ± 0.4	2.9 - 4.3	47.7
p060362	RCA	210.0 ± 38.6	97.96	3.6 ± 0.6	2.4 - 4.5	71.3
p061104	LCX	279.7 ± 42.7	113.01	3.1 ± 0.4	2.3 - 3.8	49.4
p061150	LAD	331.8 ± 76.3	102.37	2.4 ± 0.6	1.4 - 3.7	80.8
p062128	RCA	294.4 ± 41.1	140.50	3.3 ± 0.4	2.3 - 4.0	56.9
p062143	RCA	297.7 ± 64.1	130.10	3.3 ± 0.5	1.7 - 3.9	58.3

Table 3.1 - Patients, corresponding coronaries and some geometric and flow features of the ANGUS reconstructed vessels

3.1. Computational Fluid Dynamics

Computational fluid dynamics (CFD) simulations were executed thereafter, to solve the Navier-Stokes equations (described in the Background chapter), which govern fluid motion.

Firstly, the discretization of the Navier-Stokes equations was executed by the finite elements method (FEM). The geometries of the vessels were subdivided into small cells (hexahedra) to form a mesh, by the finite element package Sepran (SEPRA Analysis, Den Haag, The Netherlands). An example of the meshing of one cross-section is shown in the left side of figure 3.1, while an example of the finite element mesh of an entire coronary artery segment is shown in the right side of figure 3.1.

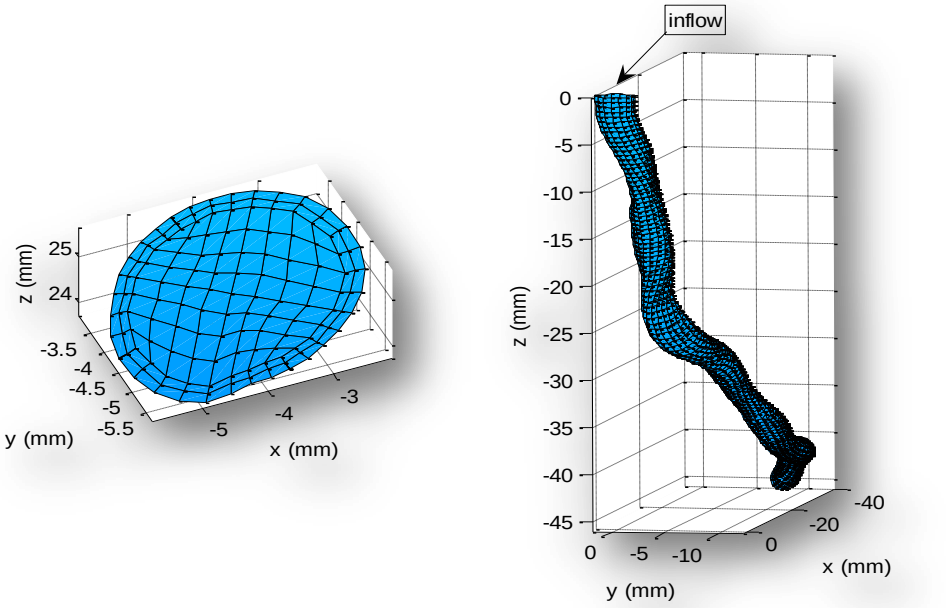

Figure 3.1 - Example of the finite element mesh of a coronary artery

Furthermore, in order to solve the Navier-Stokes equations (described in Chapter 1.Background), it is necessary to prescribe both initial and boundary conditions.

3.1.1. Assumptions and Boundary conditions

- No slip conditions at the walls: $\mathbf{u}(u_x,u_y,u_z)=0$;
- Rigid walls;
- Blood was modeled as an incompressible, homogenous and Newtonian;
- The prescribed inflow and pressure (in and out) – are presented below, at table 3.2.

Patients	Pressure (Pa)		Inflow rate (ml/min)			
	In	Out	Physiologic	50%	10%	1%
p060028	464.02	-0.89	105.27	52.64	10.53	1.05
p060065	251.82	-0.13	73.57	36.79	7.36	0.74
p060125	178.99	-0.35	93.45	46.73	9.35	0.93
p060204	747.62	-0.66	165.30	82.65	16.53	1.65
p060233	288.74	-1.42	156.59	78.30	15.66	1.57
p060362	287.97	-0.85	97.96	48.98	9.80	0.98
p061104	407.31	-1.67	113.01	56.51	11.30	1.13
p061150	2518.70	-7.83	102.37	51.19	10.24	1.02
p062128	322.42	-0.31	140.50	70.25	14.05	1.41
p062143	828.96	-0.26	130.10	65.05	13.01	1.30
Average	629.66 ± 697.00	-1.44 ± 2.30	117.81 ± 29.42	58.91 ± 14.71	11.78 ± 2.94	1.18 ± 0.29

Table 3.2 - Inflow rate and pressure (in and out) values for the CFD calculations

3.2. Analysis

CFD calculations were performed for the three different geometries, according to the ANGUS, QCA-3D and Straight 3D reconstruction method, of all ten vessels. The output files from the CFD calculations, which contained information of the local SS, flow velocity, pressure and geometry, were processed in MATLAB (Mathworks, Natick, USA). The analysis of the calculations outcomes is hereby described.

3.2.1. ANGUS vs. Poiseuille

Primarily, the relationship between the average SS per cross-section based on the CFD calculations and the lumen area were analyzed, and thereafter, the same relationship was investigated using the SS based on the Poiseuille equation. The average SS per cross section from the CFD calculations and the one based on Poiseuille were then compared.

The next step was to analyze the influence of blood flow in the relationships aforementioned. The input blood flow values in the CFD calculations were changed to 50%, 10% and 1% of the original (physiological) values, and new CFD calculations were executed. Average SS and Poiseuille based SS, of the four different blood flow values, were compared using regression analysis. In the Appendix is presented a table with the input blood flow values used in all the CFD calculation mentioned.

Furthermore, Bland-Altman statistics were performed. Bland-Altman is a statistical method that compares two measurement techniques [20]. In a Bland-Altman plot, the x-axis stands for the average of the two techniques and the y-axis stands for the difference between the two techniques. Horizontal lines were drawn at the mean difference and at the limits of agreement, which were defined as the mean difference plus or minus two times the standard deviation of the differences [21]. In this case, the mean difference in average SS per cross section represents the systematic error in average SS, and the regression line represents the proportional error between techniques, meaning the error dependant on the mean magnitude of the average SS.

In addition, a local wall SS histogram was built to visualize the local distribution of both SS from the ANGUS method and Poiseuille based SS[1].

Finally, the blood velocity profiles, from the four different blood flow values, were analyzed. These cross-sections were located in specific regions of interest. Two of them were located in a curved region and a highly stenotic region, respectively. For the sake of comparison, the third cross-section, which was located in a "normal" region (straight, and with low lumen area gradient), was analyzed.

All the results from these analyses are presented and described in Chapter 4.

3.2.2. ANGUS vs. Straight & ANGUS vs. QCA-3D

Since the analysis in these two chapters was similar, the methods used are here described together.

In the first place, average SS per cross section and Lumen area plots for both techniques were made, and compared. Then, the average SS from both methods were compared using regression analysis. The correlation coefficients and the slope and y-intercept values of the regression lines were registered.

Bland-Altman statistics and a local SS histogram, analogous to the ones previously described, were also performed for both chapters.

[1] Since the Poiseuille equation only provides one SS value per cross section, all the elements in the same cross section were given the same SS value.

The maximum SS value per cross section was also analysed, as well as the longitudinal SS (exclusively in Chapter4. ANGUS vs. Straight).

Furthermore, high and low SS analyses were performed. These analyses were performed per cross-section and per element (exclusively in Chapter 6 - ANGUS vs. Straight). The low SS analyses, per element, consisted of locating the low SS elements (<0.5 Pa) in both methods and calculate the percentage of elements that were coincident (i.e. at the same location). The high SS analyses, per element, consisted of locating the high SS elements in both methods and calculate the percentage of coincident/overlapping elements. A high SS element was considered when the SS was higher than the average SS per cross section plus the respective standard deviation (> $\bar{x} + \sigma$ Pa). A table with the threshold high SS values is presented in Chapter 5.

The high and low SS analyses per cross section were identical to the ones per element. However, in this case, a high/low SS cross-section was counted when it contained at least one element with high/low SS.

The sensitivity and specificity of the QCA-3D and Straight method when predicting high or low SS elements (or cross-sections), comparing to ANGUS were calculated. The sensitivity is a statistical measurement of the proportion of actual positives which are correctly identified as such (e.g. the percentage of low SS cross-sections determined by the QCA-3D or Straight method that are coincident with low SS cross-sections determined by the gold standard ANGUS method). The specificity measures the proportion of negatives which are correctly identified (e.g. the percentage of non-low SS cross-sections determined by the QCA-3D or Straight method that were also considered as non-low SS by the gold standard ANGUS method.

The following table exemplifies how sensitivity and specificity were measured for the calculation of low SS cross-sections. This procedure was analogous for the other cases.

		ANGUS		Total cross-sections
		<0.5 Pa	>0.5 Pa	
QCA-3D or Straight	<0.5 Pa	Overlapping cross-sections (B)	D - B	Low SS cross-sections from QCA-3D or Straight (D)
	>0.5 Pa	C - B	(A – D) – (C – B)	A - D
Total cross-sections		Low SS cross-sections from ANGUS (C)	A - C	Total cross-section of the vessel (A)
Sensitivity = B/C x 100%			Specificity = ((A – D) – (C – B))/(A – C) x 100%	

Table 3.3 – Measure of sensitivity and Specificity

The results from these analyses are presented and described in Chapter 5 and Chapter 6.

3.2.3. Influence of geometric parameters

In Chapter 7 some geometric factors that are thought to be significant in the SS calculations outcomes were analyzed. In the first place the lumen area gradient was studied, which was compared with the average SS per cross section gradient, the average SS and the local SS.

Additionally the curvature radius was analyzed, by comparing the curvature radius and the Dean number with the maximum SS per cross section, using a regression analysis.

As explained in section 3.2.1, the blood-flow was lowered to compare the average SS based on ANGUS method and the Poiseuille equation based SS. The lowering of the blood-flow reduces the presence of non-linearities in the average SS vs. lumen area relationship. However these non-linearities do not disappear completely. So, the presence of geometrical abnormalities in those specific regions was investigated.

In the end, according to the factors previously studied, some guidelines with the purpose of meshing optimization were formulated.

Chapter 4. ANGUS vs. Poiseuille

One of the aims of this chapter was to prove the inverse relation between average SS per cross section and the lumen area, by performing CFD calculations on 3D reconstructed geometries (from ANGUS) of real coronary arteries.

The main aim was to verify the relationship between the average wall SS calculated by the finite element modeling and SS calculated by the Poiseuille equation. Furthermore, the influences of blood flow in that relationship was tested.

In figure 4.1, below, is represented an example of a left anterior descending artery reconstructed by the ANGUS method (in the left) and a straight cylinder with the same cross sectional area as the ANGUS one, which resembles a Poiseuille tube. However, this tube has separated cross-sections, which means that adjacent cross-sections have no affect on each other.

Some geometrical and flow properties from the ten coronaries in study, reconstructed by the ANGUS method, is available in the methods chapter.

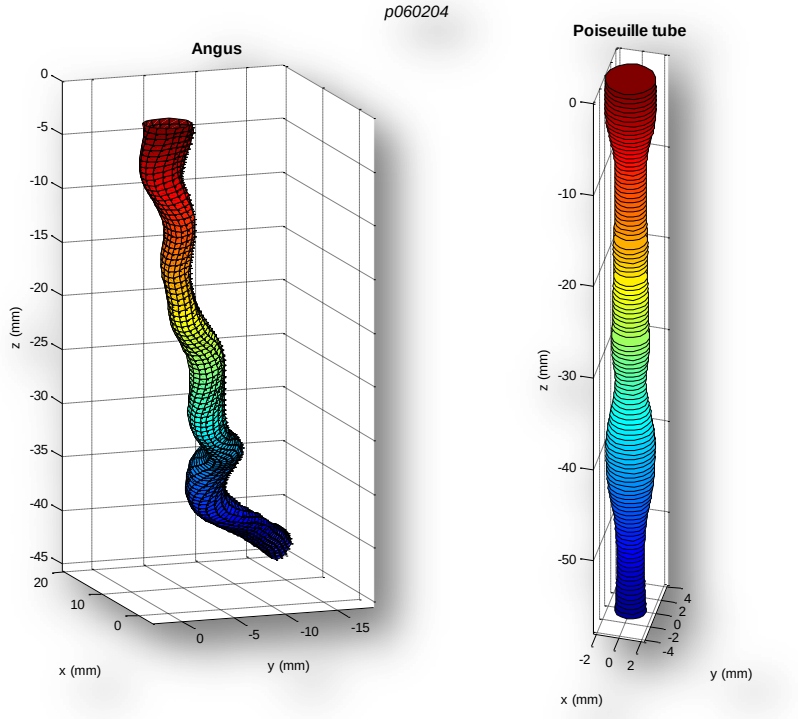

Figure 4.1 - 3D reconstruction of a left anterior descending artery by the ANGUS method (in the left) and a Poiseuille cylinder with the same cross sectional area

4.1. Results

4.1.1. Average shear stress vs. Lumen area

The first question was whether it is accurate to determine the average SS in a cross-section using the Poiseuille formula. Therefore, per cross-section, the average SS was calculated, and compared with the SS based on the Poiseuille equation.

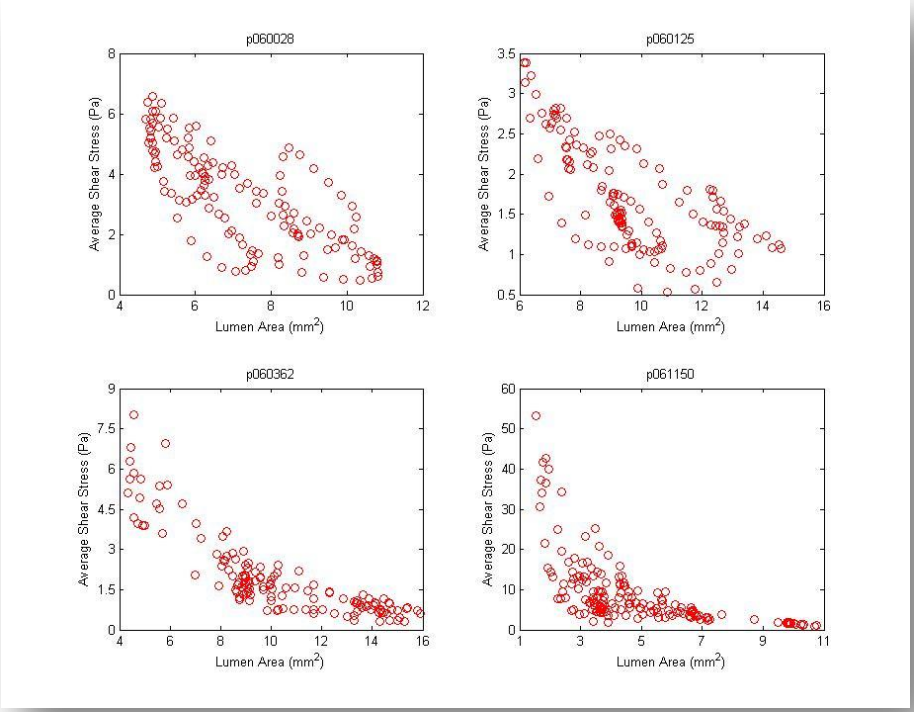

Figure 4.2 - Average SS vs. Lumen Area plots

Figure 4.2 shows the average SS vs. Lumen Area for four different arteries that were randomly picked from the 10 studied arteries. It can be seen that the ASS over a cross-section is inversely proportional to its area (see the bottom plots). Though, in some patients this relation is not as linear as expected, like in the upper plots, where the dots are more dispersed, and the inverse relationship is not so clear.

The following assignment was to calculate the average wall shear stress according to the Hagen-Poiseuille's equation: $\tau_s = \frac{4\mu Q}{\pi R^3}$, where τ_s is the shear stress (Pa), μ is the dynamic viscosity of the blood (mPa.s or cP), Q is the volume flow

(ml/min) and R is the cylindrical tube radius (m). The lumen radius was derived from the lumen area. In order to put all the variables in S.I. units, the following equation was used in MATLAB to calculate the shear stress: $\tau_s = \frac{4 \times \mu \times (Q/6000) \times 10^{-6}}{\pi \times R^3}$. The viscosity value used in this equation was 3.5 cP, which is an approximate value, because the blood viscosity can differ a lot, depending on the hematocrit, temperature and shear rate [22].

The Poiseuille SS values were plotted against the Lumen Area and then superimposed on the Average SS vs. Lumen Area plots (example of four randomly picked arteries is presented in figure 4.3).

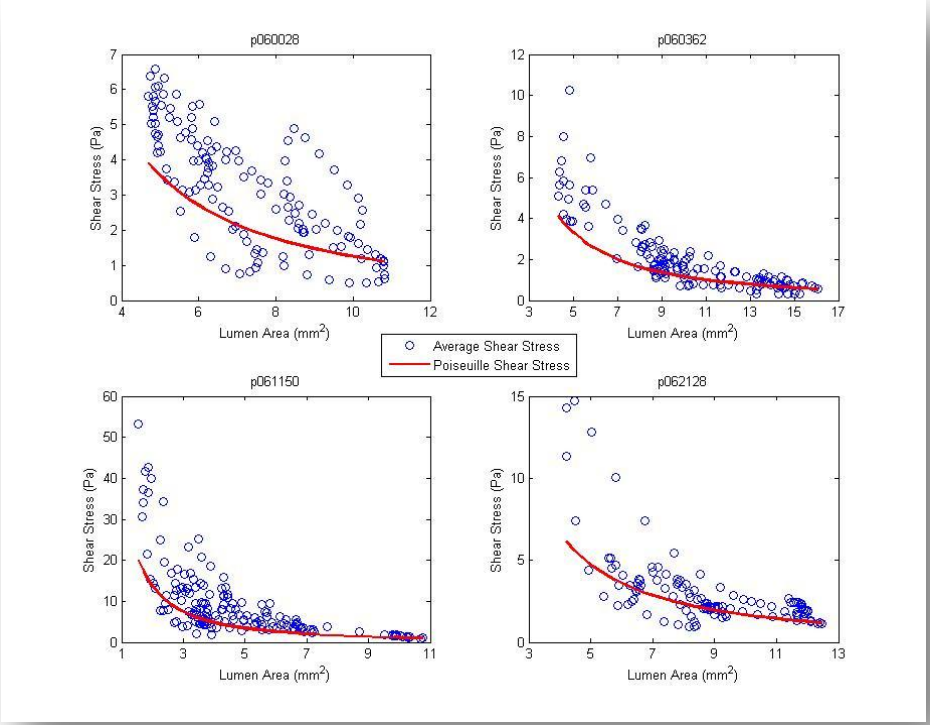

Figure 4.3 - Average SS vs. Lumen Area, based on the CFD calculations (O) and the Poiseuille formula (-)

The plots above represent the average wall SS over a cross section calculated by the finite element method (blue dots) and the wall shear stress calculated by the Poiseuille equation (red line). It is observed that the blue dots are hardly equal, and usually higher in value, to the SS values based on the Poiseuille equation. Hence, it is not very accurate to calculate the wall SS values using the Poiseuille equation. A

probable cause for this is the geometric variability of the coronary vessels, since the Poiseuille's law only describes the flow in straight cylindrical tubes. In the appendix, figure 11.1 displays analogous plots for all of the ten coronaries studied.

4.1.2. Influence of blood flow

The next question was how much the blood flow influences the relationship between average SS and the lumen area. In order to investigate that, the input blood flow rate values on the CFD simulations and in the Hagen-Poiseuille equation were changed to 50%, 10% and 1% of the physiological values. Subsequently new Average SS versus Lumen area plots were made.

By superimposing the Poiseuille based SS curve on these plots, the following plots (figure 4.4) were obtained, which permit the comparison between calculated average SS and Poiseuille SS for the different blood flows.

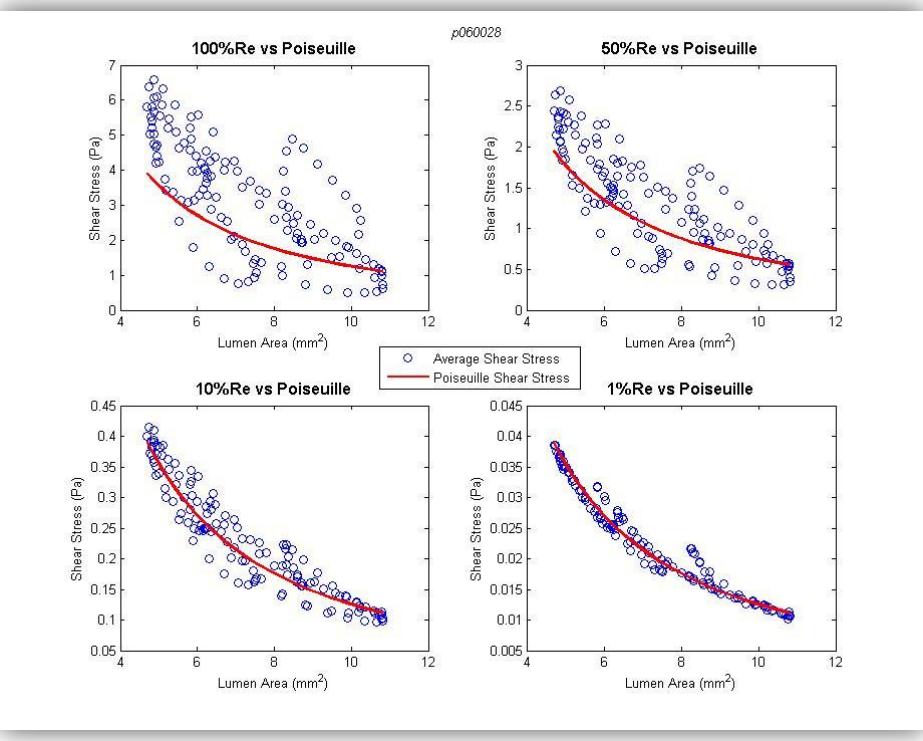

Figure 4.4 - Poiseuille shear stress versus Average shear stress – Influence of blood flow

The plot in the upper left side of the figure is the same that is shown at the same position in Figure 4.3. As said before, this plot represents the average wall SS over a cross section calculated by the finite element method (blue dots) and the wall

SS calculated by the Poiseuille equation (red line). By examining this plot it is seen that the Poiseuille equation cannot accurately predict the wall SS of realistic coronary arteries. However, when the blood flow rate is lowered (see the other three plots), the average SS resemble the ones based on Poiseuille formula. This may happen because when the flow rate is too low, geometric factors that can cause non-linearities, such as curvature, torsion, sinuosity, among others, have much less influence on the flow profile in the coronary arteries. However, even when the blood flow rate is lowered to 1% of its physiological value there are some dots that don't follow the Poiseuille based line. The reason for this deviation from the Poiseuille values will be discussed further in Chapter 7.

In addition, the Poiseuille SS was plotted versus the average SS based on CFD calculation, in a scatter plot, with the intention of deriving the correlation coefficient between them (figure 4.5).

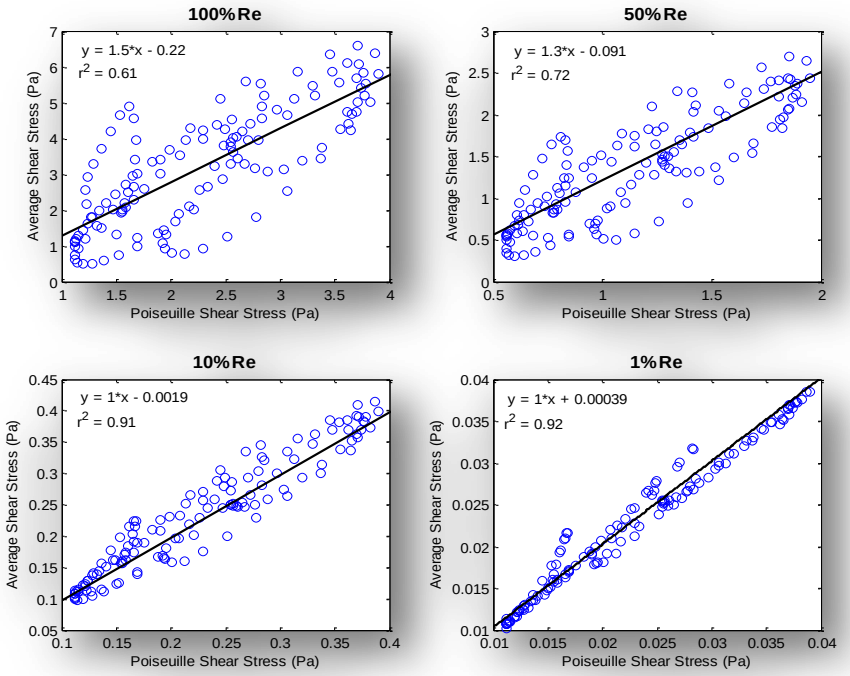

Figure 4.5 - Poiseuille and Average SS scatter plots for 100%, 50%, 10% and 1% of physiological blood flow

The correlation coefficient (r^2) between the average SS and the Poiseuille SS is presented in the table 4.1, below. A table with the regression line parameters is available in the appendix (table 11.2).

	Correlation coefficients (r^2)			
Patient	100%Re	50%Re	10%Re	1%Re
p060028	0.61	0.72	0.91	0.92
p060065	0.59	0.68	0.80	0.83
p060125	0.61	0.76	0.93	0.94
p060204	0.52	0.61	0.86	0.94
p060233	0.67	0.74	0.86	0.86
p060362	0.80	0.84	0.93	0.95
p061104	0.61	0.71	0.90	0.94
p061150	0.68	0.73	0.90	0.97
p062128	0.61	0.67	0.88	0.98
p062143	0.81	0.89	0.90	0.99
Average	0.65 ± 0.09	0.74 ± 0.08	0.89 ± 0.04	0.93 ± 0.05

Table 4.1 - Correlation coefficients (r^2)

Table 4.1 showed that, for every patient, the correlation between the average SS and the Poiseuille based SS was increasing as the flow rate, or the Reynolds number, became lower. The average r^2 for the 100% Reynolds number was 0.65 ± 0.09 and for the 1% Reynolds number was 0.93 ± 0.05, which was a significantly different. The average r^2 for the different blood flows was also presented in figure 4.6 as a bar plot.

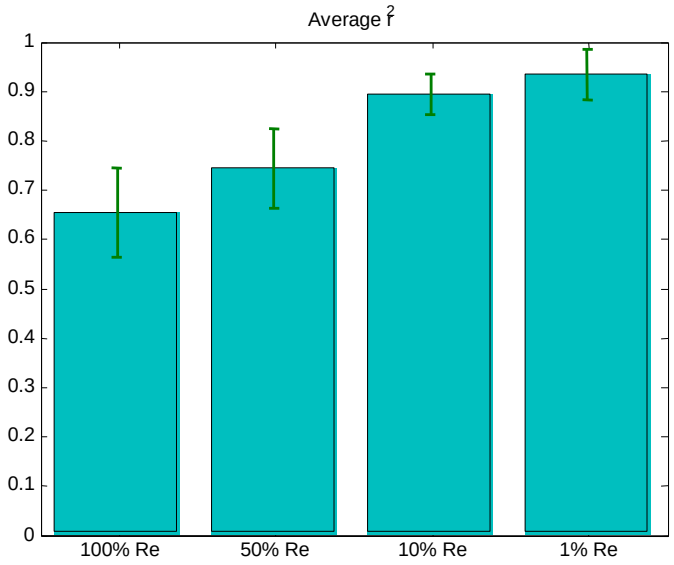

Figure 4.6 - Average r^2 – Average SS vs. Poiseuille SS

4.1.3. Bland-Altman analysis

Bland-Altman analysis was also performed to provide another type of comparison between the Poiseuille SS and the average SS from the ANGUS

geometries, for the four different blood-flow percentages (100, 50, 10 and 1% of physiological level). The Bland-Altman plot for the physiological Reynolds number is presented next (figure 4.7).

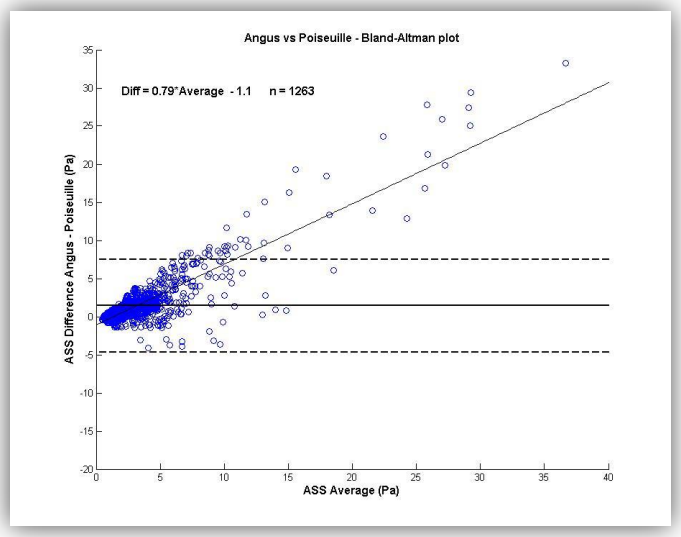

Figure 4.7 - Bland-Altman plot (ANGUS vs Poiseuille)

The Bland-Altman analysis reveals that for all patients, and for 100% of the physiological Reynolds number the average shear stress calculated from Poiseuille underestimates the SS calculated from the CFD (from ANGUS) systematically by 1.43 $\pm$ 3.05 Pa, which is a significant error. The proportional error was also noteworthy (Difference in SS = 0.79 x Average SS – 1.1), which means that the difference between methods gets larger as the average increases.

Reynolds Number	Mean Difference ANGUS – Poiseuille (Pa)	$Difference = a \times Average + b$	
		a	b
100%	1.43 ± 3.05	0.79	-1.10
50%	0.32 ± 0.99	0.55	-0.43
10%	0.13 ± 0.088	0.23	-0.044
1%	$7.65 \times 10^{-4} \pm 0.0047$	0.12	-0.0022

Table 4.2 - Bland-Altman statistic results

In table 4.2 was presented the results of Bland-Altman statistics, and, as expected, the systematic error got significantly lower (almost zero). Besides, the slope of the regression line, which represents the proportional error, also decreased from 0.79 (at 100% Reynolds number) to 0.12 (at 1% Reynolds number); this means that the magnitude of the averages had less influence in the measurements.

4.1.4. Local wall shear stress histogram

A local wall SS histogram was built (figure 4.8), to compare the local wall SS of ANGUS with the SS calculated from the Poiseuille equation. Bars were created at 0.25 Pa intervals, resulting into 120 bars, in this case. The values from the ten patients studied were included in the same histogram. A limitation of this analysis is that it does not provide any information of the location of the SS values in the vessel. Therefore geometrical information is lost.

The Poiseuille equation seems to give SS values lower than the SS derived from the ANGUS method, since the number of elements at their peaks (both located at relatively low SS values) is much higher for Poiseuille than for the ANGUS method. The peak is situated in the 1 to 1.25 Pa interval, with 1693 elements in that wall SS interval. While the Poiseuille peak is situated in the 1.25 to 1.5 Pa interval and has 4046 elements in that interval.

Taking in consideration that SS with values between 0 and 0.5 Pa is low SS and SS with values >1.5 Pa is physiological shear stress and SS higher than the mean SS plus one standard deviation ($\bar{x}+\sigma$ = 3.88 + 5.50 Pa = 9.38 Pa) is high SS; for the ANGUS vessels, the number of elements with low SS represent 7% of the total number of elements, while 57% of the elements show physiological SS and 8% of the elements exhibit high SS. For the Poiseuille based SS, there were no elements with low SS (<0.5 Pa), while the elements with physiological SS represent 64% of the total number of elements and only 2% of the elements had high SS values.

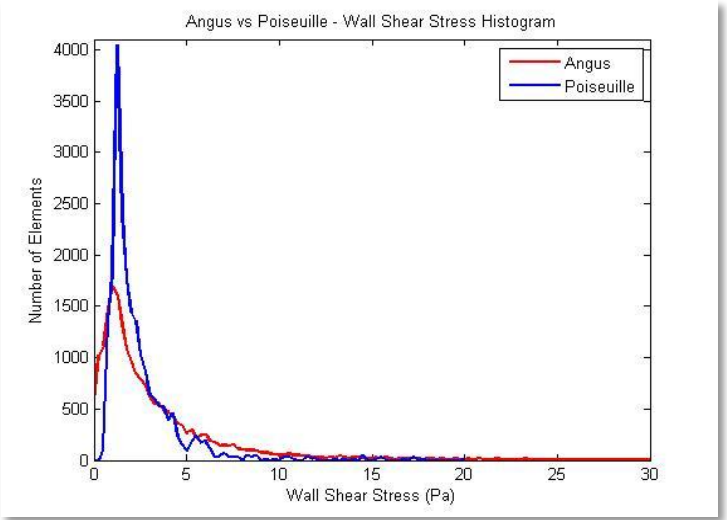

Figure 4.8 - Local Wall SS Histogram

4.1.5. Velocity profiles

At some regions, with physiologic blood flow rate, the velocity profile per cross-section exhibits an asymmetric distribution, which provokes asymmetric wall shear stress. The patterns also demonstrate that the blood flow at physiological levels is not Poiseuille like (parabolic distribution). However at low blood flow levels (10 and 1% of physiological) the velocity profile is parabolic. This, in combination to what is seen at the lower two plots in figure 4.4, demonstrates that by lowering blood flow, the calculated wall shear stresses are almost equal to the SS values based on the Poiseuille formula.

Figure 4.9 represents a cross section that has a relatively large lumen area and is located at a curved region of the artery. Consequently, the velocity profile (at physiological and 50% Reynolds number) is asymmetric. The blood velocity is higher near the outer side of the curvature and is lower at the inner side. However, at 10% and 1% of the physiological Reynolds number, the velocity profile is reasonably close to parabolic.

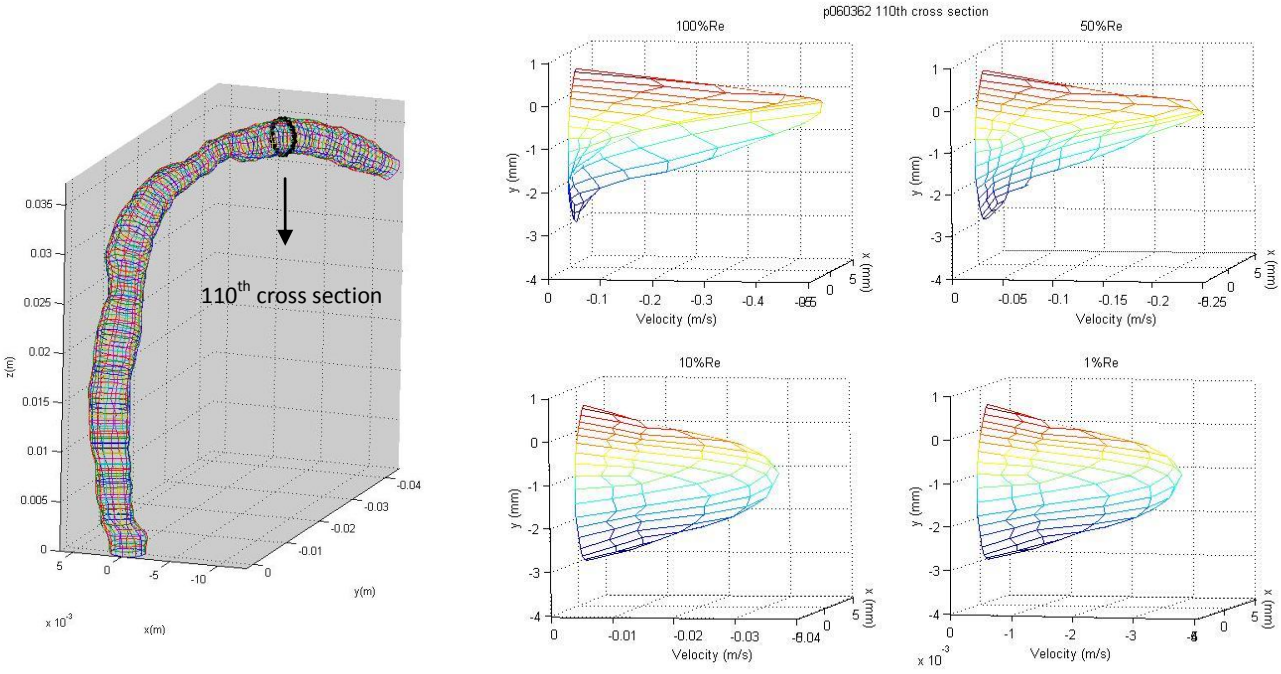

Figure 4.9 - Velocity profiles for different blood flows (100%, 50%, 10% and 1%) for a cross section located in a curved region

Furthermore, at some regions of the vessel where the lumen is narrowed, it is observed that with physiological blood flow, the velocity profile is flattened. This implicates that the wall SS at these sites is much higher than the corresponding SS values based on Poiseuille parabolic flow. Figure 4.10 shows a cross section with a small lumen area, which is located in a region where the lumen is gradually narrowing. Therefore the velocity profile at physiological and 50% flow rate is flattened, since the flow is probably turbulent. On the other hand at 10% and 1% flow rate, the velocity profile is parabolic, as expected.

In addition, the table below presents, for the same cross section illustrated in figure 4.10, the average SS from the CFD calculations, the Poiseuille SS and their ratio. As seen in the table below, the difference between the average SS and the Poiseuille SS, for 100% Reynolds number is 121% of the Poiseuille SS, while, for 1% Reynolds number, it is only 7%. These values corroborate the fact that when the average SS is much higher than the Poiseuille SS, the velocity profile in that cross section is flattened. On the other side, when the average SS is similar to the Poiseuille SS, the velocity profile is obviously parabolic.

	Average SS from CFD calculations (Pa)	Poiseuille SS (Pa)	(Average SS – Poiseuille SS) / Poiseuille SS
100% Re	6.28	2.84	121%
50% Re	2.47	1.42	74%
10% Re	0.35	0.28	25%
1% Re	0.030	0.028	7%

Table 4.3 - Average SS from CFD calculations and Poiseuille SS for the 57th cross section of patient p060233. Re is an abbreviation for Reynolds number

Figure 4.11, below, shows the velocity profiles of a cross section in a region of the vessel that is straight and has nearly constant radius. In this case, it is observed that, even for physiological blood flow, the velocity profile is parabolic. This particular cross section was chosen to serve as antagonism to the previous two examples, because its average SS (for 100% Reynolds number) is almost the same as the Poiseuille based SS (3.43 Pa ≈ 3.37 Pa).

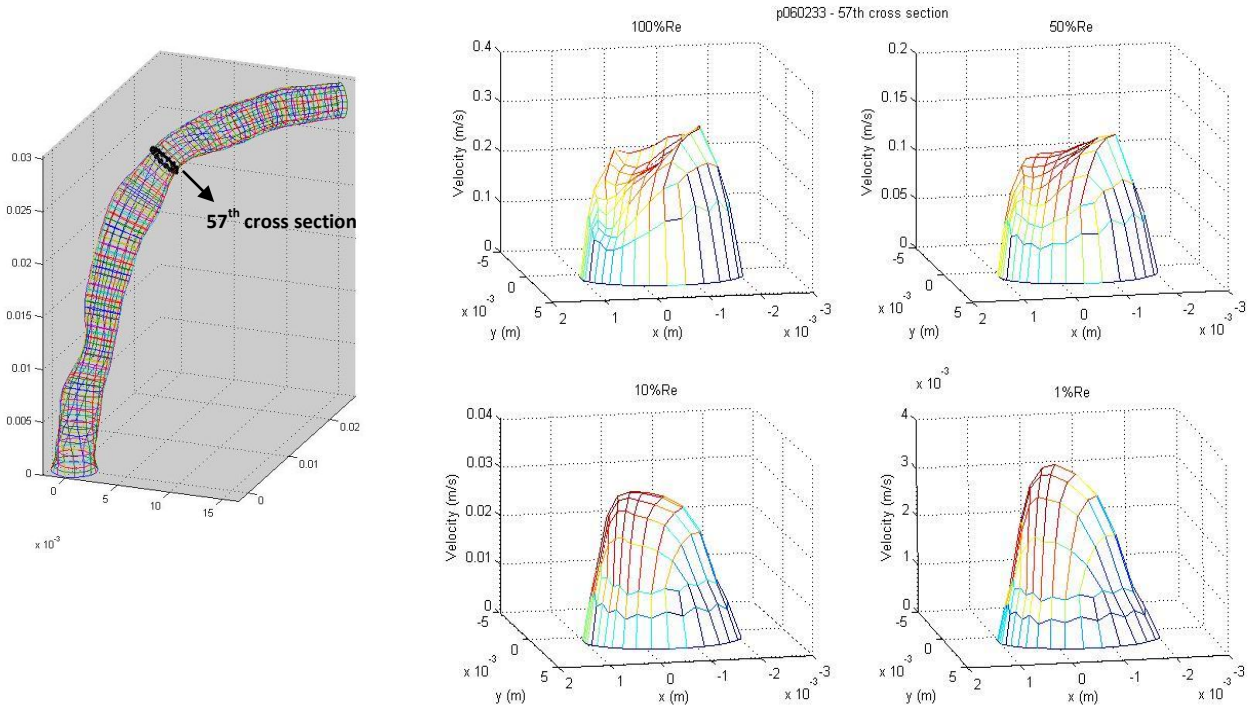

Figure 4.10 - Velocity profiles for different blood flows (100%, 50%, 10% and 1%) for a stenotic cross section

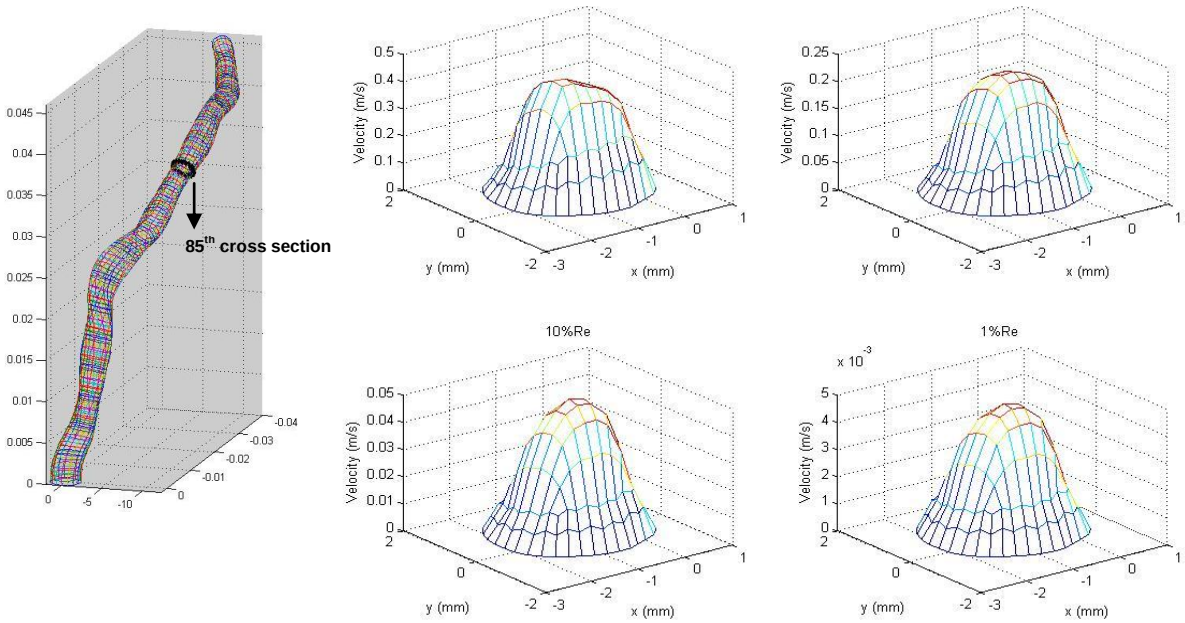

Figure 4.11 - Velocity profiles for different blood flows (100%, 50%, 10% and 1%) for a "normal" cross section

Chapter 5. ANGUS vs. QCA-3D

The ANGUS technique, as described before, is a 3D reconstruction technique based on the fusion of intravascular ultrasound (IVUS) and angiography, which provide cross sectional and curvature information of the coronary arteries, respectively. The QCA-3D is only based on multi planar angiography, so it only provides accurate curvature information, lacking the exact cross sectional information.

Therefore, the main aim of this chapter is to compare the SS based on the QCA-3D reconstruction method with the SS based on ANGUS, and see how much these differences between both methods influence the SS calculations outcome. So, the CFD calculations described in the Methods chapter were repeated using the data from the 3D reconstructions based on QCA-3D from the same vessel segments. The CFD calculations made with the meshing from the QCA-3D method were performed using analogous conditions used for the meshes from the ANGUS method, for each similar vessel.

Some geometrical and flow properties from the ten coronaries in study, reconstructed by the ANGUS method, is presented in the methods section. A similar table (11.3) for the QCA-3D method is available in the Appendix. An example of a coronary artery reconstructed by both these techniques is shown in figure 5.1, located below.

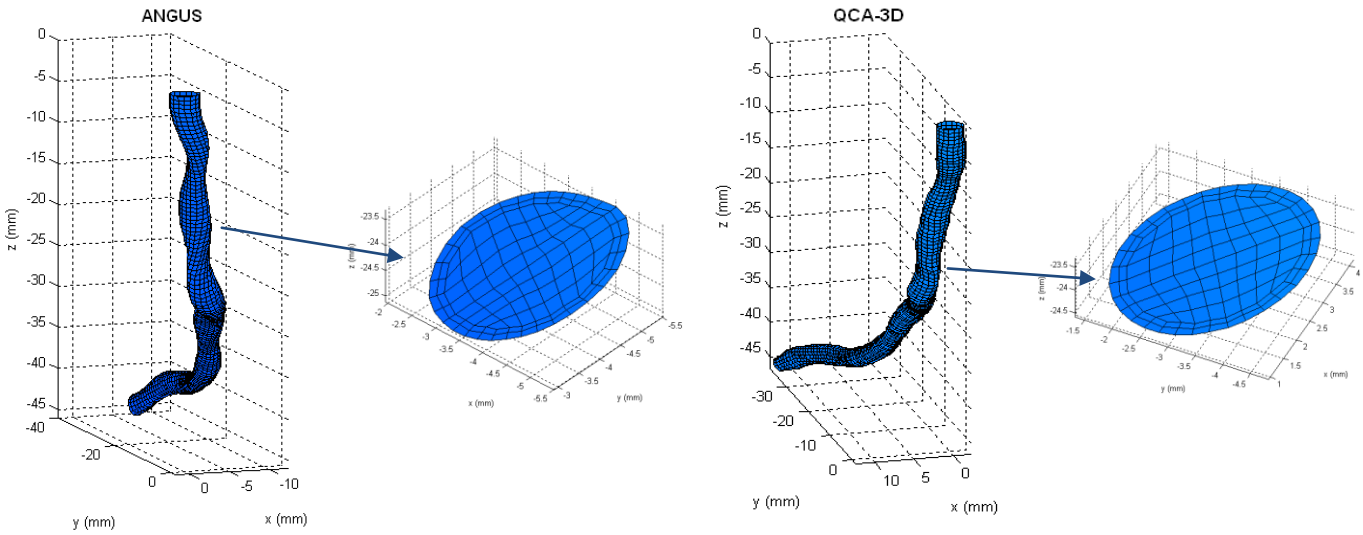

Figure 5.1 - 3D reconstructions of a left anterior descending artery by the ANGUS (in the left) and the QCA-3D techniques

5.1. Results

5.1.1. Average shear stress and lumen area

In figure 5.2 are presented the Average SS vs. Lumen area plots based on the SS calculations from ANGUS (blue dots) superimposed with the corresponding plots from QCA-3D (green dots). By looking only to the figure below, no considerable difference can be seen in the relationship between SS and Lumen Area for both techniques, since the range of SS values and its distribution along the lumen area values is similar for all the coronaries in study.

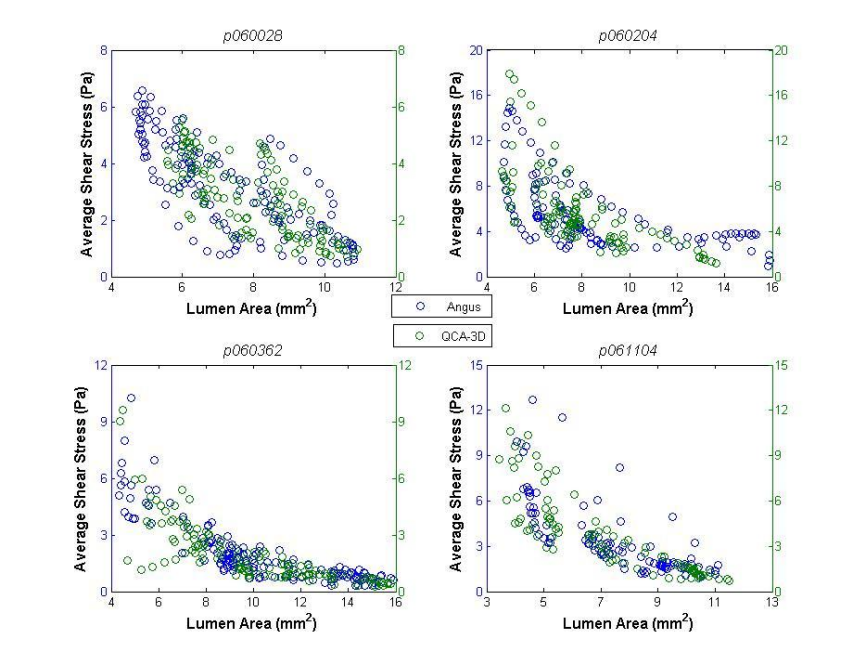

Figure 5.2 - Average SS vs Lumen Area plots from ANGUS (o) and QCA-3D (o)

The figure 5.3, presented below, shows an example of the lumen area and average SS distribution along the length of the vessel segment for both techniques (both left plots). The plots at the right show the correlation of the lumen area values and average SS from both techniques. The lumen area is shown to have a strong correlation coefficient (r^2 = 0.90) and the slope of the regression line is 0.99. The correlation in the average SS values is only moderate (r^2 = 0.55), but the slope of the regression line is 1.1, close to the expected.

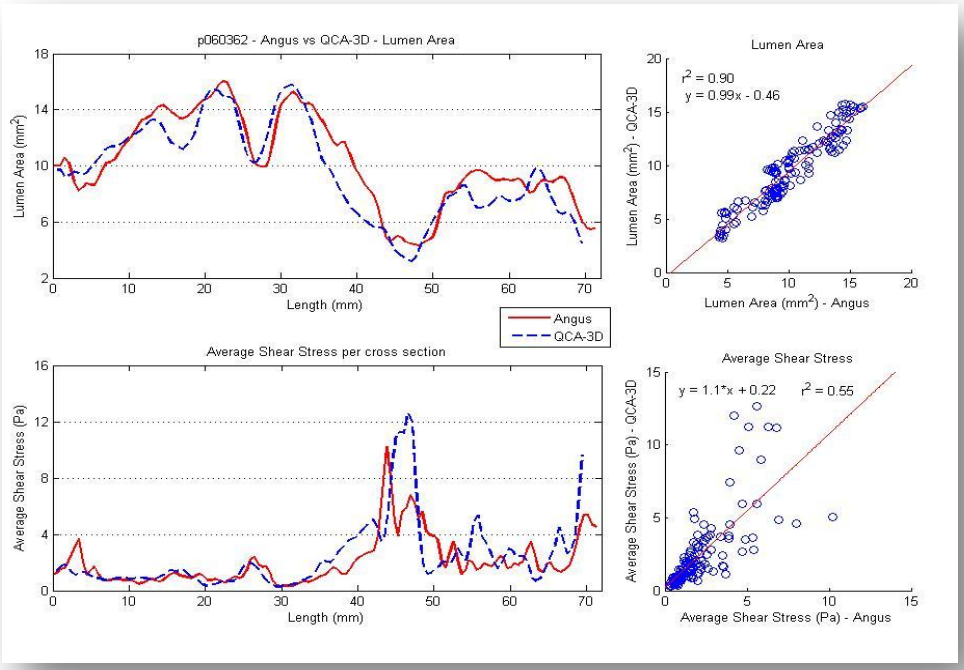

Figure 5.3 - Lumen area and average SS per cross section from ANGUS and QCA-3D

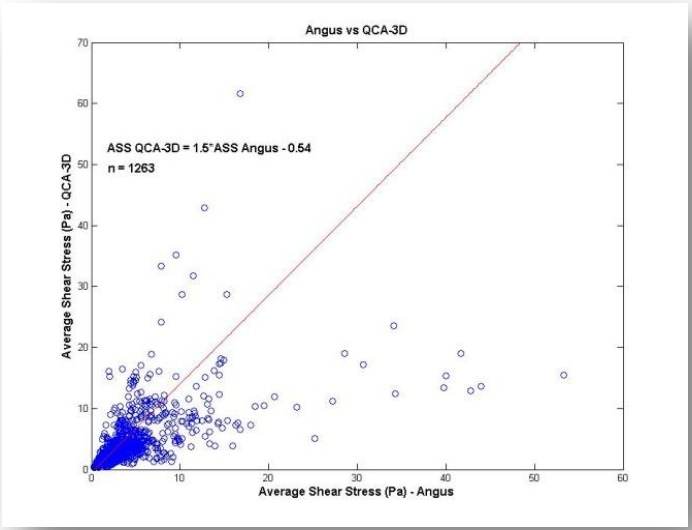

Figure 5.4 - Correlation between Average SS from ANGUS and QCA-3D

The correlation coefficients (r^2) and the linear regression equation from the correlation between the Average Shear stress from ANGUS and QCA-3D (figure 5.4) for all the patients are presented on the table 5.1. The average correlation coefficient is 0.40 $\pm$ 0.20 Pa, which suggests a low correlation. The average slope value (a) is 0.84 $\pm$ 0.45, which includes the optimal value (1) within the confidence interval. The average y-intercept value (b) is 1.12 $\pm$ 0.93, which was higher than the optimal value

(0), revealing that the QCA-3D shear stress values overestimated the ANGUS ones. In the last row of the table are also presented the correlation values if using the data from all the vessels together, instead of averaging them. This type of information will be present in further tables of this report.

Patient	r^2 Values	Linear Regression equation QCA-3D = a × ANGUS + b	
		a – slope	b – y-intercept
p060028	0.26	0.68	0.91
p060065	0.091	0.19	1.40
p060125	0.44	0.81	0.54
p060204	0.54	0.79	1.50
p060233	0.50	1.30	0.059
p060362	0.55	1.10	0.22
p061104	0.50	0.94	0.73
p061150	0.047	1.70	3.30
p062128	0.36	0.46	1.60
p062143	0.66	0.39	0.95
Average	0.40 ± 0.20	0.84 ± 0.45	1.12 ± 0.93
All	0.073	1.50	-0.54

Table 5.1 - Average Shear Stress correlation parameters

5.1.2. Bland-Altman Analysis

In order to provide another comparison between both techniques, the Bland-Altman analysis was included. Figure 5.5 represents the Bland-Altman plot of the average shear stress per cross section.

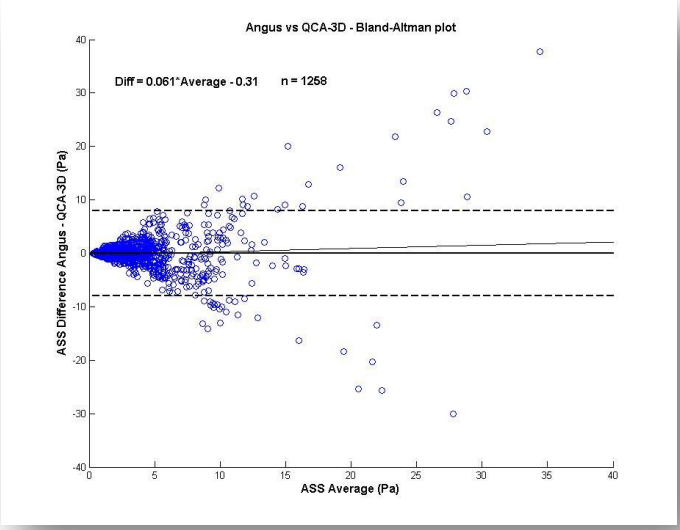

Figure 5.5 - Bland-Altman plot of the average SS per cross section

The Bland-Altman analysis reveals that the average shear stress from the QCA-3D is overestimated systematically by 0.077 ± 3.96 Pa. This value shows that the average of all differences is almost zero; however it is of less value due to its high standard deviation. The proportional error was also very small (Difference in SS = 0.061 x Average SS – 0.31). However it can be seen in the plot that the differences got larger as the averages increased.

5.1.3. Maximum Shear Stress

In figure 5.6 is presented an example of the comparison between ANGUS and QCA-3D of the lumen area, average SS and Maximum SS per cross-section along the length of a vessel. Furthermore, in table 5.2 are presented the correlation coefficient (r^2), and the linear regression parameters of the scattering between the maximum SS per cross-section calculated from the ANGUS and QCA-3D geometries.

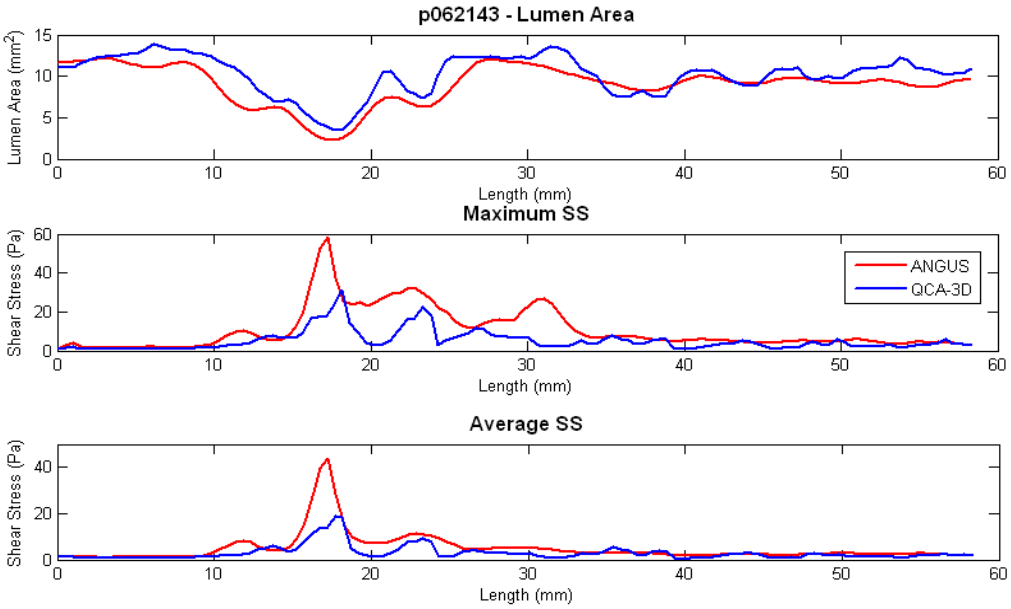

Figure 5.6 - Lumen Area, Maximum and Average SS per cross section – ANGUS vs QCA-3D (example)

Patient	Maximum SS		
	r^2 Value	$y = ax + b$	
		a - slope	b - y-intercept
P060028	0.32	0.75	1.40
P060065	0.01	0.042	2.70
P060125	0.08	0.41	1.90
P060204	0.41	0.71	2.8
P060233	0.37	1.40	0.20
P060362	0.48	0.73	0.92
P061104	0.46	0.67	1.90
P061150	0.23	0.78	3.10
P062128	0.32	0.41	2.50
P062143	0.52	0.35	1.50
Average	0.32 ± 0.17	0.63 ± 0.36	1.89 ± 0.91

Table 5.2 - Correlation coefficients (r^2) for the Maximum SS per cross section

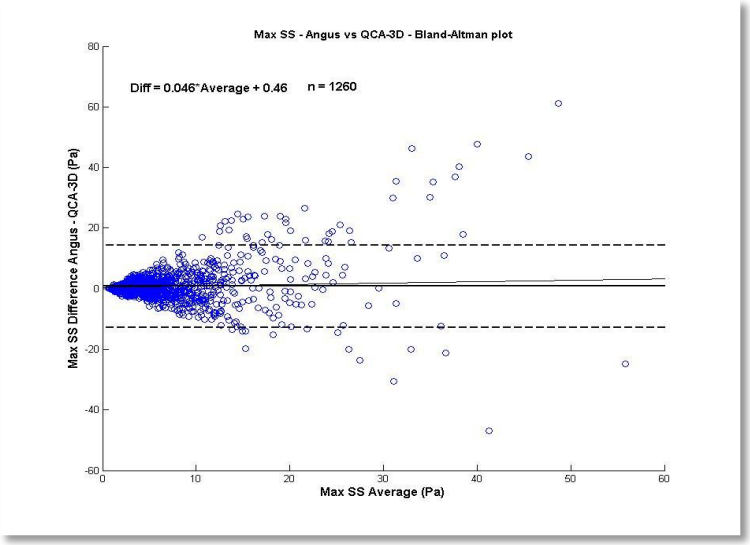

Figure 5.7 - Bland-Altman plot – Maximum SS per cross section

By analyzing the Bland-Altman plot for the maximum SS it can be seen that the QCA-3D method underestimates the maximum SS per cross section by 0.78 ± 6.78 Pa (very high standard deviation) in relation to ANGUS. The proportional error was determined by the following equation: Difference = 0.046*Average + 0.46. The slope value (0.046) is very close to the one expected (0).

5.1.4. Local wall shear stress histogram

A local wall SS histogram was built (figure 5.6), with the purpose of comparing the local wall SS of both techniques. Bars were created at 0.25 Pa intervals, resulting into 80 bars, in this case.

The ANGUS and the QCA-3D histograms were very similar. Both of the peaks are situated in the 1.25 to 1.5 Pa interval. The ANGUS vessels have 1657 elements in that wall shear stress interval, while the QCA-3D ones have 1612 elements in that same interval.

Assuming that SS with values between 0 and 0.5 Pa is considered low SS, SS with values >1.5 Pa is considered physiological SS and SS > $\bar{x} + \sigma$ = 3.88 + 5.50 Pa = 9.38 Pa is high SS; for the ANGUS vessels, the number of elements with low SS represent 7% of the total number of elements, while 57% of the elements show physiological SS and 8% of the elements exhibit high SS. For the QCA-3D vessels, the elements with low SS represent 6% of the total number of elements; while the elements with physiological SS represent 58.5% of the total number of elements and 9.5% of the elements have high SS values.

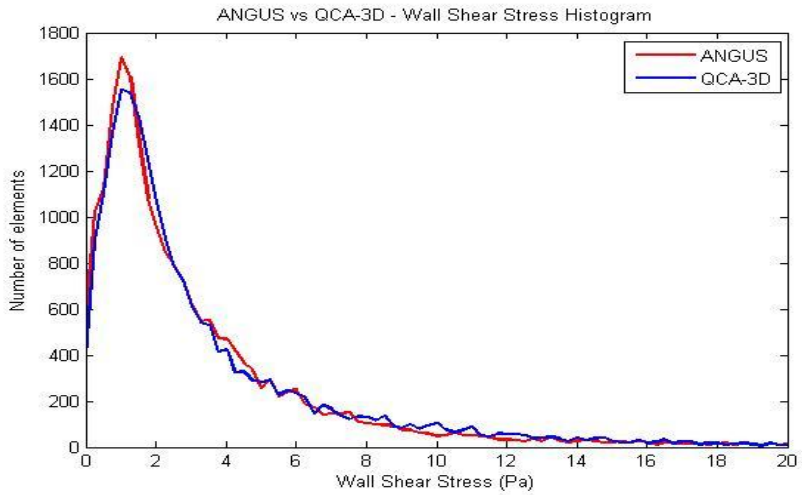

Figure 5.8 - Local wall SS histogram (ANGUS vs QCA-3D)

5.1.5. Low SS Analysis

Patients	Number of cross sections with low SS (<0.5 Pa)			Sensitivity	Specificity
	ANGUS	QCA-3D	Overlapping		
P060028	18	26	10	56%	86%
P060065	65	29	21	32%	91%
P060125	40	41	35	88%	94%
P060204	21	9	6	29%	97%
P060233	32	22	21	66%	98%
P060362	79	68	62	78%	90%
P061104	13	12	7	54%	94%
P061150	44	26	17	39%	92%
P062128	36	23	17	47%	93%
P062143	39	39	29	74%	87%
All	387	295	225	58%	92%
Average	39 ± 21	30 ± 17	23 ± 17	$56 \pm 20\%$	$92 \pm 4\%$

Table 5.3 – Cross-sections with low SS (<0.5 Pa) by ANGUS and QCA-3D method

In table 5.2 was presented an analysis of the number of cross-sections with low SS (<0.5 Pa) for the ANGUS and the QCA-3D method, as well as the percentage of those cross sections that are coincident (sensitivity) and the specificity. The total number of cross-sections analyzed was 1263.

This analysis showed that the sensitivity of the QCA-3D method to predict cross-sections with low SS comparing to ANGUS is 58% (225 out of 387 cross-sections). The average sensitivity is 56 $\pm$ 20%. The specificity of the QCA-3D method in determining cross-sections with low SS comparing to ANGUS is 92%.

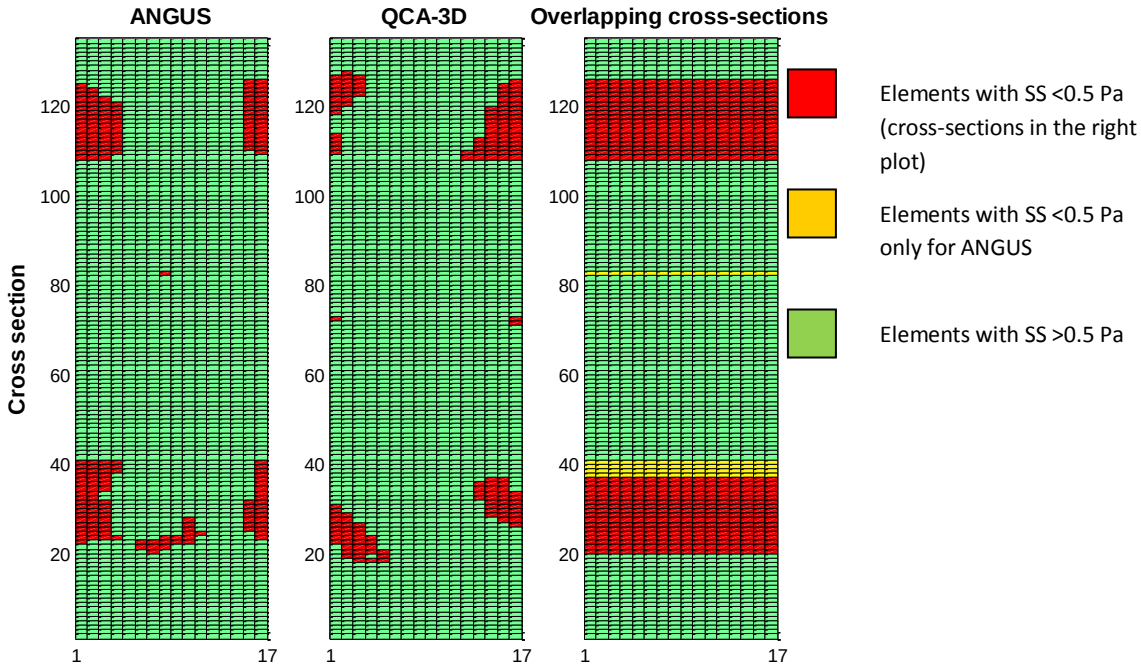

Figure 5.9 - Example of a vessel with low SS elements (<0.5 Pa) for the ANGUS, the QCA-3D method and the overlapping cross-sections.

In figure 5.9, above, is shown a randomly picked example of the distribution of the low SS elements for both techniques (left and center plot) and the overlapping cross-sections with low SS. The green squares represent the elements with SS superior to 0.5 Pa. The red squares, in the left and center plot, represent the elements with SS lower than 0.5 Pa, while in the right plot they represent the elements with low SS (<0.5 Pa) that are predicted by both techniques. The yellow squares, only present in the right plot, represent the cross-sections with low SS elements from ANGUS that are not determined by QCA-3D. The sensitivity is calculated dividing the number of red cross-sections by the number of yellow and red

cross-sections. In this case, the sensitivity of the QCA-3D in determining low SS cross-sections is of 88%.

5.1.6. High SS Analysis

In this analysis, high SS was defined as all values above the mean SS for each vessel plus one standard deviation (from the ANGUS calculations outcome). So high SS is > $\bar{x}+\sigma$ Pa. The total number of cross-sections analyzed was 1263. In table 5.3, below, is presented the mean SS, standard deviation and the sum of both, for the ten coronaries studied.

Patients	Mean SS (Pa)	Standard deviation (Pa)	$\bar{x}+\sigma$ (Pa)
P060028	3.20	2.00	5.20
P060065	1.78	1.49	3.27
P060125	1.69	0.89	2.59
P060204	5.40	3.93	9.32
P060233	3.16	1.85	5.01
P060362	2.04	2.22	4.26
P061104	3.46	2.85	6.31
P061150	9.16	10.57	19.73
P062128	3.05	2.91	5.95
P062143	4.99	7.36	12.35

Table 5.4 – High SS threshold for each patient.

The number of cross-sections with high SS, for the ANGUS, the QCA-3D method and the percentage of coincident cross-sections with high SS, were presented below in table 5.5. It shows that 58% of the QCA-3D cross-sections with high SS were coincident with the ANGUS cross-sections with high SS (155 out of 261 cross-sections). The average percentage of overlapping high SS cross-sections per patient was 58 $\pm$ 20%. The specificity of the QCA-3D method in predicting cross-sections with high SS relatively to ANGUS is 78%.

In figure 5.10, below, is shown a randomly picked example (patient p060233) of the distribution of the high SS elements for both techniques (left and center plot) and the overlapping cross-sections with high SS. The green squares represent the elements with SS inferior to 5.01 Pa (see table 5.4 for the value). The red squares, in the left and center plot, represent the elements with SS higher than 5.01 Pa, while in the right plot they represent the elements with high SS (>5.01 Pa) that are predicted by both techniques. The yellow squares, only present in the right plot, represent the cross-sections with high SS elements from ANGUS that are not determined by QCA-

3D. The sensitivity is calculated dividing the number of red cross-sections by the number of yellow and red cross-sections. In this case, the sensitivity of the QCA-3D in determining high SS cross-sections is of 87%.

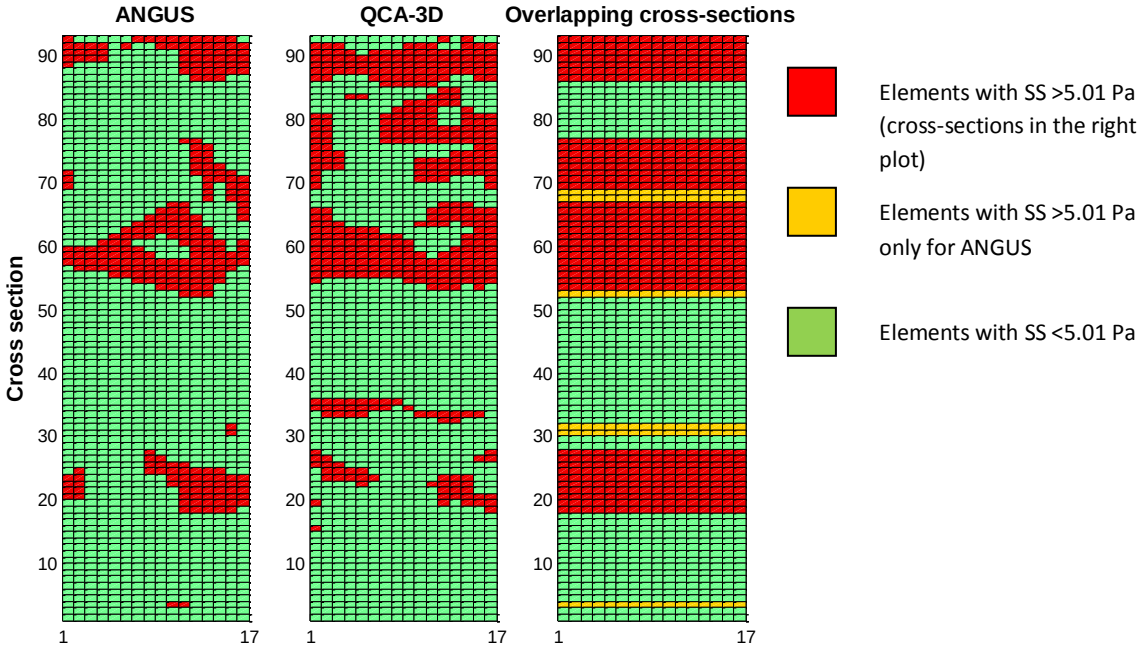

Figure 5.10 - Example of a vessel with high SS elements (in this case <5.01 Pa) for the ANGUS, the QCA-3D method and the overlapping cross-sections.

Patients	Number of cross sections with high SS (> $\bar{x}+\sigma$ Pa)			-	
	ANGUS	QCA-3D	Overlapping	Sensitivity	Specificity
P060028	68	61	47	69%	79%
P060065	60	43	20	33%	76%
P060125	84	84	58	69%	49%
P060204	59	56	30	51%	55%
P060233	46	54	40	87%	70%
P060362	52	50	37	71%	85%
P061104	26	32	20	77%	83%
P061150	50	42	21	42%	81%
P062128	40	34	19	48%	80%
P062143	34	10	10	29%	100%
All	519	466	302	58%	78%
Average	52 ± 17	47 ± 20	30 ± 15	$58 \pm 20\%$	$76 \pm 15\%$

Table 5.5 - Percentage of cross sections with high SS (> $\bar{x}+\sigma$ Pa) in the ANGUS and QCA-3D method

Chapter 6. ANGUS vs. Straight

Stacking up the cross-sections obtained by IVUS, on a straight centerline, a 3D reconstruction of the artery, leaving out the curvature, is created. This way, it is eliminated the vessel curvature influence in the SS calculations outcomes.

Consequently, the aim of this chapter was to verify if the curvature of the coronary arteries has an important influence in the final outcome of the SS calculations. In order to accomplish that, originally curved vessels from ANGUS were compared with the corresponding straight vessels.

Some geometrical and flow properties from the ten coronaries in study, reconstructed by the ANGUS method, is presented in the methods section. A similar table for the Straight method is available in the Appendix (table 11.4). In figure 6.1 an example of the 3D reconstruction of a coronary artery was presented; namely, a left anterior descending artery, using the ANGUS method (in the left) and using the Straight method (in the right).

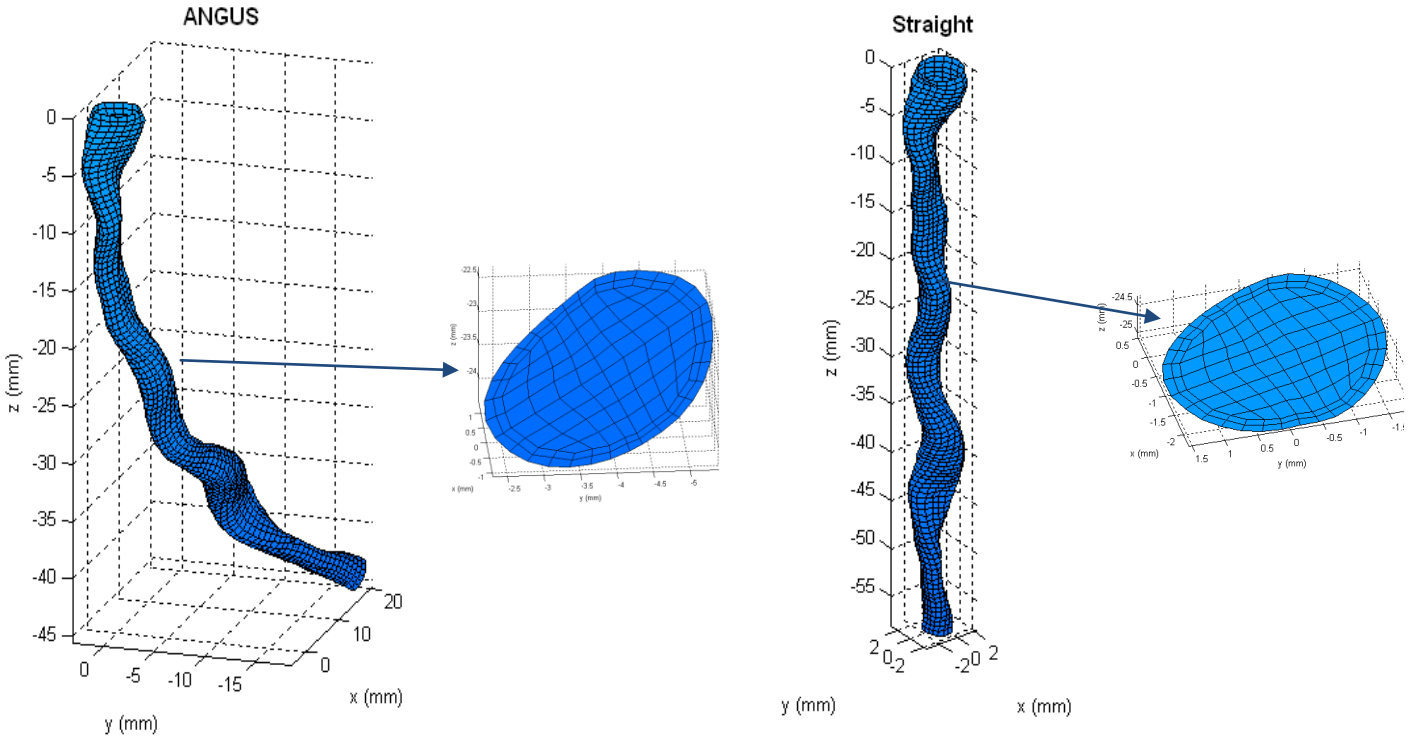

Figure 6.1 - 3D reconstruction of the curved ANGUS vessel (left) and from the corresponding straight vessel (right)

6.1. Results

As described in the Methods chapter, CFD simulations were performed on the straight meshes to calculate the SS on its walls. A randomly picked example of the local wall SS distribution, in both straight and normal arteries, was presented in figure 6.2.

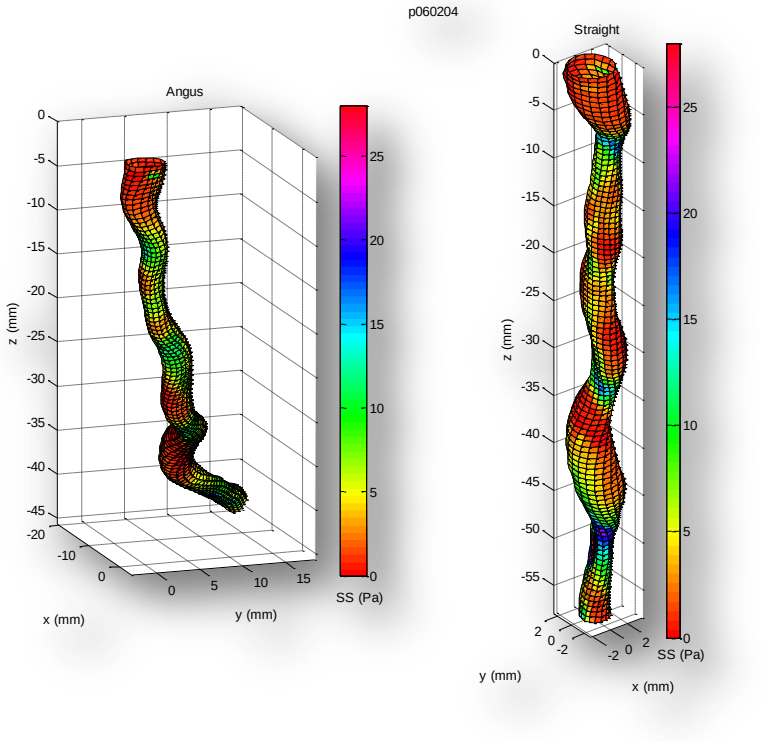

Figure 6.2 - 3D view of the local wall SS distribution in both ANGUS original vessel and in the straight vessel

6.1.1. Average shear stress and lumen area

Figures 6.3 and 6.4 show the relation between the lumen area (top left plot) and the relation between the average SS per cross section (bottom left plot) for ANGUS and Straight vessels. The plots in the right side of the figures present the correlation of the average SS per cross section between ANGUS and Straight vessels.

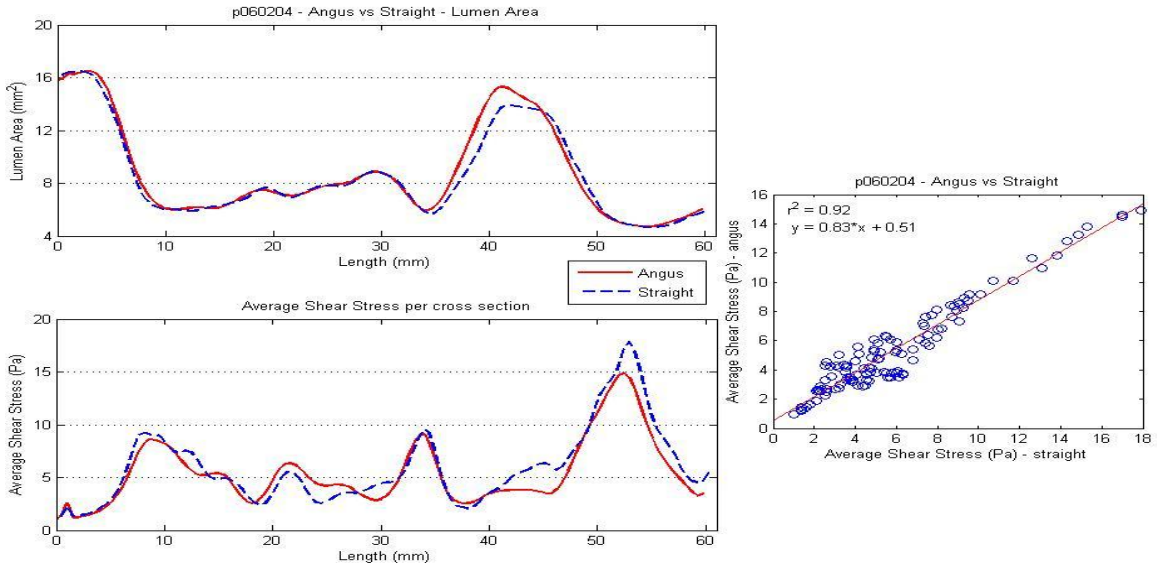

Figure 6.3 - Lumen Area and Average SS comparison between ANGUS and Straight vessels

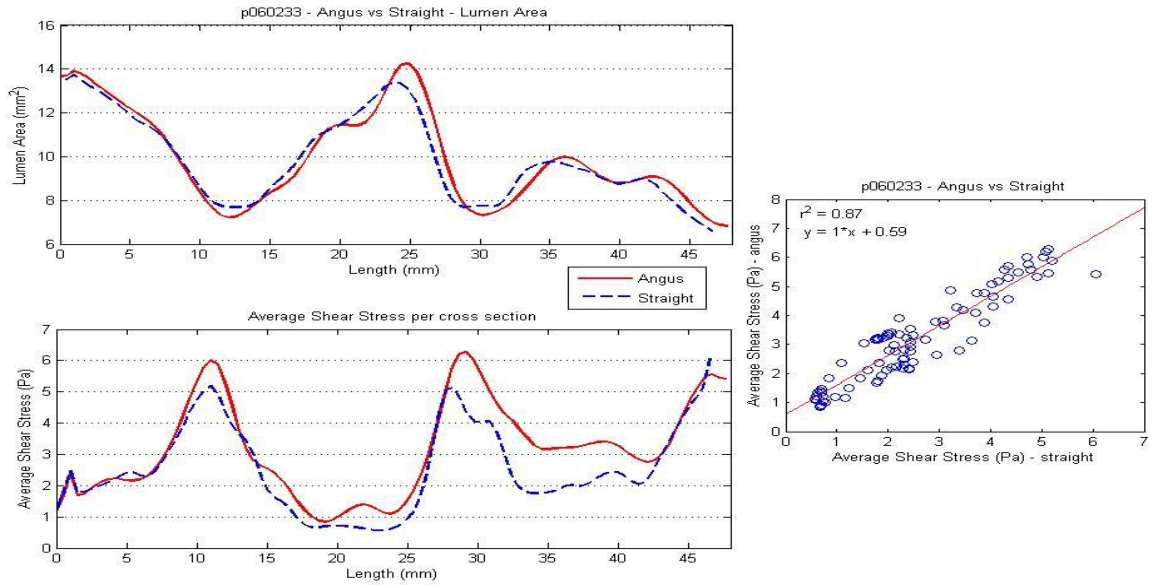

Figure 6.4 - Lumen Area and Average SS comparison between ANGUS and Straight vessels

In both figure 6.3 and 6.4 it is observed that the average SS per cross section at ANGUS and the Straight vessel are very much alike. This is confirmed by the strong correlation seen in the scatter plots (r^2 = 0.92 and 0.87). If we perform this analysis for all patients, we found an average r^2 value of 0.79 $\pm$ 0.11, and although it is smaller than the ones presented, it is still a high correlation coefficient (see table 6.1).

Consequently, only considering the average SS per cross section, it can be said that the results from the SS based on the ANGUS method and from the Straight vessel are fairly similar.

However, by analyzing the maximum SS per cross section and the average longitudinal shear stress from both techniques, some significant differences were found, which are presented further in this chapter.

Patient	Average SS			Maximum SS		
	r^2 Value	$y = ax + b$		r^2 Value	$y = ax + b$	
		a - slope	b - y-intercept		a - slope	b - y-intercept
P060028	0.58	0.62	1.30	0.55	0.65	1.70
P060065	0.66	1.20	0.12	0.56	1.80	-0.61
P060125	0.79	0.81	0.59	0.45	0.64	1.60
P060204	0.92	0.83	0.51	0.69	0.65	2.30
P060233	0.86	1.00	0.59	0.74	0.92	1.50
P060362	0.81	1.00	0.43	0.66	1.40	1.00
P061104	0.83	1.20	0.12	0.67	1.60	-0.23
P061150	0.76	1.20	1.40	0.66	1.50	4.20
P062128	0.90	1.10	0.24	0.74	1.00	1.30
P062143	0.83	1.30	1.00	0.42	1.20	4.60
Average	0.79 ± 0.11	1.03 ± 0.22	0.63 ± 0.46	0.61 ± 0.11	1.14 ± 0.43	1.74 ± 1.66

Table 6.1 - Correlation coefficients (r^2) for the Average and Maximum SS per cross section

6.1.2. Bland-Altman Analysis

As in the two previous chapters, a Bland-Altman analysis was performed on the average SS per cross section. The Bland-Altman plot is shown in figure 6.5.

The Bland-Altman analysis reveals that the average SS from the Straight vessels underestimated systematically the one from ANGUS by 0.76 ± 2.24 Pa. The proportional error was defined by the following equation: Difference in SS = 0.29 x Average SS – 0.25. A slope of 0.29 means that the differences between techniques got slightly larger as the averages increased.

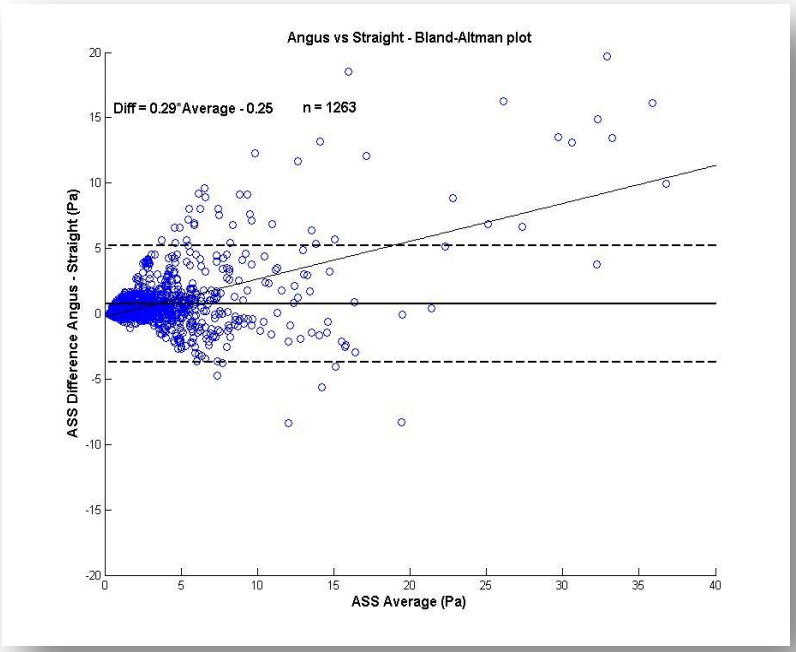

Figure 6.5 - Bland-Altman plot of the average SS per cross section for all patients

In table 6.2 are presented the systematic error (mean SS difference between techniques) and the proportional error (represented by the equation Difference = a*Average + b) for all the ten patients individually.

Patient	Systematic error	Proportional error (Difference = a*Average + b)	
	Mean SS Difference (Pa)	a	b
P060028	0.061 ± 1.32	-0.21	0.74
P060065	0.34 ± 0.58	0.39	-0.29
P060125	0.34 ± 0.32	-0.095	0.48
P060204	-0.52 ± 1.06	-0.15	0.35
P060233	0.63 ± 0.55	0.092	0.37
P060362	0.50 ± 0.74	0.16	0.22
P061104	0.56 ± 1.05	0.31	-0.43
P061150	2.77 ± 4.59	0.35	0.036
P062128	0.41 ± 0.74	0.11	0.092
P062143	2.04 ± 3.04	0.40	0.46
All	0.76 ± 2.24	0.29	-0.25
Average	0.71 ± 0.97	0.14 ± 0.23	0.20 ± 0.36

Table 6.2 - Bland-Altman analysis results for all patients individually

6.1.3. Maximum shear stress

In figure 6.6 an example is given of the comparison between the lumen area, the average SS per cross section and the maximum SS per cross section, between ANGUS and the Straight method. Figure 6.7 shows an example (the same vessel presented in figure 6.6) of the local wall SS for both ANGUS and Straight vessels, while figure 6.8 shows the 3D view of the same local wall SS distribution.

Analyzing figure 6.6 shows that the lumen area and the average SS per cross section of ANGUS and the Straight vessel, are, again, very much similar. However, by looking at the maximum SS, there are some visible differences. The average r^2 for the maximum SS per cross section is lower than the one for the average SS, suggesting a weaker correlation (table 6.1). For the ANGUS reconstructed vessel there are maximum SS peaks from 40th cross section to 50th and from 60th to 70th cross section, that don't occur for the Straight vessel. This information is confirmed by figure 6.7, in particular by the blue areas (high SS locations) around the 45th and the 60th cross sections. Finally, when analyzing figure 6.8, it becomes obvious that the differences in shear stress at these locations are due to the curvature in the original ANGUS vessel, and are located, as expected, at the outer side of the curvature.

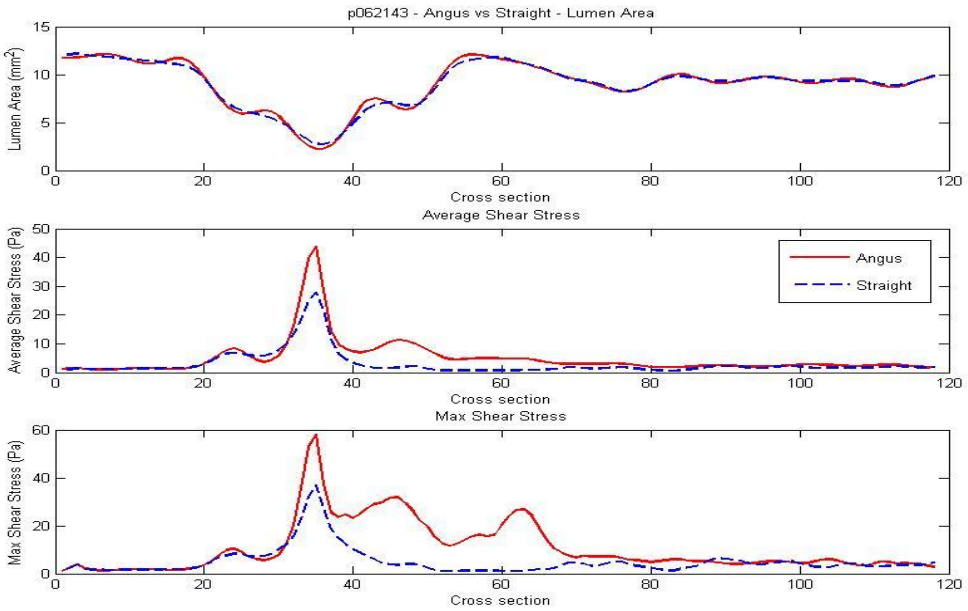

Figure 6.6 - Lumen Area, Average SS and Maximum SS per cross section comparisons, between ANGUS and Straight vessels

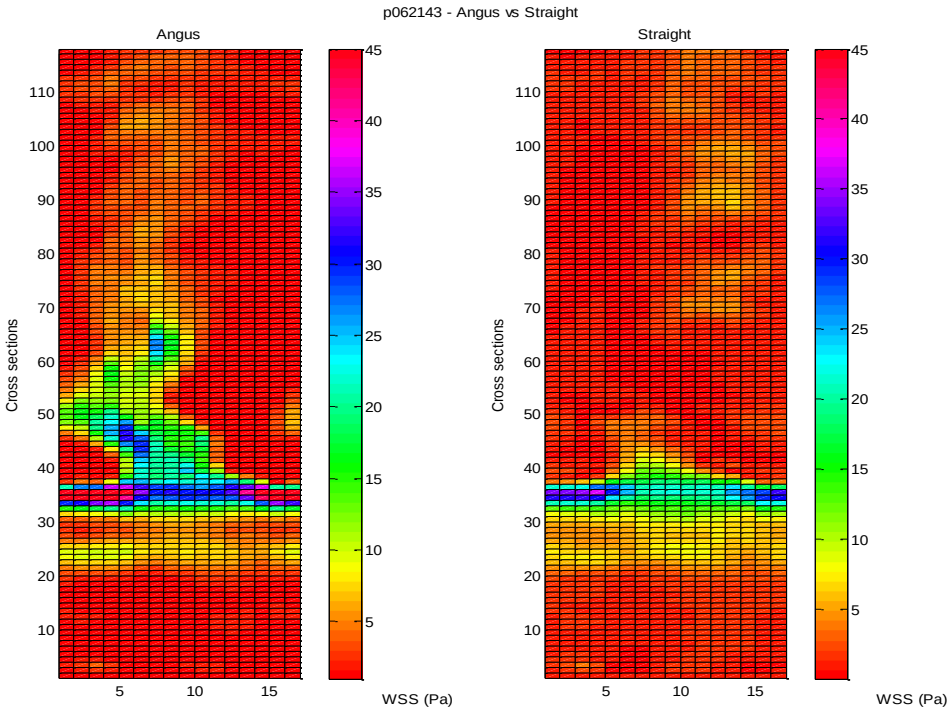

Figure 6.7 - Wall SS distribution of an ANGUS and a Straight geometry

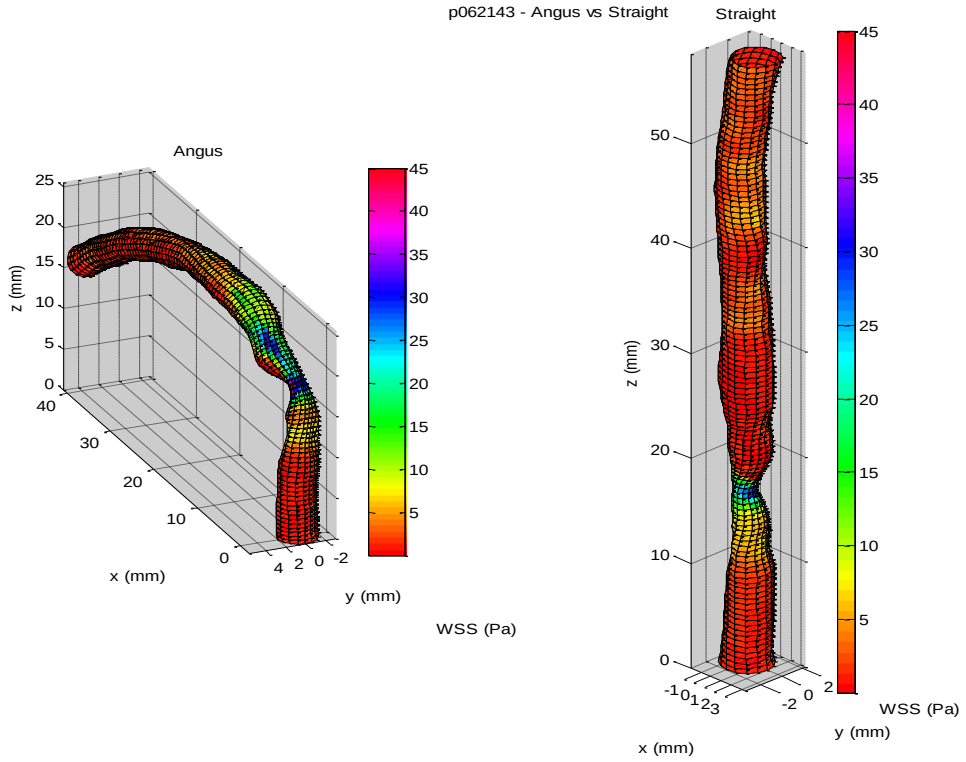

Figure 6.8 - 3D view of the SS distribution in the reconstructed ANGUS and Straight vessels

6.1.5. Local wall shear stress histogram

A wall SS histogram was built (figure 6.12) with the purpose of comparing the local wall SS taken from the ANGUS and the Straight vessels. Each point in the plot represents a 0.25 Pa interval.

Figure 6.12 shows that the ANGUS and the Straight histograms were identical. Both of their peaks are situated in the 1 to 1.25 Pa interval. The ANGUS vessels have 1693 elements in that wall SS, while the Straight ones have 1952 elements in the same gap.

Having in consideration that SS with values between 0 and 0.5 Pa is low SS, SS with values >1.5 Pa is physiological SS and SS > $\bar{x} + \sigma$ = 3.88 + 5.50 Pa = 9.38 Pa is high SS; for the ANGUS vessels, the number of elements with low SS represent 7% of the total number of elements, while 57% of the elements show physiological SS and 8% of the elements exhibit high SS. For the Straight vessels, the elements with low SS represent 9.5% of the total number of elements, while the elements with physiological SS represent 51.5% of the total number of elements and 5.5% of the elements have high SS values.

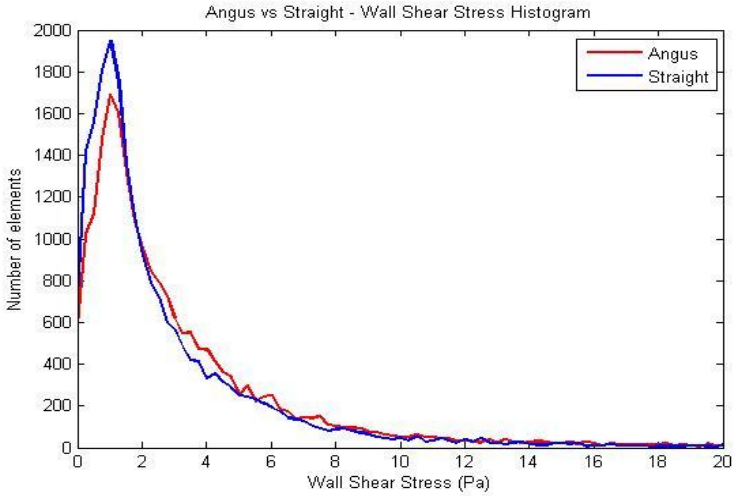

Figure 6.9 - Wall shear stress histogram (Angus vs Straight)

6.1.6. Low SS Analysis

Patients	Number of elements with low SS (<0.5 Pa)			Sensitivity	Specificity
	ANGUS	Straight	Overlapping		
P060028	77	104	44	57%	97%
P060065	209	246	84	40%	93%
P060125	228	405	193	85%	90%
P060204	49	61	29	59%	98%
P060233	102	122	53	52%	95%
P060362	463	539	373	81%	91%
P061104	55	69	24	44%	97%
P061150	102	158	49	48%	96%
P062128	135	119	47	35%	96%
P062143	117	212	16	14%	90%
All	1537	2035	912	59%	94%
Average	154 ± 124	204 ± 156	91 ± 111	$52 \pm 21\%$	$94 \pm 3\%$

Table 6.3 - Percentage of elements with low SS (<0.5 Pa) in the ANGUS and Straight method

In table 6.3 is presented an analysis of the number of elements with low SS (<0.5 Pa) for the ANGUS and the Straight method, as well as the percentage of those elements that are coincident by both methods. The total number of elements in study was 21471.

The result of this analysis, for all patients, revealed that the sensitivity was 59%. This means that 59% of the number of elements from the Straight method with low SS (912 out of 1537 elements) was coincident with the low SS elements from the ANGUS method. The average sensitivity of the Straight method to predict low SS elements per patient was $52 \pm 21\%$.

In figure 6.10, below, is shown an example of the distribution of the low SS elements for both techniques (left and center plot) and the overlap of them. The green squares represent the elements with SS superior to 0.5 Pa. The red squares, in the left and center plot, represent the elements with SS lower than 0.5 Pa, while in the right plot they represent the elements with low SS (<0.5 Pa) that are coincident in both techniques. The yellow squares, only present in the right plot, represent the low SS elements from the ANGUS method that were not predicted by the Straight method. In this example, the sensitivity of the Straight method of predicting low SS elements was of 81%.

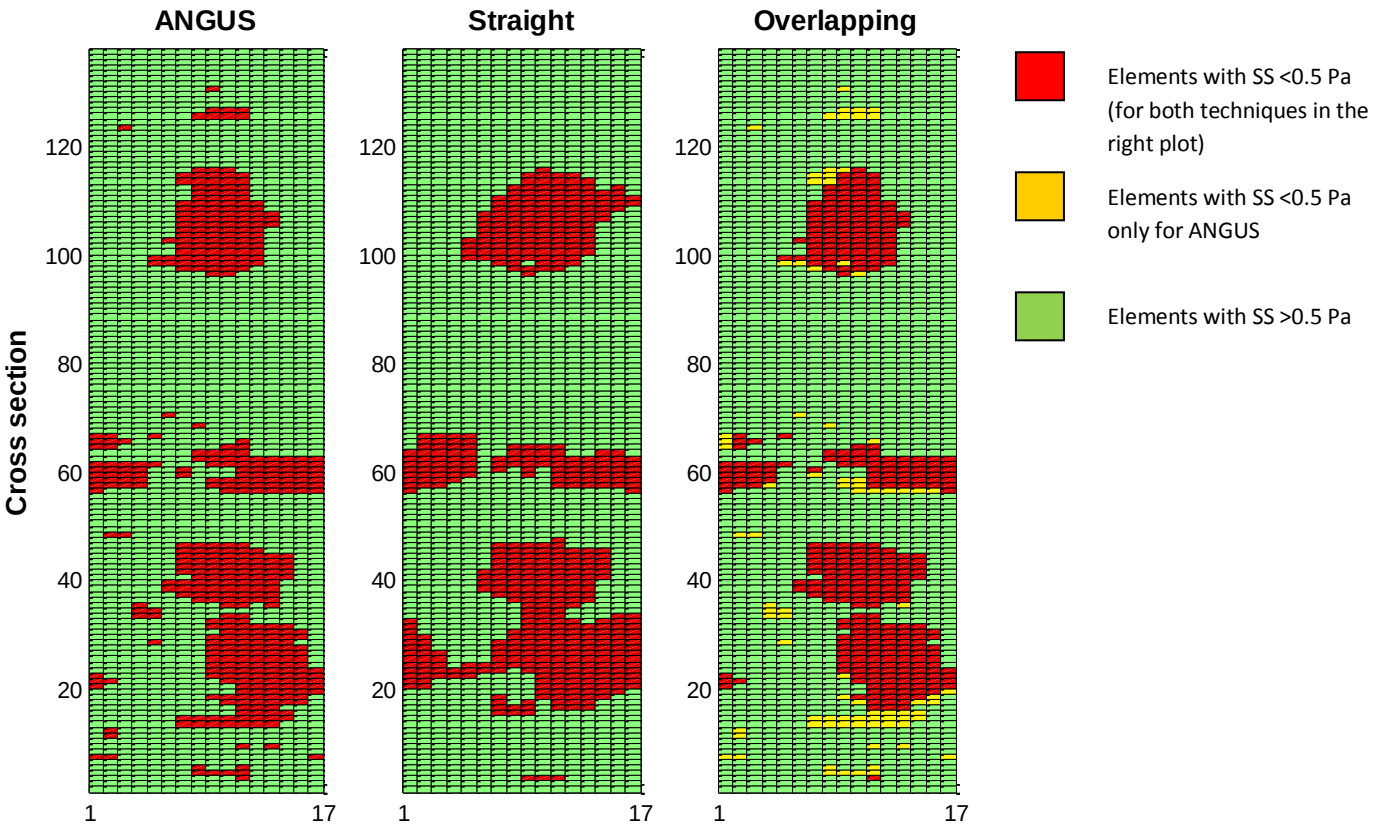

Figure 6.10 - Example of a vessel with elements with low SS (<0.5 Pa) for the ANGUS, the Straight method and the overlap of both

Patients	Number of cross sections with low SS (<0.5 Pa)				
	ANGUS	Straight	Overlapping	Sensitivity	Specificity
P060028	18	25	17	94%	93%
P060065	65	31	28	43%	97%
P060125	40	43	38	95%	95%
P060204	21	28	28	86%	90%
P060233	32	29	26	81%	95%
P060362	79	65	64	81%	98%
P061104	13	14	9	69%	94%
P061150	44	40	30	68%	92%
P062128	36	30	22	61%	90%
P062143	39	62	37	95%	68%
All	387	367	289	75%	91%
Average	39 ± 21	37 ± 16	29 ± 15	$77 \pm 17\%$	$91 \pm 9\%$

Table 6.4 - Percentage of cross sections with low SS (<0.5 Pa) in the ANGUS and Straight method

In table 6.4 was presented an analysis of the number of cross-sections with low SS (<0.5 Pa) for the ANGUS and the Straight method, as well as the percentage of

those cross sections that are coincident (or overlapped). This is a more general approach than looking at the all the elements, as was previously done. This analysis showed that the sensitivity of the Straight method in predicting cross-section with low SS was of 75% comparing to ANGUS (289 out of 387 cross-sections). Again, the total number of cross-sections analyzed was 1263.

In figure 5.9, below, is shown a randomly picked example of the distribution of the low SS elements for both techniques (left and center plot) and the overlapping cross-sections with low SS. The green squares represent the elements with SS superior to 0.5 Pa. The red squares, in the left and center plot, represent the elements with SS lower than 0.5 Pa, while in the right plot they represent the elements with low SS (<0.5 Pa) that are predicted by both techniques. The yellow squares, only present in the right plot, represent the cross-sections with low SS elements from ANGUS that are not determined by the Straight method. The sensitivity of the Straight method, in this case was 95%.

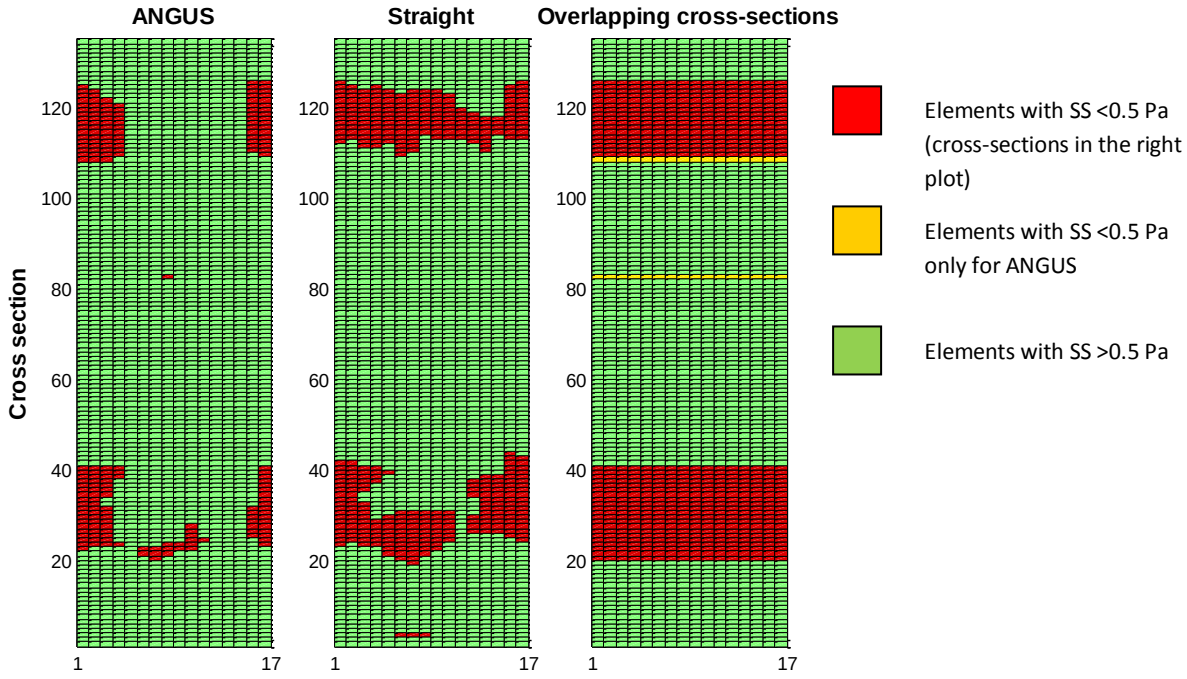

Figure 6.11 - Example of a vessel with low SS elements (<0.5 Pa) for the ANGUS, the Straight method and the overlapping cross-sections

6.1.7. High SS Analysis

In this analysis, high SS was defined as all values above the mean SS plus one standard deviation for each vessel (from the ANGUS calculations outcome). So high SS is > $\bar{x}+\sigma$ Pa (these values were previously presented in table 5.3 in Chapter 5. ANGUS vs. QCA-3D). The total number of elements in study was 21471.

The result of this analysis, for all patients, presented in table 6.5, revealed that 46% of elements from the Straight vessels with high SS (1370 out of 2952 elements) were coincident with the high SS elements from the ANGUS vessels. The average percentage of overlapping high SS elements per patient was 46 $\pm$ 15%. The specificity of the Straight method in calculating high SS elements was 97% relatively to the gold-standard ANGUS method.

In figure 6.14, below, is shown an example of the distribution of the high SS elements for both techniques (left and center plot) and the overlap of them in one of the vessels studied. In this example, the average SS was 5.40 Pa and the standard deviation was 3.93 Pa, so the high SS was considered as higher than 9.32 Pa. The green squares represent the elements with SS inferior to 9.32 Pa. The red squares, in the left and center plot, represent the elements with SS equal or higher than 9.32 Pa, while in the right plot they represent the elements with high SS (>9.32 Pa) that are coincident in both techniques. The yellow squares, only present in the right plot, represent the high SS elements that are calculated only by ANGUS. In the example shown in figure 6.14, the sensitivity of the Straight method in calculating high SS elements was 77% comparing to ANGUS.

Patients	Number of elements with high SS (> $\bar{x}+\sigma$ Pa)			Sensitivity	Specificity
	ANGUS	Straight	Overlapping		
P060028	412	348	187	45%	91%
P060065	280	111	88	31%	99%
P060125	413	224	190	46%	98%
P060204	302	375	232	77%	92%
P060233	301	132	99	33%	97%
P060362	299	198	136	45%	97%
P061104	196	75	54	28%	99%
P061150	333	190	153	46%	98%
P062128	214	152	136	64%	99%
P062143	202	95	95	47%	100%
All	2952	1900	1370	46%	97%
Average	295 $\pm$ 78	190 $\pm$ 102	137 $\pm$ 55	46 $\pm$ 15%	97 $\pm$ 3%

Table 6.5 - Elements with high SS (> $\bar{x}+\sigma$ Pa) in the ANGUS and Straight method

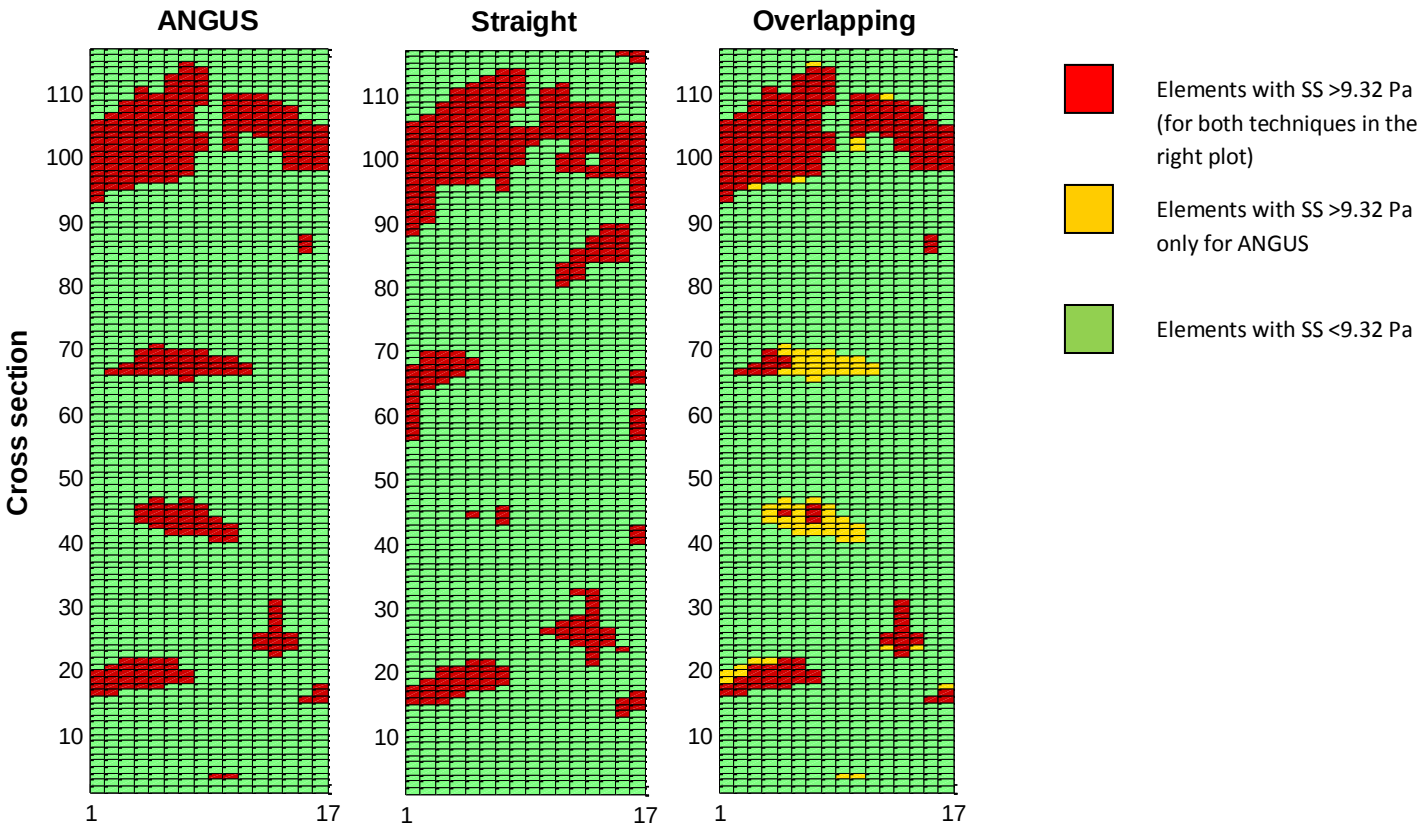

Figure 6.12 - Example of a vessel with elements with high SS (>9.32 Pa) for the ANGUS and the Straight method, and the overlap of both

The number of cross-sections with a least an element with high SS, for the ANGUS, the Straight method, the percentage of coincident cross-sections with high SS (sensitivity) and the specificity, were presented in table 6.6. It shows that 51% of the ANGUS cross-sections with high SS were coincident with the Straight cross-sections with high SS (124 out of 261 cross-sections). The total number of cross-sections analyzed was 1263. The average percentage of overlapping high SS cross-sections per patient was 49 $\pm$ 19%. The specificity of the Straight method in predicting cross-sections with high SS relatively to ANGUS is 96%.

In figure 6.13, below, is shown a randomly picked example (patient p060204) of the distribution of the high SS elements for both techniques (left and center plot) and the overlapping cross-sections with high SS. The green squares represent the elements with SS inferior to 9.32 Pa (see table 5.4 for the value). The red squares, in the left and center plot, represent the elements with SS higher than 9.32 Pa, while in the right plot they represent the elements with high SS (>9.32 Pa) that are predicted

by both techniques. The yellow squares, only present in the right plot, represent the cross-sections with high SS elements from ANGUS that are not determined by QCA-3D. In this case, the sensitivity of the QCA-3D in determining high SS cross-sections is of 86%.

Patients	Number of cross sections with high SS ($> \bar{x} + \sigma$ Pa)			Sensitivity	Specificity
	ANGUS	Straight	Overlapping		
P060028	68	55	47	69%	88%
P060065	60	23	23	38%	100%
P060125	84	43	42	50%	98%
P060204	59	77	51	86%	55%
P060233	46	28	26	57%	96%
P060362	52	20	18	35%	98%
P061104	26	14	13	50%	99%
P061150	50	19	17	34%	98%
P062128	40	21	21	53%	100%
P062143	34	7	7	21%	100%
All	519	307	265	51%	94%
Average	52 ± 17	31 ± 21	27 ± 15	$49 \pm 19\%$	$93 \pm 14\%$

Table 6.6 - Percentage of cross sections with high SS ($> \bar{x} + \sigma$ Pa) in the ANGUS and Straight method

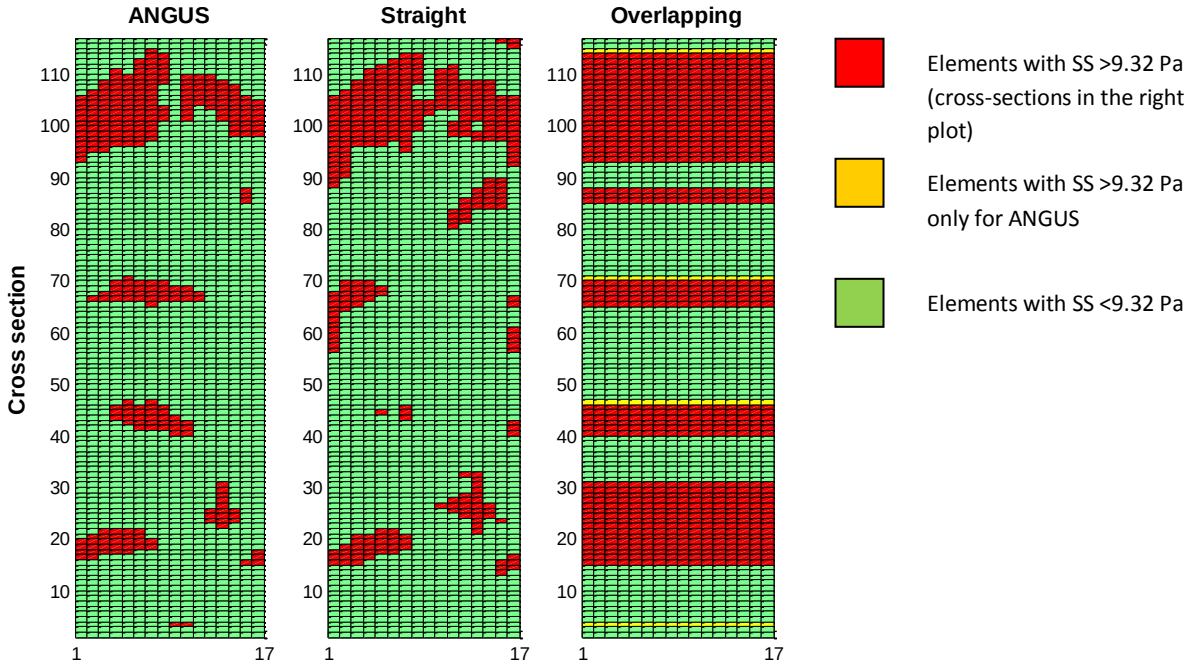

Figure 6.13 - Example of a vessel with elements with high SS (>9.32 Pa) for the ANGUS and the Straight method, and the overlapping cross-sections.

6.1.8. Longitudinal shear stress

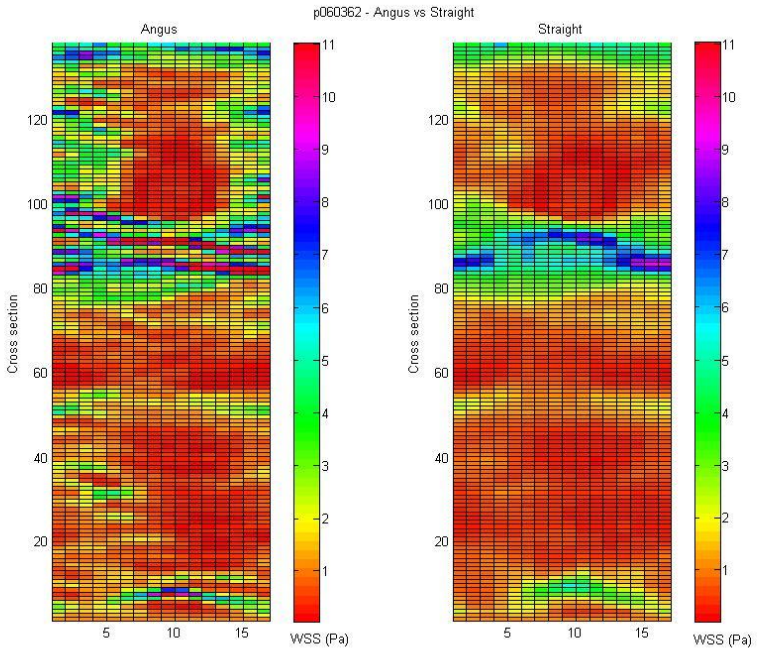

Figure 6.14 - Wall SS distribution an ANGUS and a Straight geometry

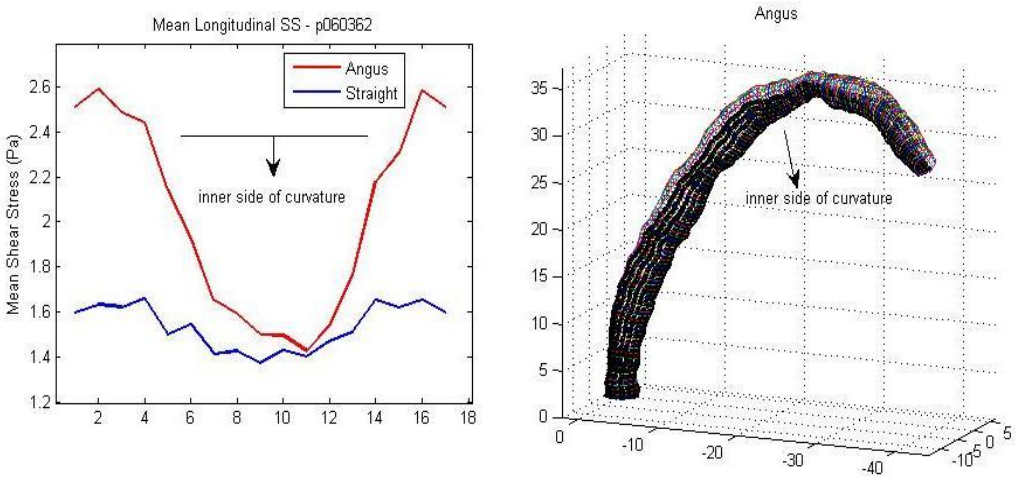

Figure 6.15 - Mean Longitudinal SS for ANGUS and the Straight vessel (p060362)

The left side of Figure 6.9 and the ANGUS (red) curve of Figure 6.10 suggest that the average longitudinal SS is not constant for the whole vessel. The columns from 6 to 13 have lower SS than the columns 1 to 5 and 14 to 17. The 3D image in Figure 6.10 reveals that the columns that have the lowest SS correspond to the inner side of the curvature in the ANGUS vessel, while the columns that have the highest SS correspond to the outer side of curvature.

On the other hand, the right side of Figure 6.9 and the Straight (blue) curve of Figure 6.10 suggest that the average longitudinal SS is almost constant for the whole vessel. This is expected, since the straight vessel has obviously no curvature.

So, at the outer side of the vessel curvature, the SS is higher than the correspondent area in the straight vessel. Otherwise at the inner side of curvatures the SS is lower or equal to the correspondent location in the straight vessel. Therefore, there is some difference between calculating SS in a curved or in a straight vessel.

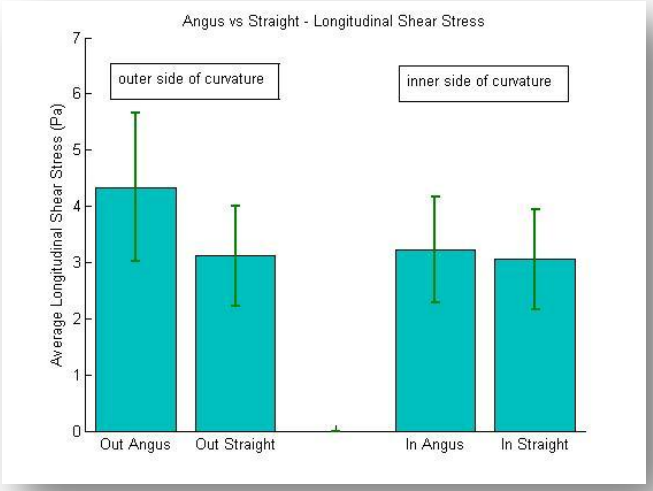

Figure 6.16 - Longitudinal Shear Stress

The bar plot shown in figure 6.11 illustrates the average longitudinal SS of the ten vessels in study. The plot is divided in four bars. The first two bars represent the average longitudinal SS in the outer side of the ANGUS vessels curvature and the correspondent region in the straight vessels. The two bars on the right represent the average longitudinal SS in the inner side of the ANGUS vessels curvature and the correspondent region in the straight vessels.

The average SS values are shown in the following table:

	Outer side		Inner side	
	ANGUS	Straight	ANGUS	Straight
Average SS (Pa)	4.34 ± 2.65	3.11 ± 1.77	3.23 ± 1.89	3.05 ± 1.79

Table 6.7 - Average longitudinal SS

This data confirms the previous assumption that the vessel curvature provokes higher SS on the outer side and lower SS on the inner side. The average SS on the outer side of curvature in the ANGUS vessels is 39% higher than in the Straight vessels, while on the inner side is only 6% higher. When comparing the inner and outer side of the same method, the outer side of ANGUS is 34% higher than the inner side and the outer side of the Straight vessels is only 2% higher than the inner side.

Chapter 7. Geometric factors

The vessel geometry was acknowledged as a major influence on the mechanical stress in and out the vessel wall, so the concept of *geometric risk factors* for the development of atherosclerosis was proposed [23]. The conjecture is that some geometric features of the human vasculature may be risk factors that increase the vessel's vulnerability to atherosclerotic disease by creating an adverse mechanical environment [24]. Wall SS distribution is largely determined by arterial geometry, but also by other factors, such as flow pulsatility, flow rates and blood rheology [25].

In this chapter, some factors, related to the vessels' geometry, that are known to influence the SS calculations outcome in the coronary arteries were presented and discussed. These factors do not depend on the blood flow and can even manifest themselves in situations with very low flow (as done in the Chapter 4 - ANGUS vs. Poiseuille). The geometric factors that were considered in this chapter were:

- Lumen area gradient;
- Local curvature;
- Geometrical anomalies (such as torsion).

It is important to know the influence of these factors in the SS calculations outcome in order to optimize the finite element meshing. In this way, regions with high SS need a coarser mesh, while regions of low SS will need finer meshes, saving precious computing time.

7.1. Results

7.1.1. Lumen Area Gradient

In this paragraph the relationship between the lumen area gradient and some SS parameters (such as average SS per cross-section, local SS and average SS gradient) was analyzed. The aim was to verify if the lumen area gradien is an accurate predictor of the SS results.

In figure 7.1, below, the relationship between the average SS per cross-section gradient versus the lumen area gradient was presented, for all ten patients in study.

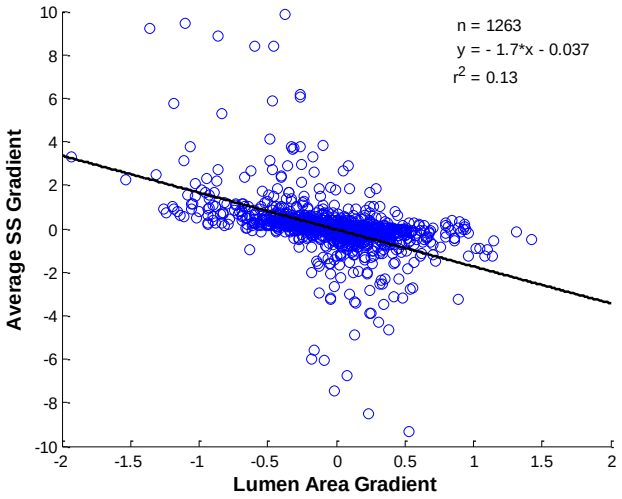

Figure 7.1 - Average SS Gradient vs Lumen Area Gradient

In this scatter plot, in the x-axis is represented the lumen area gradient. Negative values imply a lumen narrowing, while positive values imply a increase in lumen area. The analysis of this scatter plot showed that there is an inverse relationship between them, since the slope of the linear regression line is –1.7. When the lumen area gradient is negative, the average SS gradient is positive, meaning an increase in average SS, and vice-versa. However, the correlation coefficient (r^2) is only 0.13, showing a weak correlation. These results suggest that the lumen area gradient is a factor that can help to predict the SS calculations outcome.

In addition, the results of this analysis, per patient, were presented in table 7.1, below.

Patients	r^2	$y = ax + b$	
		a – slope	b – y-intercept
P060028	0.48	-0.93	-0.013
P060065	0.33	-0.88	0.0004
P060125	0.39	-0.31	0.005
P060204	0.30	-0.79	-0.040
P060233	0.51	-0.65	0.0005
P060362	0.29	-0.69	0.003
P061104	0.40	-1.4	-0.052
P061150	0.29	-6.2	-0.26
P062128	0.45	-1.7	0.010
P062143	0.18	-2.5	-0.033
All	0.13	-1.7	-0.037
Average	0.36 ± 0.10	-1.61 ± 1.73	-0.04 ± 0.08

Table 7.1 - Average SS Gradient vs Lumen Area Gradient – correlation coefficient and linear regression line slope and y-intercept

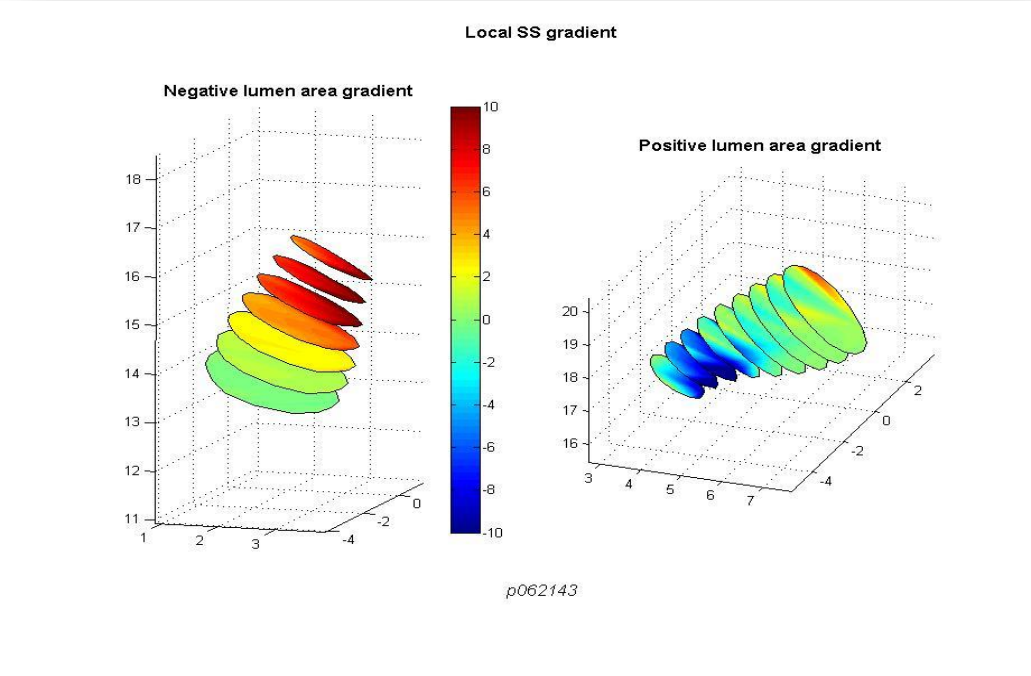

Figure 7.2 - Example of the relation between the lumen area gradient and the gradient in SS

In figure 7.2 an example is presented, showing both a positive and negative SS gradient because of a negative and positive lumen area gradient.

Additionally, the relationship between the gradient in lumen area and the average SS per cross-section was analyzed. In figure 7.3 was shown the lumen area gradient (top plot) and the average SS (bottom plot) along the length of one of the coronaries in study. Cross-sections with negative area gradient (o) and with positive area gradient (o) were highlighted, as well as the corresponding cross-sections in the average SS plot. As expected, when the gradient in lumen area is positive, or when the lumen area is increasing, the average SS over a cross section is decreasing. On the other hand, when the gradient in lumen area is negative (lumen area decreasing), the average SS over a cross section increases.

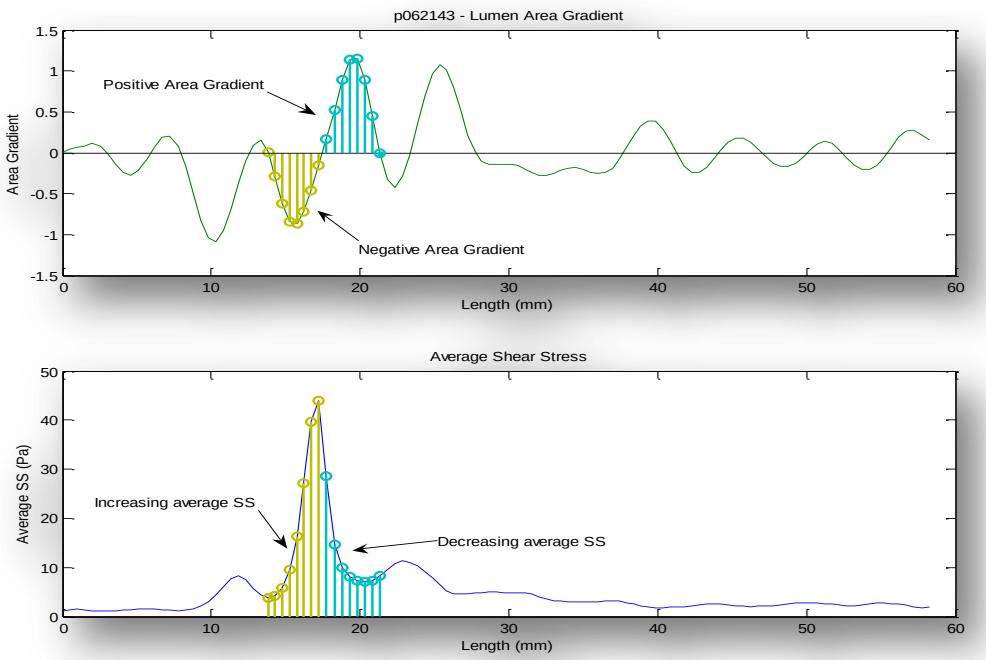

Figure 7.3 - Lumen area gradient and average SS per cross section along a coronary length

In figure 7.4 is presented a local example (same region which is highlighted in figure 7.3) of the relation between the lumen area gradient and the local SS.

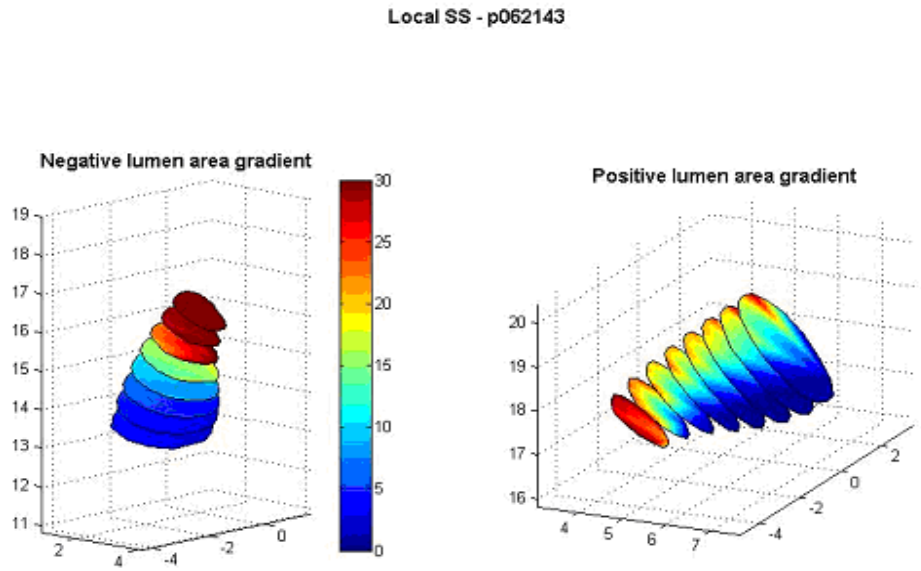

Figure 7.4 - Example of the relation between the lumen area gradient and the local SS

7.1.2. Local Curvature

In this paragraph the importance of the vessels local curvature in the SS calculations was analyzed.

The local curvature (mm^{-1}) is the angular velocity of the tangent $\vec{t}(s)$ at a location *s* of the centerline. The normal vector $\vec{n}(s)$ always points towards the origin of the curvature radius (see figure 7.5) [26]. The curvature radius *r*(mm) is the inverse of the local curvature.

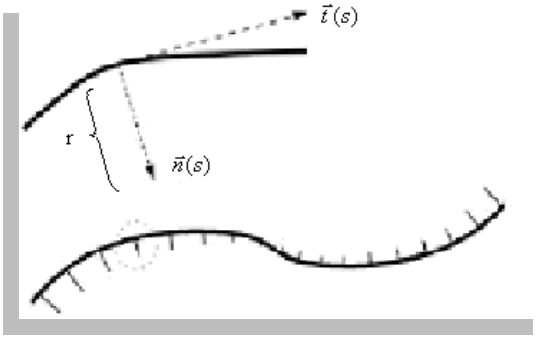

Figure 7.5 - Curvature parameters

The local curvature or the curvature radius was analyzed against the maximum SS stress per cross section and against the Dean Number. The Dean Number is dimensionless quantity used in the study of flow in curved pipes. It can be calculated using the following equation: $De = \mathrm{Re}\sqrt{r/R}$ Where Re is the Reynolds number, r is the vessel radius (mm) and R is the curvature radius (mm). The Dean Number is also a "measure" of the effect of curvature on a secondary flow development [27].

In figure 7.6 the scatter plot of the curvature radius versus the maximum SS per cross section was presented. For low curvature radius values (<50mm) the maximum SS has a wide range of values (from ≅0 to 80 Pa), while for high curvature radius values (>100mm) the maximum SS has a restricted range of values (from ≅0 to 10 Pa). This reveals that regions of high local curvature (low curvature radius) are more prone to have higher SS values.

In figure 7.7 the scatter plot of the Dean Number against the maximum SS per cross-section was presented, for all the patients in study together. The Dean Number revealed to be directly proportional to the maximum SS magnitude.

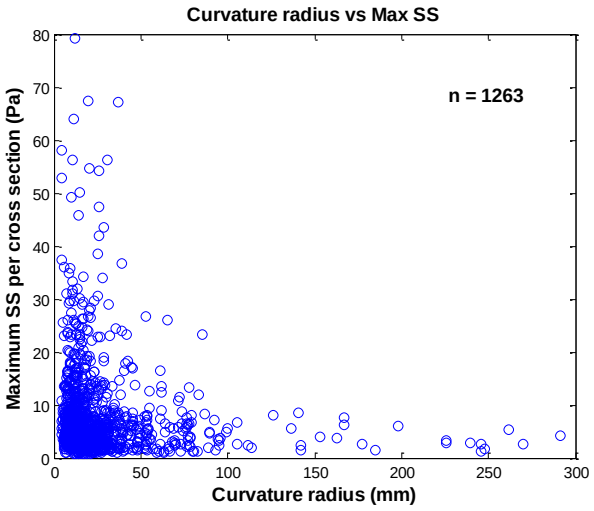

Figure 7.6 - Curvature radius vs. maximum SS per cross-section

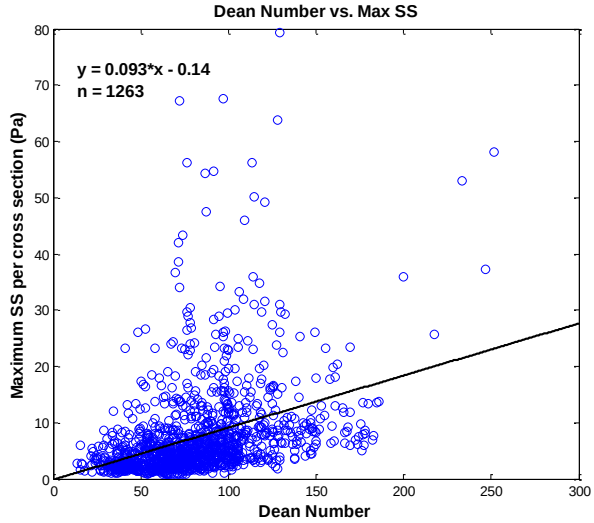

Figure 7.7 – Dean Number vs. maximum SS per cross-section

7.1.3. Other geometrical abnormalities

As described before, in Chapter 4. ANGUS vs. Poiseuille, the CFD calculations on ANGUS geometries were repeated using blood flow values, down to 1% of its physiological value. After analyzing the plots shown in figure 4.4 (in Chapter 4 - ANGUS vs. Poiseuille), it was noticed, for these low flow values that there were some locations where the average SS for that lumen area, deviated from the SS calculated based on the Poiseuille formula. Therefore it was verified if those locations corresponded to specific and continuous areas in the vessel in study, by marking those locations (figure 7.8) and examining them in the 3D reconstruction of the vessel and in the flat surface plot of those vessels (figure 7.9).

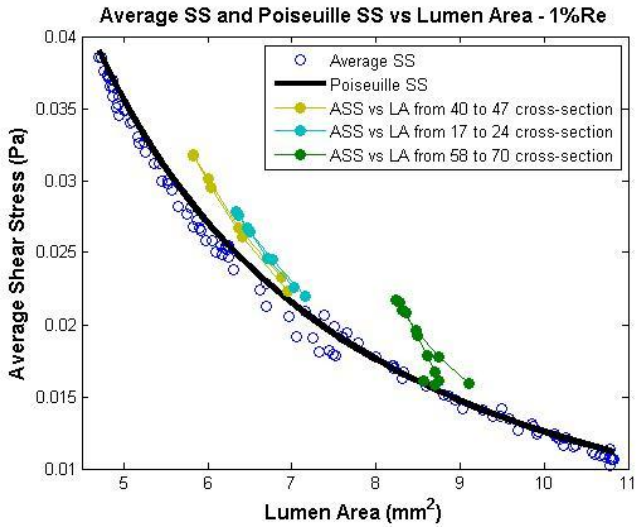

Figure 7.8 - Highlight of the dots deviated from the line based on the Poiseuille equation

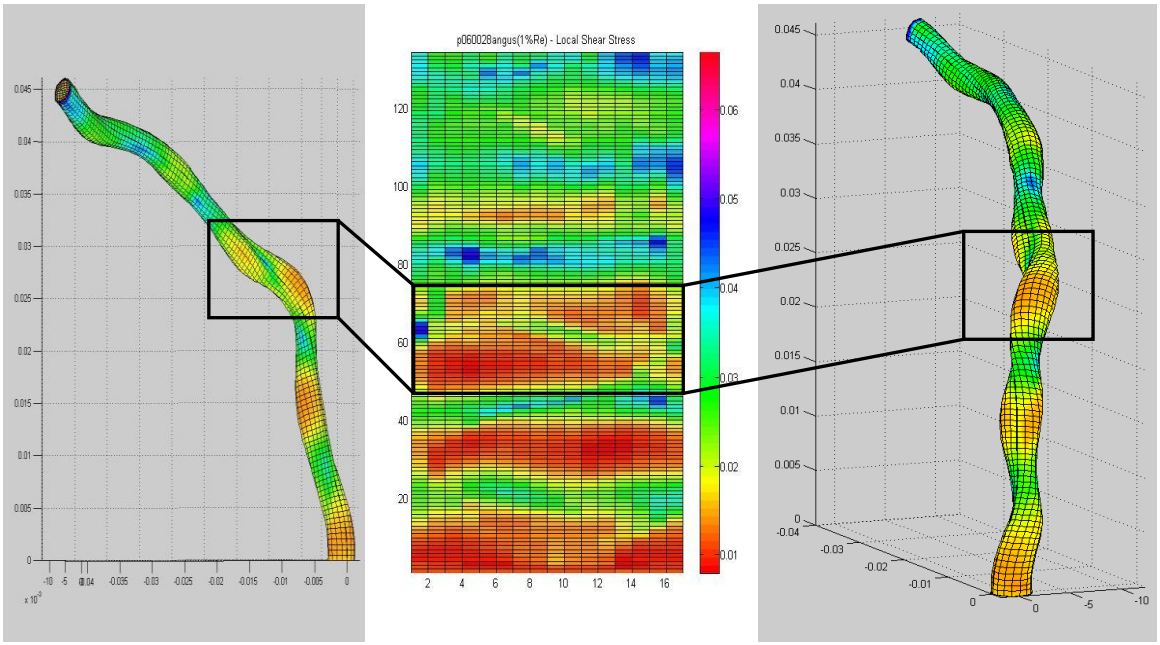

Figure 7.9 - Local SS distribution of a coronary artery – two views of the 3D reconstruction and a flat surface plot

The green dots (●) showed in Figure 7.8 represent the SS in the region between the 58th cross section and the 70th, for 1% of the physiological Reynolds number. These dots are clearly far from the ones based on Poiseuille formula. Thus, by analyzing figure 7.9, it can be seen that in this location the vessel has some torsion, which can be the cause of this difference between the Average SS and the Poiseuille SS. The Average SS dots illustrated in light blue (●) and dark yellow (●) are also non-coincident with the Poiseuille based SS, probably because of some torsion in the corresponding regions of the vessel

The two figures below represent another case. In figure 7.10.a) the average SS values, from cross section 30 to 44, calculated with 1% of the physiological flow, are represented by green dots. Again, these dots were selected because they have a large deviation from the values calculated with Poiseuille formula. By looking at figure 7.10.b) and 7.11 it was observed that in this region of the vessel, there is some abrupt lumen narrowing, and therefore a high gradient in lumen area. This quick change in lumen area (high gradient) is believed to be the cause of the abnormally high shear stress in the previously referred location. It was also observed that in the referred region of the vessel there is some torsion, or sinuosity, which could have caused this difference in the SS calculations.

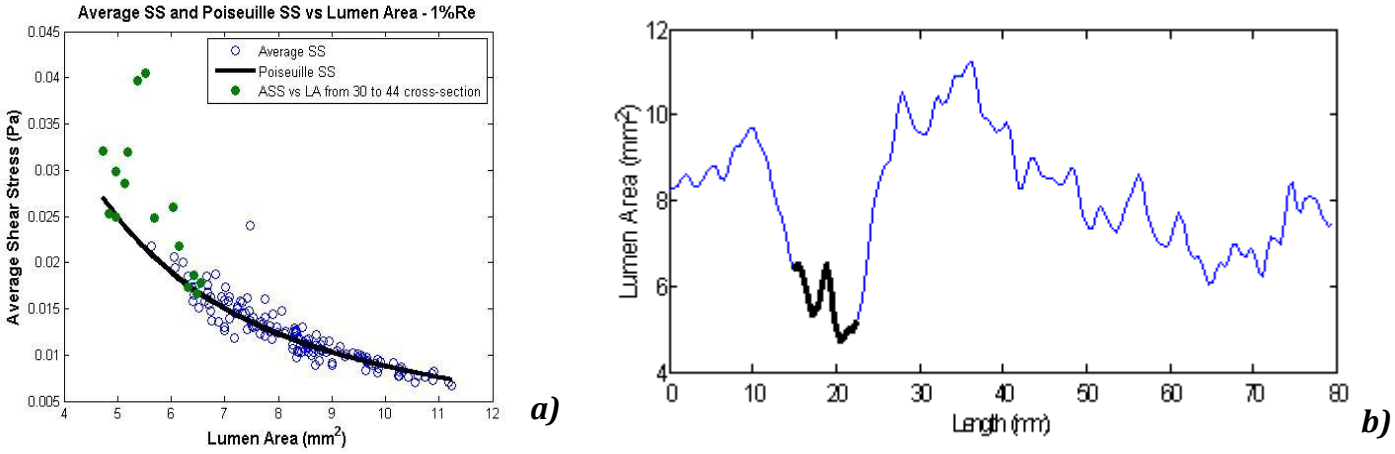

Figure 7.10 - Highlight of the dots deviated from the line based on the Poiseuille equation (a); lumen area highlight of the 30th to 44th cross-sections (b)

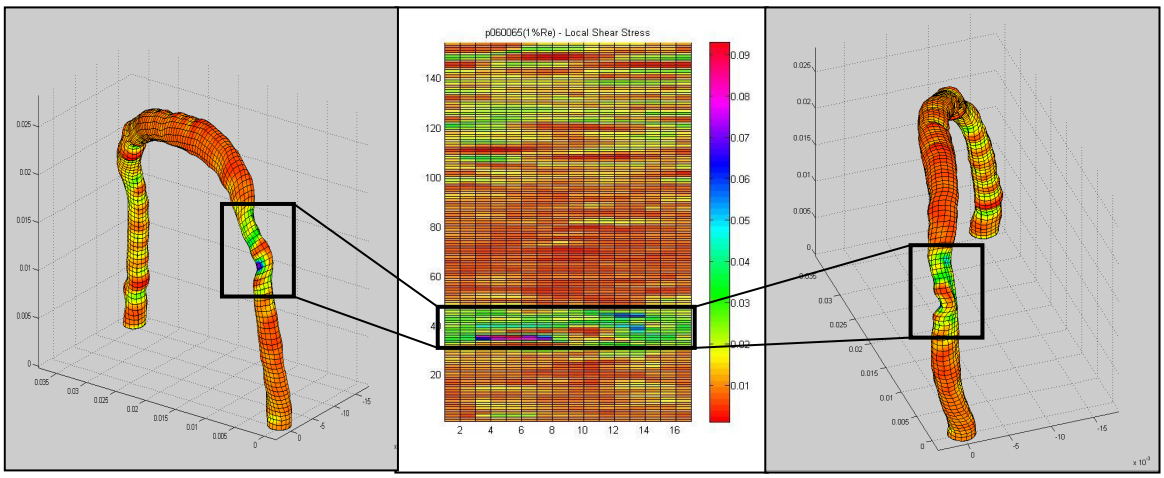

Figure 7.11- Local SS distribution – highlight of the 30th to 44th cross-sections

7.1.4. Guidelines to mesh optimization

The results previously presented in this manuscript show that geometric factors are of most importance in the SS outcome of CFD calculations. These calculations are difficult and time-consuming. So, if regions of low SS were found, meshing could be made finer in those regions, whereas areas of higher SS could have coarser meshes. Therefore some guidelines to improve the finite element meshing locally in coronary arteries reconstructions were given and compiled in this paragraph.

- Regions with positive lumen area gradient should have finer meshing, as they help create low SS locations. On the other hand, regions with negative lumen area gradient should have coarser meshing, since they are a predictor of high SS locations.

- Regions with high local curvature values and, therefore, high Dean number values, should also have finer meshing; since the Dean number is a predictor of secondary flow development. Therefore, those are regions of predilection for atherosclerotic plaque formation.

- The inner side of curvatures should also have a finer mesh, since those are regions commonly with low SS and where plaques are known to develop. In contrast, the outer side of curvatures should have coarser meshing as SS is known to have higher magnitudes at those regions.

- Regions with detectable torsion or sinuosity should also have finer meshing than the overall, since they cause non-linearities, even at extremely slow flow conditions, where they should be absent.

- On the other side, regions that don't exhibit any of the factors above mentioned could have coarser meshing. Computing time depends, among other factors, on the number of elements. Therefore if meshing is made coarser in these areas, precious time is saved.

Chapter 8. Discussion

8.1. Limitations

Some of the limitations in this study concern the CFD calculations, since it is difficult to account for all exact physiological conditions. The fluid was assumed as incompressible, homogenous Newtonian, while blood has a non-Newtonian behavior. However these previous assumptions are common and found reasonable for medium and large arteries by Friedman et al. in 1992 [28]. The flow was prescribed as steady, instead of pulsatile. The coronary vessel walls were also assumed as rigid, however at physiological conditions, the coronary walls are complaint; and due to the cardiac contraction, the coronaries contract and deform.

Furthermore, sometimes SS artifacts might have occurred due to the different smoothing in the 3D reconstructions. This fact had some residual effect on the data obtained from the Straight geometries. One presumption of the Straight method was that the geometries obtained from it had cross-sections with the exact shape and size as the ones from the ANGUS method. However, due to the different smoothing in the reconstructions, sometimes, the area of corresponding cross-sections was not exactly equal. Nevertheless, these differences in lumen area between methods had residual effects on the SS calculations outcomes.

The fact that these 3D reconstructions do not include bifurcations and side branches are a limitation in this study, since ignoring the side branches might have an impact in the SS distribution.

8.2. ANGUS vs. Poiseuille

In this chapter, one of the goals was to confirm the inverse relationship between the average SS per cross section and the lumen area of the corresponding cross-section. However, the main goal was to verify if the SS calculated based on the

Poiseuille equation[2] was accurate enough to predict the average SS per cross section in a 3D reconstructed coronary artery (by the gold-standard ANGUS method)[3], which is not a straight cylinder with perfectly circular cross-sections.

According to the results obtained, that was not a correct assumption. Though the average SS and the Poiseuille SS have similar distribution per lumen area (inverse relation), a large number of cross-sections diverged significantly in terms of value. Their correlation was only average, with average $r^2 = 0.65 \pm 0.09$.

Other goal of this chapter was to quantify the influence of the blood flow, whether in the average SS versus lumen area relationship, as in the relationship between the average SS and the Poiseuille SS. Given the results, it was evident that by lowering the blood flow, the average SS versus lumen area relation became more linear. The average SS versus Poiseuille SS correlation grew up to an $r^2 = 0.93 \pm 0.05$. This reveals that at 1% of the physiological blood flow, it is so low that the coronaries exhibit parabolic, Poiseuille-like flow. This means that most of the factors, related to flow, that caused non-linearities in the results, were suppressed.

The Bland-Altman statistics results showed that the Poiseuille SS systematically underestimated the average SS and that when the magnitude of the averages increased, the difference between the methods got larger. A probable cause for this occurrence may be the presence of the results of a specific vessel (p061150), which had really high average SS peaks comparing to the estimated Poiseuille SS.

The results from the local wall SS histogram revealed that the Poiseuille equation did not calculate any low SS (<0.5 Pa) cross-section. While according to the ANGUS method 7% of the elements had low SS. This fact may indicate that the Poiseuille equation has difficulties in predicting the low SS regions, which are of great importance, since the low SS is a cause of the development of an atherogenic phenotype in the inner surface cells of the arteries. The Poiseuille equation was also found to have difficulties in predicting the higher magnitudes of SS per cross-section, comparing to ANGUS. Furthermore, the SS histogram revealed that the SS magnitudes

[2, 3] From hereby will be referred only as Poiseuille SS and average SS, respectively.

obtained from the ANGUS geometries were in agreement with the SS range of magnitudes presented by Malek et al. in 1999 [5].

The results from the analysis of velocity profiles in some specific cross-sections were important to confirm and visualize the blood flow/SS behavior inside the coronaries. The cross section in a curved region of the vessel revealed an asymmetric profile, with high velocity near the outer side of curvature and low velocity near the inner side of curvature. The cross section with small lumen area, revealed a flattened velocity profile. This implies that the SS in this cross section is much higher than what is predicted by the Poiseuille equation, probably due to abrupt lumen narrowing. Still, for low blood flow values, these effects were eliminated and the velocity profiles became parabolic.

In the end, the Poiseuille equation revealed to be a fairly poor method of calculating SS in coronaries arteries. The main reason is that the SS distribution is strongly dependent of on the geometry of the vessel, which is not accounted in the Poiseuille equation. A similar result was found by Berthier et al., who compared the SS distribution in a model of a realistic RCA and a model with the physiological trajectory but with circular and constant cross-sections [29].

8.3. ANGUS vs. QCA-3D

In this chapter the primary objective was to compare the SS calculated from 3D geometries created by two different techniques: ANGUS and QCA-3D. The QCA-3D is based only on biplane angiography, lacking cross-sectional information. Consequently, the importance of the cross-sectional information was studied

The average SS versus lumen area relationship of both techniques was analyzed. Both demonstrated an inverse relationship and no relevant differences were found. On the other side, when comparing the average SS from both methods a low correlation coefficient was found, $r^2 = 0.40 \pm 0.20$. This lack of correlation in the average SS was mainly due to the different shape of corresponding cross-sections between each technique, since the difference in lumen area between corresponding cross-sections are highly correlated, as stated by Schuurbiers et al[19]. Those shape differences occur because QCA-3D is only based on biplane Angiography, therefore

has a limited cross sectional information, contrarily to ANGUS which has the cross sectional information given by IVUS.

It was also studied the sensitivity and the specificity of the QCA-3D method comparing to the gold-standard ANGUS method, in predicting cross-section with low or high SS. This analysis revealed that the average sensitivity of the QCA-3D method to predict low SS cross-sections was 56 ± 20%, while the specificity was 92 ± 4%. As for high SS, the average sensitivity was 58 ± 20% while the specificity was 76 ± 15%. These results state that the QCA-3D method has a similar sensitivity in predicting low SS cross-sections and high SS cross-sections.

In the end, the cross-sectional information (namely the shape of each cross-section), which lacks in the QCA-3D method, revealed to have some relevance in the SS outcomes. However, the SS results of the QCA-3D were fairly similar to the ones from ANGUS. Since the QCA-3D is a simpler approach and less time consuming, it can be affirmed that QCA-3D has the potential to become a useful tool in the catheterization laboratory, as it was stated by Schuurbiers et al [19]. Goubergrits et al. also studied the wall SS profiling of a biplane angiography-based reconstruction technique (QCA-3D) on a LCA phantom [30], and concluded that it is a practical approach.

8.4. ANGUS vs. Straight

The purpose of this chapter was to compare the SS results of the CFD calculations from ANGUS geometries and Straight geometries, therefore studying the influence of curvature on the SS distribution.

Like in Chapters 4 and 5, the first parameter analyzed was the average SS per cross section from both techniques. The average correlation coefficient, r^2 = 0.79 $\pm$ 0.11, was significantly higher than the one obtained for the ANGUS vs. QCA-3D results. The Straight geometries had similar cross-sectional shape as the ANGUS geometries, contrasting to the QCA-3D ones. Therefore these results show that when it comes to predict the average SS per cross-section the shape of the cross-section is a much more important factor than the curvature of the vessel.

The analysis of the maximum SS per cross-section or even locally, revealed that a weaker correlation (r^2 = 0.61 $\pm$ 0.11) comparing to the average SS. When observing the maximum SS locally in the ANGUS vessels, the locations at the outer side of the vessel curvature had much higher values than the corresponding locations in the Straight vessels. These results are consistent with the prevalence of atherosclerosis in the inner side of curvatures, since low SS is promotes atherosclerosis.

The local SS histogram disclosed that the peak for both techniques was situated at the same interval, 1 to 1.25 Pa. However, there were a higher percentage of elements with low SS from the Straight geometries than from the ANGUS ones. On the other hand, a lower percentage of physiological and high SS elements were found in the Straight geometries comparing to the ANGUS ones.

Like in Chapter 5 - ANGUS vs. QCA-3D, an analysis of the sensitivity and specificity of the Straight method was performed. However, in this chapter the sensitivity and the specificity were analyzed per element, as well as on a cross-sectional basis. The analysis per cross-section revealed that the average sensitivity of the Straight method in predicting cross-section with low SS was 77 ± 17% comparing to ANGUS, while the average specificity was 91 ± 9%. As for high SS, the average sensitivity was only 49 ± 19% and the average specificity was 93 ± 14%. Therefore, the Straight method seems to have more sensitivity in predicting the cross-sections with low SS than the cross-sections with high SS. Comparing with the analogous analysis for the QCA-3D method, it is observed that the Straight method has better sensitivity than QCA-3D in the prediction of low SS cross-sections. However, the QCA-3D method has better sensitivity to predict high SS cross-sections.

The sensitivity and specificity analysis per element showed that, for low SS elements, the Straight method has an average sensitivity of 52 ± 21% and an average specificity of 94 ± 3%, comparing to the ANGUS method. Concerning the high SS elements, the average sensitivity of the Straight method was 46 ± 15%, while the specificity was 97 ± 3%. From these results can be concluded that, comparing to the cross-sectional analysis, the sensitivity results are slightly worse. However this is expected, since it is a more specific analysis. Furthermore, the analysis per element showed that the Straight method has a similar average sensitivity in predicting low SS

elements and high SS elements, contrarily to the results of the analysis per cross-section.

As a conclusion, the curvature influence in the SS results revealed to have a limited importance, in contrast to the cross-sectional shape, since the SS results from the Straight method were fairly similar to the ones from ANGUS. The Straight method also revealed to be more accurate in mimicking the ANGUS results than the QCA-3D method.

8.5. Geometric Factors

The first factor analyzed in this chapter was the lumen area gradient. The scattering of the lumen area gradient and the average SS gradient from all patients together, revealed an inverse relationship between them, with a regression line slope of –1.7. So, as expected, it was observed that when the area gradient was negative the average SS was increasing in proportion, and vice-versa. These results confirm that analyzing the lumen area gradient (complemented by the lumen area values), it can be given an accurate prediction of where SS peaks may occur, and consequently optimize the meshing in those areas, by making it finer or coarser.

Another parameter analyzed was the local curvature/curvature radius. The curvature radius showed an inverse relationship with the maximum SS per cross section, which implies that low curved regions have a predominance of low SS, while highly curved regions exhibit both high and low SS. Analyzing the maximum SS per cross-section against the Dean number, a direct relationship was found. This implied that regions with high local curvature might develop secondary flow. According to Honda et al [31], the vessel bending together with the pulsatile flow causes areas of flow reversal; therefore those areas are of predilection for atherosclerosis development.

The results of the analysis of the Average SS per cross section and the Poiseuille SS for the lowest blood flow magnitude (1% of the physiological level), suggested that, even for such a slow flow, the Average SS was not similar to the Poiseuille SS. A further analysis on the local SS and the geometry in those specific

locations contributed to the assumption that this occurs due to the torsion or sinuosity exhibited in that location. The presence of these sinuous regions in the coronaries impedes the blood flow to behave in a parabolic way even at such low magnitudes. So, when transported to physiological conditions, these effects might have a much higher impact on the SS distribution.

Regarding these geometric factors, some guidelines to mesh optimization were given. In the future, these simplifications in the finite element meshing might save some precious computing time while allowing the CFD approach in SS calculation to be transported from bench to bedside.

Chapter 9. Conclusion

In the course of this project, the distribution of wall SS in coronary arteries was studied. These studies are important due to the relevance of the SS in the modulation of endothelial biology and consequent predisposal to atherogenesis.

The methods used revealed to be appropriate, since convergence was reached in all the CFD calculations executed.

Blood flow was confirmed to have a strong effect on the relationship between average SS and the lumen area, since it was found out that by lowering blood flow, non-linearities in that inverse relationship almost vanished and the average SS per cross section assumed a distribution identical to the SS based on the Poiseuille equation.

The QCA-3D method, based on biplane angiography, with elliptical cross sections, revealed to have more accuracy than the Poiseuille in mimicking the SS results based on the ANGUS geometries.It is essential to know that the results from QCA-3D geometries are comparable to the state-of-the-art ANGUS, since it is a more practical approach that can be performed on-site at the catheterization laboratory.

The Straight geometries also revealed to provide results similar to the ones from the ANGUS geometries. However, originally extremely curved vessels exhibited significantly higher SS magnitudes on the outer side of the curvature, comparing to the corresponding sites in the Straight geometries.

Geometric factors, such as lumen area gradient, local curvature or torsion, were revealed to be important in predicting SS peaks, low SS areas and sites predisposed to secondary flow development, which contribute to atherosclerotic plaque formation.

In the future, based on the knowledge of these geometric features, meshes can be optimized and CFD calculations on 3D reconstructed arteries may become a faster and bedside approach.

10. References

[1] http://www.rjmatthewsmd.com/Definitions/coronary_arteries.htm - adapted from Waller, B.F., MD, Schlant, R.C., MD, Anatomy of the Heart, Hurst's The Heart, 8th edition, p 84-86 (accessed 13 April,2009).

[2] Mosseri M, Zolti E, Rozenman Y, Lotan C, Ershov T, Izak T, Admon D, Gotsman MS. The diameter of the epicardial coronary arteries in patients with dilated cardiomyopathy. Internacional Journal of Cardiology. 62 (1997) 133–141.

[3] Guyton&Hall. Textbook of Medical Phisiology - ninth edition, Unit 4, Chapter 21, page 257.

[4] Guyton&Hall. Textbook of Medical Phisiology - ninth edition, Unit 4, Chapter 15, page 171.

[5] Malek AM, Alper SL, Izumo S. Hemodynamic Shear Stress and Its Role in Atherosclerosis. JAMA, December 1, 1999 – Vol 282, No.21

[6] Atherosclerosis: The new view. Peter Libby. Scientific American 2002 – www.ahs.uwaterloo.ca/~kh346/pdf/libby.pdf

[7] Chatzizisis YS, Coskun AU, Jonas M, Edelman ER, Feldman CL, Stone PH. Role of endothelial shear stress in the natural history of coronary atherosclerosis and vascular remodeling – molecular, cellular and vascular behavior. JACC Vol. 49, No. 25, June 26, 2007:2379–93

[8] Helderman F, Segers D, de Crom R, Hierck BP, Poelmann RE, Evans PC, Krams R. Effect of shear stress on vascular inflammation and plaque development. Curr Opin Lipidol. 2007. 18:527-533.

[9] Cunningham KS, Gotlieb AI. The role of shear stress in the pathogenesis of atherosclerosis. Laboratory Investigation (2005) 85, 9–23.

[10] Slager CJ, Wentzel JJ, Gijsen FJH, Schuurbiers JCH, van der Wal AC, van der Steen AFW, Serruys PW. The role of shear stress in the destabilization of vulnerable plaques and related therapeutic implications. Nature Clinical Practice Cardiovascular Medicine. 2005 Vol.2 No.9:456-464.

[11] Slager CJ, Wentzel JJ, Gijsen FJH, Schuurbiers JCH, van der Wal AC, van der Steen AFW, Serruys PW. The role of shear stress in the generation of rupture-prone vulnerable plaques. Nature Clinical Practice Cardiovascular Medicine. 2005 Vol.2 No.8:401-407

[12] Falk E, Shah PK, Fuster V. Coronary plaque disruption. (1995) Circulation 92: 657-671.

[13] http://www.cfd-online.com/Wiki/Navier-Stokes_equations (accessed June 15, 2009)

[14] http://www.grc.nasa.gov/WWW/K-12/airplane/nseqs.html_(accessed June 15, 2009)

[15] Segal A., Vuik C. 2006. Computational Fluid Dynamics II. Delft Institute of Applied Mathematics, Delft, The Netherlands.

[16] Poelma C. Blood-tissue interaction; the role of wall shear stress. Biological Fluid Mechanics lecture (2008). Delft University of Technology.

[17] Slager CJ, Wentzel JJ, et al. True 3-Dimensional Reconstruction of Coronary Arteries in Patients by Fusion of Angiography and IVUS (ANGUS) and Its Quantitive Validation. Circulation. 2000; 102*:511-516.*

[18] Gijsen FJH, Migliavacca F, Schievano S, Socci L, Petrini L, Thury A, Wentzel JJ, Van der Steen AFW, Serruys PWS, Dubini G. Simulation of stent deployment in a realistic human coronary artery. BioMedical Engineering OnLine 2008, 7:23.

[19] Schuurbiers JCH, Lopez NG, Ligthart J, Gijsen FJH, Dijkstra J, Serruys PW, Van der Steen AF, Wentzel JJ. In vivo validation of CAAS QCA-3D coronary reconstruction using fusion of angiography and intravascular ultrasound (ANGUS). Catheterization and Cardiovascular Interventions 73:620–626 (2009).

[20] Bland JM, Altman DG. Statistical methods for assessing agreement between two methods of clinical measurement. Lancet 1986 Feb 8;1(8476):307-10.

[21] http://www.medcalc.be/manual/blandaltman.php (accessed August 24, 2009)

[22] Rand PW, Lacombe E, Hunt HE, Austin WH. Viscosity of normal human blood under normothermic and hypothermic conditions. J.Appl. Physiol. 19(1): 117-122. 1964.

[23] Friedman MH, Deters OJ, Mark FF, Bargeron CB, Hutchins GM. Arterial geometry affects hemodynamics — a potential risk factor for atherosclerosis. Atherosclerosis 1983; 46(2):225–31.

[24] Zhu H, Ding Z, Piana RN, Gehrig TR, Friedman MH. Catologuing the geometry of human coronary arteries: A potential tool for predicting risk of coronary artery disease. International Journal of Cardiology 135(2009) 43-52.

[25] Feldman CL, Stone PH. Intravascular hemodynamic factors responsible for progression of coronary atherosclerosis and development of vulnerable plaque. Current Opinion in Cardiology 2000, 15:430–440.

[26] Wahle A, Lopez JJ, Olszewski ME, Vigmostad SC, Chandran KB, Rossen JD, Sonka M. Plaque development, vessel curvature, and wall shear stress in coronary arteries assessed by X-ray Angiography and intravascular ultrasound. Medical Image Analysis 10 (2006) 615-631.

[27] Wood NB, Zhao SZ, Zambanini A, Jackson M, Gedroyc W, Thom SA, Hughes AD, Xu XY. Curvature and tortuosity of the superficial femoral artery: a possible risk factor for peripheral arterial disease. Journal of Applied Physiology 101: 1412–1418, 2006.

[28] Friedman MH, Bargeron CB, Duncan DD, Hutchins GM, Mark FF. Effects of arterial compliance and non-Newtonian rheology on correlations between intimal thickness and wall shear. Journal of Biomechanical Engineering.1992 Aug; 114(3):317-320.

[29] Berthier B, Bouzerar R, Legallais C. Blood flow patterns in an anatomically realistic coronary vessel: influence of three different reconstruction methods. Journal of Biomechanics 35 (2002) 1347-1356.

[30] Goubergrits L, Wellnhofer E, Kertzscher U, Affeld K, Petz C, Hege HC. Coronary artery WSS profiling using a geometry reconstruction based on biplane angiography. Annals of Biomedical Engineering 37 (2009) 4:682-691

[31] Honda HM, Hsiai T, Wortham CM, Chen M, Lin H, Navab M, Demer LL. A complex flow pattern of low shear stress and flow reversal promotes monocyte binding to endothelial cells. Atherosclerosis 158 (2001), 385-390.

11. Appendix

Patients	100% Re - $y = ax + b$		50% Re - $y = ax + b$		10% Re - $y = ax + b$		1% Re - $y = ax + b$	
	a	b	a	b	a	b	a	b
p060028	1.5	-0.22	1.3	-0.091	1.0	-0.0019	1.0	0.0004
p060065	1.9	-0.67	1.6	-0.3	1.3	-0.038	1.3	-0.0033
p060125	1.2	0.12	1.2	-0.071	1.1	-0.012	1.0	-0.0007
p060204	1.5	0.8	1.4	0.21	1.2	-0.02	1.2	-0.0023
p060233	2	-0.93	1.7	-0.42	1.2	-0.033	1.1	-0.002
p060362	1.7	-0.41	1.5	-0.2	1.1	-0.017	1.1	-0.0012
p061104	1.6	-0.44	1.3	-0.18	1.1	-0.016	1.0	-0.0012
p061150	1.9	-1.1	1.6	-0.73	1.2	-0.095	1.1	-0.0049
p062128	1.8	-1.1	1.5	-0.47	1.1	-0.033	1.0	-0.0015
p062143	2.5	-0.92	2.5	-0.46	1.4	-0.075	1.2	-0.0044
Average	1.76 ± 0.35	-0.49 ± 0.60	1.56 ± 0.37	-0.27 ± 0.26	1.17 ± 0.12	-0.03 ± 0.03	1.10 ± 0.11	-0.002 ± 0.002

Table11.1 - Regression line coefficients from the scattering of ANGUS based Average SS versus Poiseuille based SS

Patient	Coronary Artery	Mean Reynolds Number	Inlet flow rate (ml/min)	Average lumen diameter (mm)	Range of diameter (mm)	Artery Length (mm)
p060028	LCX	252.9 ± 30.5	105.27	3.1 ± 0.3	2.0 – 3.7	67.7
p060065	RCA	171.5 ± 15.0	73.57	3.2 ± 0.3	2.7 – 4.0	77.6
p060125	RCA	204.4 ± 20.4	93.45	3.4 ± 0.3	2.7 – 4.0	66.5
p060204	LAD	396.5 ± 53.1	165.30	3.2 ± 0.4	2.4 – 4.2	59.0
p060233	LCX	355.3 ± 43.6	156.59	3.3 ± 0.4	2.5 – 4.0	47.0
p060362	RCA	218.5 ± 44.6	97.96	3.5 ± 0.6	2.0 – 4.5	69.5
p061104	LCX	291.2 ± 54.6	113.01	3.0 ± 0.5	2.0 – 3.8	46.7
p061150	LAD	333.0 ± 125.4	102.37	2.5 ± 0.6	0.6 – 3.9	77.7
p062128	RCA	304.5 ± 28.9	140.50	3.5 ± 0.3	2.8 – 4.3	57.8
p062143	RCA	272.5 ± 44.0	130.10	3.6 ± 0.5	2.1 – 4.2	58.3
Average	**-**	**280.0 ± 70.6**	**117.81 ± 29.42**	**3.2 ± 0.3**	**2.2 ± 0.6 – 4.1 ± 0.2**	**62.7 ± 11.0**

Table 11.2 - Some geometric and flow parameters of the QCA-3D reconstructed vessels

Patient	Coronary Artery	Mean Reynolds Number	Inlet flow rate (ml/min)	Average lumen diameter (mm)	Range of diameter (mm)	Artery Length (mm)
p060028	LCX	263.3 ± 34.3	105.27	3.0 ± 0.4	2.3 – 3.7	67.9
p060065	RCA	173.1 ± 16.1	73.57	3.2 ± 0.3	2.5 – 3.7	77.7
p060125	RCA	209.5 ± 22.2	93.45	3.5 ± 0.4	2.8 – 4.3	67.8
p060204	LAD	397.6 ± 68.6	165.30	3.3 ± 0.6	2.4 – 4.6	60.3
p060233	LCX	327.7 ± 31.9	156.59	3.5 ± 0.4	2.9 – 4.2	46.6
p060362	RCA	212.9 ± 37.5	97.96	3.6 ± 0.6	2.4 – 4.4	69.1
p061104	LCX	272.6 ± 39.2	113.01	3.1 ± 0.4	2.4 – 3.7	48.0
p061150	LAD	330.5 ± 69.4	102.37	2.4 ± 0.5	1.6 – 3.6	81.2
p062128	RCA	320.6 ± 41.9	140.50	3.3 ± 0.4	2.4 – 4.0	58.1
p062143	RCA	306.0 ± 59.3	130.10	3.3 ± 0.5	1.9 – 3.9	58.9
Average	-	**281.4 ± 68.5**	**117.81 ± 29.42**	**3.2 ± 0.3**	**2.4 ± 0.4 – 4.0 ± 0.3**	**63.5 ± 11.4**

Table 11.3 - Some geometric and flow parameters of the Straight reconstructed vessels

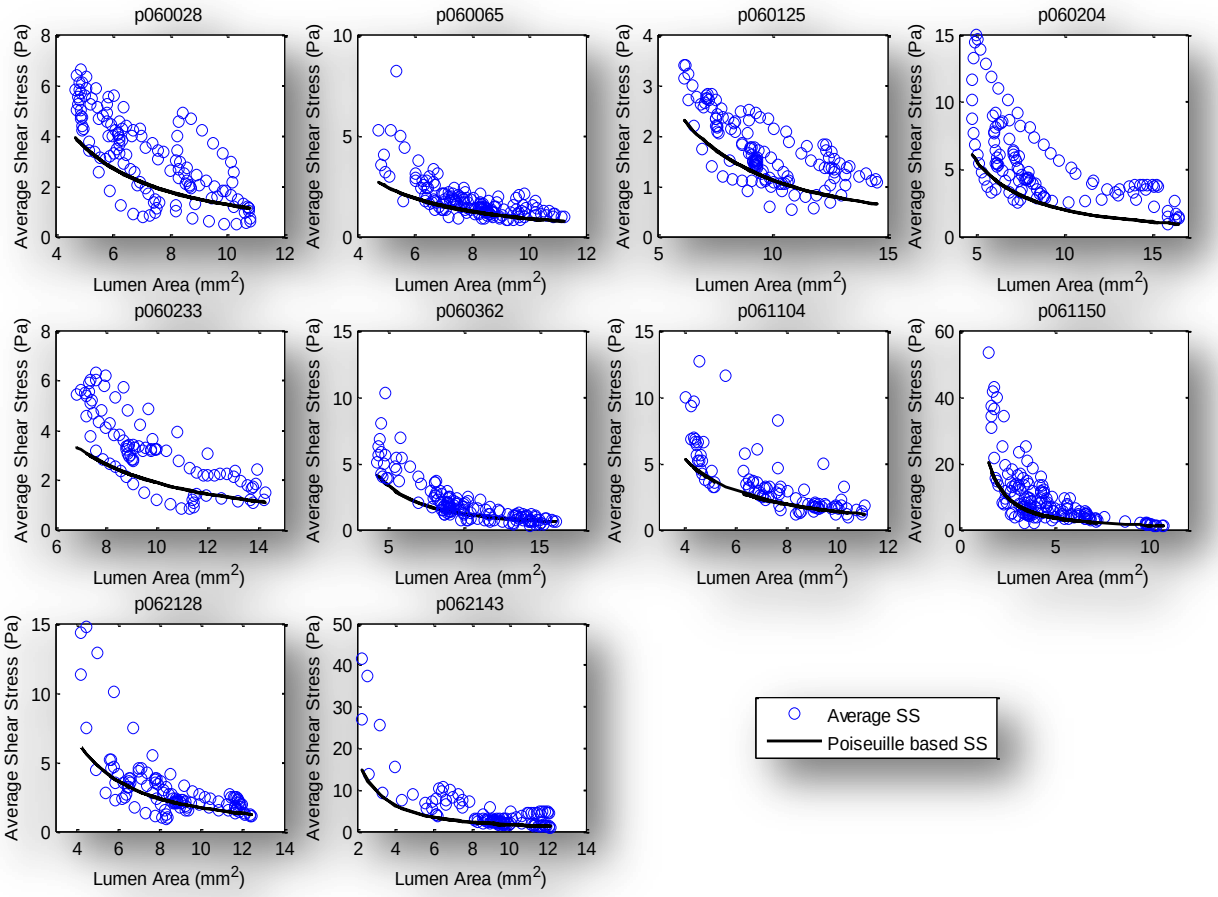

Figure 11.1 – Average Shear Stress vs. Lumen Area, based on the CFD calculations (O) and the Poiseuille formula (-), of all ten coronaries

11.1. CFD script – example

```
problem
types
 elgrp1=900
 essbouncond
  surfaces(s1)
  surfaces(s3)
end

matrix
  method=2
end

essential boundary conditions, sequence_number =    1
  surfaces(s1 ), degfd3=(func=1)
end

# two steps:
# step 1: creat a good initial solution
# step 2: get final solution thru Re stepping

# coefficients step 1: initial solution

coefficients, sequence_number =    1
elgrp1 (nparm=20)
  icoef2 = 1       # Newtonian fluid
  icoef5 = 0       # Stokes, linearization
  coef6  = 1d-6    # eps
  coef7  = 1000    # density
  coef12 = 0.030   # viscosity
end

# coefficients step 2: Re stepping

coefficients, sequence_number =    2
elgrp1 (nparm=20)
  icoef2 = 1       # Newtonian fluid
  icoef5 = 2       # Newtonian linearization
  coef6  = 1d-6    # eps
  coef7  = 1000    # density
```

```
  coef12 = 0.010   # viscosity
end

# change coeffients for the initial solution: 1 and 2

change coefficients, sequence_number =     1
elgrp1
  icoef5 = 1       # Picard lin
end

change coefficients, sequence_number =     2
elgrp1
  icoef5 = 2       # Newtonian lin
end

# change coeffients for final solution: 3 till 5

change coefficients, sequence_number =     3
elgrp1
  coef12 =  0.0075   # viscosity
end

change coefficients, sequence_number =     4
elgrp1
  coef12 =  0.005   # viscosity
end

change coefficients, sequence_number =     5
elgrp1
*   icoef2=101
  coef12 =  0.0035   # viscosity
end

# for deriva we need the same coefficients as in the last iteration
# of the non_linear problem
# it has to be the same as the last change coefficients

coefficients, sequence_number =     3
elgrp1 (nparm=20)
  icoef2 = 1       # Newtonian fluid
  icoef5 = 2       # Newtonian linearization
  coef6  = 1d-6    # eps
```

```
  coef7  = 1000     # density
  coef12 = 0.0035
end

#step1
nonlinear_equations, sequence_number =     1
 global_options, maxiter=100,accuracy=5d-3,print_level=2, lin_solver =1
 equation 1
 fill_coefficients     1
 change_coefficients
 at_iteration 2, sequence_number 1
 at_iteration 3, sequence_number 2
end

#step2
nonlinear_equations, sequence_number =     2
 global_options, maxiter=100,accuracy=1d-4,print_level=2, lin_solver =1
 equation 1
 fill_coefficients     2
 change_coefficients
 at_iteration 2, sequence_number 3
 at_iteration 3, sequence_number 4
 at_iteration 4, sequence_number 5

end

end_of_sepran_input
 0.001829 105.384185
 0.003600  0.012300 -0.400000

output
 to_avs
end
```